The Henryk Niewodniczański Institute of Nuclear Physics
Polish Academy of Sciences

Processes with a hard scale at the LHC as a signature of partonic structure of the proton

Emilia Lewandowska

Thesis submitted for the Degree of Doctor of Philosophy in Physics
prepared under the supervision of Prof. Krzysztof Golec-Biernat

KRAKÓW 2014

Abstract

The main aim of this thesis is a theoretical analysis of selected processes with a hard scale observed in the high-energy proton collisions at the LHC. These processes are considered in the limit of high energies available at the LHC, which allows a closer examination of the parton correlations inside the proton and, in consequence, leads to new information on the partonic structure of hadrons. The analysis carried out in this thesis concerns several problems. First, the Drell-Yan processes were analyzed in the formalism of the color glass condensate. The obtained results were compared with those obtained in the collinear approximation. The rest of the discussed issues concern the double parton scattering. In particular, we analyzed the problem of the specification of initial conditions for QCD evolution equations for double parton distributions, which satisfy non-trivial momentum and valence quark number sum rules. Within the double parton scattering studies, we analyzed the production of electroweak bosons W^+W^- and Z^0Z^0 taking into account the so called splitting terms in the QCD evolution equations. The found results show the importance of these terms for the predictions of the cross sections for the considered processes.

Streszczenie

Celem niniejszej pracy jest szczegółowa analiza teoretyczna wybranych procesów z twardą skalą obserwowanych w wysokoenergetycznych zderzeniach protonów na akceleratorze LHC. Procesy te są rozpatrywane w granicy wysokich energii, dostępnych na LHC, co umożliwia dokładniejsze zbadanie korelacji między partonami wewnątrz protonu i w konsekwencji prowadzi do otrzymania nowej informacji na temat partonowej struktury hadronów. Przeprowadzone w pracy analizy dotyczą kilku wybranych zagadnień. Po pierwsze, dokonana została analiza procesów Drella-Yana w formaliźmie szkła kolorowego. Otrzymane wyniki zostały porównane z wynikami uzyskanymi w ujęciu kolinearnym. Pozostałe analizowane zagadnienia dotyczą procesów podwójnego rozpraszania partonów. W szczególności, analizowane było zagadnienie specyfikacji warunków początkowych dla równań ewolucji QCD rozkładów dwupartonowych, które spełniają nietrywialne reguły sum: pędową i liczbową dla kwarków walencyjnych. W ramach badań podwójnego rozpraszania partonów wykonana została analiza produkcji elektrosłabych bozonów W^+W^- oraz Z^0Z^0 z uwzględnieniem członów typu *splitting* w równaniach ewolucji QCD. Otrzymane wyniki pokazują jak istotne są te człony dla przewidywań przekrojów czynnych dla rozważanych procesów.

Contents

Preface

In the last 60 years, studies of particle collisions gave the possibility to deepen the knowledge of the structure of hadrons and high energy processes. Experiments conducted at particle accelerators led to the discovery of the fundamental constituents of matter - "elementary particles" and allowed to examine the interactions between them. A model of matter, called the Standard Model, assumes the existence of elementary particles - a total of six quarks and six leptons, interacting with each other through the exchange of intermediate bosons: gluons which mediate the strong force, photon which carries the electromagnetic force and $W^{\pm}$ and Z^0 bosons mediating the weak force.

One of the basic issues of high energy physics are the interactions between hadrons. For decades, physicists have been conducting intensive studies in this field to understand the dynamics of hadron collisions and to confront existing theoretical models with experimental data. The technical progress in the construction of accelerator and detector systems has allowed to analyze these processes at increasingly higher energies.

The Large Hadron Collider (LHC), built by the European Organization for Nuclear Research (CERN) in the years 1998 - 2008, is currently the largest and the most powerful accelerator in the world. The LHC has been designed to collide two opposing proton beams with the total collision energy equal to 14 TeV. The analyzes of the particle collisions at such high energies provide important information on interaction of hadrons and thus on the structure of matter. Many of the fundamental particles are produced only in high energy collisions, thus it is hard or near impossible to study them in other ways. In the year 2012, the last missing element of the Standard Model, the Higgs boson, was discovered, which proved the physical potential of the LHC.

The processes with a hard scale at the LHC, which are the main subject of the research proposed in this thesis, belong to the area of fundamental science. They concern the basic building blocks of matter - quarks and gluons which are fundamental constituent of hadrons in general and nucleons in particular. Our analysis is based on quantum chromodynamics (QCD), the fundamental theory of strong interactions.

The outline of the dissertation is the following.

Chapter 1 serves as a theoretical introduction in which we review basic facts concerning the quantum chromodynamics and its applications such as color forces, quarks

and gluons, deep inelastic scattering, the Feynman's parton model and the phenomena of parton saturation. We introduce here the parton distribution functions which are intensively used in the description of the measured cross sections for high energy scattering processes.

In Chapter 2, we present an analysis of the Drell-Yan lepton pair production at forward rapidities at the LHC kinematics. In particular, we show that using the dipole framework leads to a significant suppression of the DY cross section in comparison to the collinear factorization result. This is due to saturation effects in a dipole cross section.

In Chapters 3 and 4, we perform theoretical studies of the double parton scattering processes in the context of the LHC experiments. The key element in the description of these processes are the double parton distribution functions (DPDFs) which describe correlations between partons inside a hadron. Therefore, they provide the basic knowledge of the partonic structure of a nucleon which goes beyond the description with the standard single parton distribution functions, determined so far in the scattering experiments. In particular, we concentrate on the QCD evolution equations of the double parton distributions, addressing the question of initial conditions for these equations. For this purpose, we constructed a numerical program which solves the DPDFs evolution equations. The observation of the double parton scattering processes at the Tevatron experiments strongly suggests that the deep theoretical understanding of the double parton scattering is mandatory for the interpretation of experimental results from the LHC.

In Chapter 5, we present an application of the results from the previous section to the analysis of the W^+W^- and Z^0Z^0 electroweak boson production in the double parton scattering at the LHC. In particular, we quantify the role of splitting terms in the QCD evolution equations for the double parton distribution functions. We find that these terms give important contributions to the cross sections under the study.

The results discussed in this thesis are based on the following publications:

1. "Drell-Yan process at forward rapidity at the LHC",
   Krzysztof Golec-Biernat, Emilia Lewandowska and Anna M. Stasto,
   Phys. Rev. **D82**, 094010 (2010),

2. "The Drell-Yan processes at forward rapidities at the LHC",
   Emilia Lewandowska, Acta Phys. Pol. B, Vol. **42** (2011) - No 7,

3. "Initial conditions for evolution of double parton distributions",
   Krzysztof Golec-Biernat and Emilia Lewandowska, Proceedings of Science,
   PoS DIS2013 (2013) 075, arXiv:1311.7392 [hep-ph],

4. "How to impose initial conditions for QCD evolution of double parton distributions?", Krzysztof Golec-Biernat and Emilia Lewandowska,
   Phys. Rev. **D90**, 014032 (2014),

5. "Double parton distribution functions and their QCD evolution equations",
   Emilia Lewandowska, Acta Phys. Pol. B, Vol. **45** (2014) - No 7,

6. "Electroweak boson production in double parton scattering",
   Krzysztof Golec-Biernat and Emilia Lewandowska, Phys. Rev. **D90**, 094032 (2014).

Chapter 1

Introduction

1.1 Quarks and the strong interactions

In 1964, Murray Gell-Mann and George Zweig hypothesized the existence of certain elementary particles called quarks. At first, they assumed the existence of three quarks, u, d and s, together with the corresponding antiparticles - called antiquarks. The later experimental researches conducted over the strong interactions discovered of three more quarks of different flavors, c, b and t, discovered in the years 1974, 1977 and 1995, respectively. Quarks are the basic elementary particles and the fundamental constituents of matter which make up hadrons: baryons which are built with three quarks (qqq) and mesons formed by a quark antiquark pair $(q\overline{q})$.

Quarks are point-like fermions with spin $\frac{1}{2}$, fractional baryon number $A = \frac{1}{3}$ and fractional electric charge $+\frac{2}{3}|\mathrm{e}|$ or $-\frac{1}{3}|\mathrm{e}|$. The exact specification of the quark properties is given in Table 1.1. Each quark has its antiquark which is characterized by the opposite sign of additive quantum numbers, e.g. the electric charge Q, baryon number A or the third component of isospin I_3. Quarks do not exist in nature as free particles but are confined in hadrons. All experiments, made by the analogy to the break up of a nucleus during which its components, nucleons, are released, failed to observe free quark. Even in the highest energy collisions, the free quarks were never directly observed in the detectors.

Quarks can be divided into two groups according to their mass (called current mass):

- light quarks: u, d, s with mass $m_q < 0.5$ GeV,
- heavy quarks: c, t, b with mass $m_q > 1$ GeV.

The individual quark masses are shown in Table 1.2. In addition, from the point of view of electroweak interactions, all quarks are grouped into two-quark families, called gener-

Table 1.1: The properties of quarks

	Quantum numbers			
Quark flavors	A	Q	I	I_3
u (up)	$\frac{1}{3}$	$+\frac{2}{3}$	$\frac{1}{2}$	$+\frac{1}{2}$
d (down)	$\frac{1}{3}$	$-\frac{1}{3}$	$\frac{1}{2}$	$-\frac{1}{2}$
s (strange)	$\frac{1}{3}$	$-\frac{1}{3}$	0	0
c (charm)	$\frac{1}{3}$	$+\frac{2}{3}$	0	0
b (bottom, beauty)	$\frac{1}{3}$	$-\frac{1}{3}$	0	0
t (top, truth)	$\frac{1}{3}$	$+\frac{2}{3}$	0	0

ations,

$$\begin{pmatrix} u \\ d \end{pmatrix}, \quad \begin{pmatrix} c \\ s \end{pmatrix}, \quad \begin{pmatrix} t \\ b \end{pmatrix},$$

wherein, only the first-generation quarks occur commonly (as constituent quarks) in nature, e.g. in the proton (uud) and the neutron (ddu).

Quark structure of hadrons have to be considered as a proven fact. Experiments on deep inelastic scattering (DIS) of leptons off hadrons are beautifully explained as scattering of leptons on individual, point-like quarks. In the infinite momentum frame, the duration of these collisions is too small for quarks to exchange gluons among themselves. Consequently, quarks interacts with leptons as free particles.

The development of the quark theory caused a re-review of the existing forces in nature. Due to the Pauli exclusion principle, which excludes the existence of identical quarks in the same quantum state, the existence of the structure of the three quarks in a baryon requires quarks with different quantum numbers. It turned out that quarks carry

Table 1.2: Quark masses

m_u	m_d	m_s
2 - 8 MeV/c^2	5 - 15 MeV/c^2	0.1 - 0.3 GeV/c^2
m_c	m_b	m_t
1.0 - 1.6 GeV/c^2	4.1 - 4.5 GeV/c^2	168 - 192 GeV/c^2

a color charge and are held in nucleons by a fundamental force - color force. The concept of a color force, introduced in 1964 by O. W. Greenberg, allowed to fulfill the Pauli exclusion principle for quarks in baryons. According to this theory, the interaction between quarks are determined by their color charge which allows to identify a quantum state of each quark, called conventionally red, blue or green. As for the electric charge, quarks have positive values of the color charge, while antiquarks have opposite, negative value. The process of the transition of the quark color into a different color is done by an emission of gluons. Such interactions between quarks are called strong interactions. It was proven experimentally in 1980 at the high energy e^+e^- scattering experiments at DESY that the strong interactions between quarks are carried out through the vector gauge bosons of spin 1, gluons, which are massless, electrically neutral particles. However, they carry color charge.

1.2 Fundamentals of QCD

Over the past 60 years, numerous theoretical and experimental studies in particle physics allowed to formulate the theory of strong interactions, called quantum chromodynamics (QCD). Quantum chromodynamics describes the interactions between quarks and gluons within hadrons. It is based on mathematical methods used in quantum electrodynamics (QED) and quantitatively describes the physics of quarks, gluons and their compound systems.

One of the basic concepts of QCD is *color* - the charge of the strong interactions. According to this theory, the elementary particles interact strongly by the exchange color charges carried by intermediary gluons. Gluons not only mediate the color charges between quarks, they also interact with each other due to their color charges. This stays in contrast to photons which do not carry electric charges, thus they do not interact directly between themselves. The fact that gluons interact with each other makes the mathematical analysis of the color forces extremely difficult. The already mentioned absence of free quarks and gluons in an isolated form in nature is a key concept of quantum chromodynamics, called *color confinement*. In recent years, quantum chromodynamics has enabled the formulation of a number of phenomenological models describing the interactions of elementary particles. It was also realized that the results of perturbative QCD could be seen in numerous hadronic processes involving hard scales, much bigger than the fundamental parameter of QCD, $\Lambda_{QCD} \sim 300$ MeV, that is in hard processes.

Quantum chromodynamics is a quantum field theory with a non-abelian local gauge symmetry group. The three quark color fields, called customary: red, green and blue, form a fundamental representation of the $SU(3)$ gauge group. The eight gauge fields corresponding to gluons are necessary for the local gauge symmetry and form the adjoint representation of $SU(3)$. The Lagrangian of QCD, required to be invariant under the

$SU(3)$ gauge group transformations, has the following form [1]

$$\mathscr{L} = \sum_{k=1}^{3} \bar{q}_k \left\{ i\gamma^\mu \partial_\mu - m_k \right\} q_k - \sum_{k,l=1}^{3} \sum_{a=1}^{8} g_s \left\{ \bar{q}_k \gamma^\mu \left(T^a\right)_{kl} q_l \right\} A^a_\mu - \frac{1}{4} \sum_{a=1}^{8} G^a_{\mu\nu} G^{\mu\nu}_a \,, \quad (1.1)$$

in which g_s is the strong interaction coupling constant, q_k are quark color fields with mass m_k and A^a_μ are gluon fields. In addition, γ^μ are the Dirac matrices and T_a are generators of the $SU(3)$ group which fulfill the following commutation relations

$$[T^a, T^b] = i \sum_{c=1}^{8} f^{abc} T^c \,. \quad (1.2)$$

Here f^{abc}, with $a,b,c = 1,2,\ldots,8$, are the structure constants of the group. The gauge strength fields,

$$G^a_{\mu\nu} = \partial_\mu A^a_\nu - \partial_\nu A^a_\mu - g_s f^{abc} A^b_\mu A^c_\nu \,, \quad (1.3)$$

contain the nonlinear part in gauge fields, responsible for self-interaction of gluons.

In 1973, F. Wilczek, D. Gross, and H. D. Politzer theoretically predicted *asymptotic freedom* of the strong interactions by computing the effective coupling constant in QCD,

$$\alpha_s(Q^2) = \frac{g_s^2(Q^2)}{4\pi} = \frac{12\pi}{(33 - 2n_f)\ln(Q^2/\Lambda^2_{QCD})} \,, \quad (1.4)$$

where n_f is the number of active quark flavors f and Q^2 is the four-momentum transfer squared and Λ_{QCD} is the already mentioned internal scale of QCD. The effective coupling constant of QCD is the decreasing function of Q^2. Thus, for $Q^2 \gg \Lambda^2_{QCD}$ the coupling constant is small, $\alpha_s(Q^2) \ll 1$. From Heisenberg uncertainty principle, this means that the strength of the strong interactions is small at sufficiently small distances. Thus, quarks and gluons interact as free particles at small distances, which is a property called *asymptotic freedom*. It allows to apply perturbative methods to compute the QCD predictions, e.g. for the deep inelastic scattering of leptons on hadrons where the values of Q^2 are very large. On the other hand, at large distances *color confinement* forces bind quarks and gluons in hadrons. The precise nature of this phenomenon is yet to be understood analytically. The perturbative methods are of no use in such a case because of large values of the strong coupling constant at large distances.

1.3 Deep inelastic scattering

One of the most important tests of quantum chromodynamics is the issue of breaking of the Bjorken scaling of the nucleon structure functions, F_1 and F_2, in the deep in-

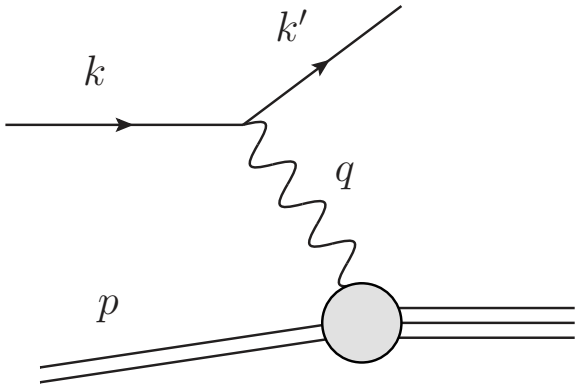

Figure 1.1: Deep inelastic lepton-proton scattering.

elastic scattering (DIS). Deep inelastic scattering is a high-energy process attempted from 1960s until the year 2007 which provides information about the structure of the hadrons. In DIS, charged leptons (electrons, muons) or neutrinos are deflected on a hadron target. In consequence of such a scattering, many new particles are created. The graphical illustration of the deep inelastic electron-proton scattering is presented in Fig. 1.1 in which a target proton is being probed *"deep inside"* by virtual photon emitted by the point-like lepton. The target proton absorbs some kinetic energy of the electron, thus this process can be called *inelastic*.

The kinematics of the DIS is characterize by the square of the four-momentum transfer q, being the photon virtuality,

$$Q^2 \;=\; -q^2 = -(k-k')^2\,, \tag{1.5}$$

and by the invariant mass of the produced particles,

$$W^2 = (p+q)^2 = M^2 + 2Ms + q^2\,, \tag{1.6}$$

in which k and k' are lepton incoming and outgoing four-momenta, and M and p are mass and a four-momentum of the target proton (in the colliding mode). The standard variables used in the description of DIS process are the Bjorken variable x and inelasticity y [2],

$$x \;=\; \frac{Q^2}{2p\cdot q} = \frac{Q^2}{2M(E'-E)}\,, \tag{1.7}$$

$$y \;=\; \frac{q\cdot p}{k\cdot p} = 1 - \frac{E'}{E}\,, \tag{1.8}$$

where the last equalities show these variables in the proton target rest frame (E and E' are energies of the incoming and outgoing lepton, respectively). These variables obey the

equations

$$xy(s-M^2) = Q^2\,, \tag{1.9}$$

where $s = (k+p)^2$ is the Mandelstam invariant, equal to the total energy squared of the incoming particles in their center-of-mass frame.

The structure of the target proton in DIS is encoded in the *structure functions*, F_1 F_2 and F_3, which parametrize the DIS cross section integrated over momenta of all the produced particles except the scattered lepton. In the case of a charged lepton scattering, $lp \to lX$, the differential cross section has the following form

$$\frac{d^2\sigma}{dxdy} = \frac{8\pi\alpha^2 ME}{Q^4}\left[\left(\frac{1+(1-y)^2}{2}\right)2xF_1 + (1-y)(F_2-2xF_1) - \left(\frac{M}{2E}\right)xyF_2\right], \tag{1.10}$$

while for a neutrino (or antineutrino) scattering, $\nu p \to lX$, the cross section can be rewritten as

$$\frac{d^2\sigma}{dxdy} = \frac{G_F^2 ME}{\pi}\left[\left(1-y-\frac{M}{2E}xy\right)F_2 + y^2xF_1 \pm y\left(1-\tfrac{1}{2}y\right)xF_3\right], \tag{1.11}$$

with the fine-structure constant α and G_F being the Fermi constant equal to [2]

$$\alpha^{-1} = 137.0359895(61)\,, \tag{1.12}$$

$$G_F = 1.16639(2)\times 10^{-5}\ \mathrm{GeV}^{-2}\,. \tag{1.13}$$

The sign $(\pm)$ in the above formula equals $(+)$ for the neutrino scattering and $(-)$ for the antineutrino scattering.

In 1967, James D. Bjorken suggested that for the very large values the four-momentum transfer squared, $Q^2 \to \infty$, the structure functions depend only on one variable - the Bjorken variable x,

$$F_i(x,Q^2) \to F_i(x)\,, \qquad i = 1,2,3\,. \tag{1.14}$$

This behavior, called the *Bjorken scaling*, was found in the first DIS data from SLAC.

1.4 The parton model

Parton model was proposed in 1969 by Richard Feynman as a way to analyze the high-energy hadron collisions. According to this model, an inelastic scattering process can be interpreted as an elastic scattering of a lepton on a free, point-like particle - parton. Currently, partons are identified as quarks and gluons. Parton distributions, determined

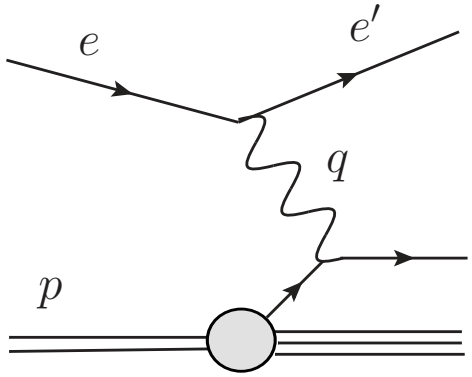

Figure 1.2: The DIS process in the parton model.

experimentally under the studies of the parton model, provide detailed description of the hadron structure and are widely used in processes occurring in high-energy collisions.

The Feynman's parton model provides a physical interpretation of the Bjorken scaling. In this model, the deep inelastic scattering can be considered in the limit of the infinite momentum of the proton in which its mass is neglected. In this limit, the proton four-momentum equals $p^\mu \approx (P,0,0,P)$ and $P \to \infty$. In such a case, cross section (1.10) can be rewritten in the following form [2]

$$\frac{d^2\sigma}{dxdQ^2} = \frac{4\pi\alpha^2}{Q^4}\left[(1+(1-y)^2)F_1 + \frac{(1-y)}{x}(F_2 - 2xF_1)\right]. \tag{1.15}$$

According to Feynman, in the infinite momentum frame, the fast moving proton can be treated as a flux of point-like partons each of which carries a momentum fraction ξ of the proton four-momentum,

$$p_q^\mu = \xi p^\mu . \tag{1.16}$$

The graphical illustration of the DIS process in parton model is shown in Fig. 1.2. Lepton scattering takes place through the virtual photon exchange with the four-momentum q on a single parton, without interfering with other. From the four-momentum conservation

$$(\xi p + q)^2 = 0 \quad \Rightarrow \quad \xi = \frac{-q^2}{2p\cdot q} = \frac{Q^2}{2p\cdot q} \equiv x. \tag{1.17}$$

Thus, the Bjorken variable equals the momentum fraction of the proton carried by the struck quark. The cross section for such a scattering can be given as [2]

$$\frac{d\hat{\sigma}}{dxdQ^2} = \frac{4\pi\alpha^2}{Q^4}[1+(1-y)^2]\,\tfrac{1}{2}\,e_q^2\,\delta(x-\xi), \tag{1.18}$$

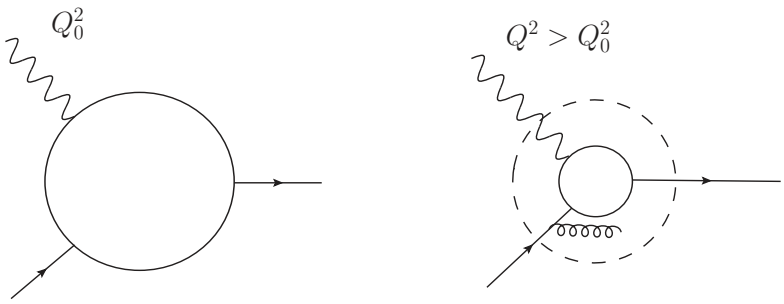

Figure 1.3: With the increase of the scale $Q^2 > Q_0^2$ a virtual photon starts to see a partonic structure of the hadron.

in which the following relation for the structure functions has been used

$$F_2 = x e_q^2 \, \delta(x - \xi) = 2x F_1 \, . \tag{1.19}$$

In the Feynman's (naïve) parton model, the probability density that parton q carries a fraction ξ of the total proton momentum is given by a function $q(\xi)$ to be determined from experiments. Thus

$$q(\xi)\, d\xi, \qquad 0 \leqslant \xi \leqslant 1 \tag{1.20}$$

is the probability that the parton momentum fraction lies in the interval $(\xi, \xi + d\xi)$. The structure functions are given in such a case as incoherent sum over all scattering possibilities,

$$F_2(x) = 2x F_1(x) = \sum_i x e_q^2 \int_0^1 d\xi \, q_i(\xi) \, \delta(x - \xi) = \sum_i e_q^2 \, x q(x) \, , \tag{1.21}$$

where i distinguishes different species of partons. We see that by measuring the structure function F_2, the parton distribution functions are determined. The relation $F_2 = 2xF_1$, valid in the naïve parton model, is called the Callan-Gross relation. It was observed to good accuracy at the first DIS data from SLAC.

1.5 Parton distribution functions

One of the achievements of perturbative QCD is the field theoretical justification of the parton model realized by the factorization theorem of deep inelastic scattering. Within this theory, the lepton-hadron DIS process can be consider as two independent parts: a short distance part which is perturbatively calculable and a long distance part to be determined experimentally. In terms of quantum chromodynamics, partons are identified as both quarks and gluons in contrast to the naïve parton model in which gluons are

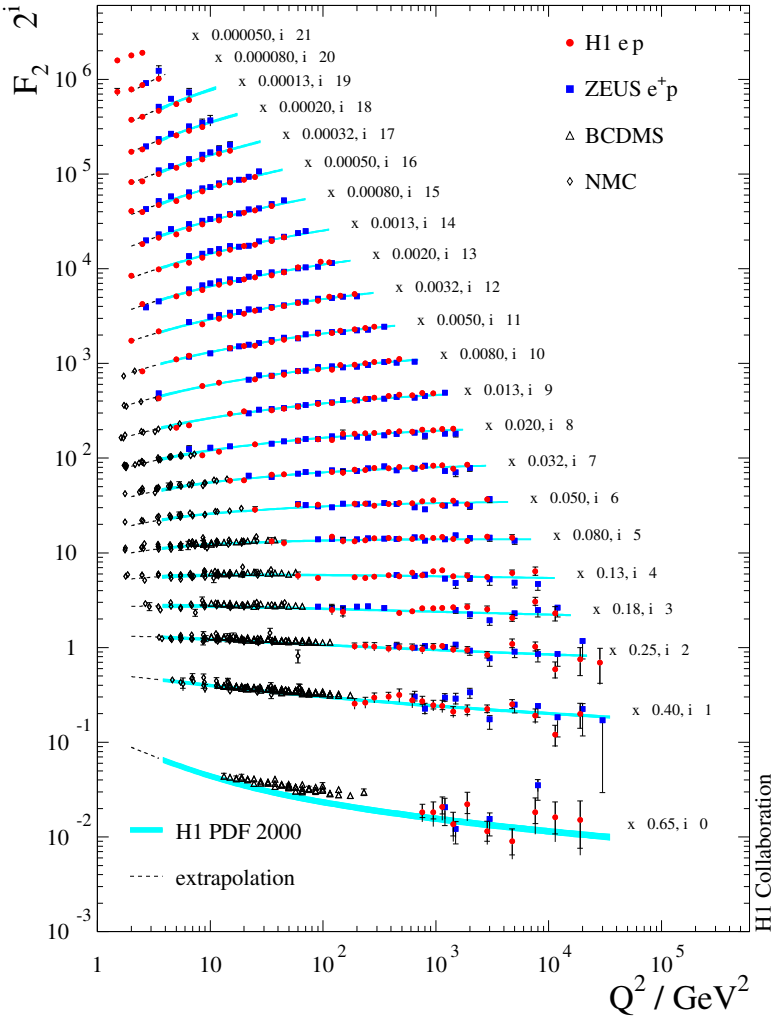

Figure 1.4: The dependence of the structure function F_2 on Q^2 for fixed values of x, obtained by the H1 Collaboration at DESY.

neglected. QCD improves the naïve parton model by taking into account the emission of gluons, which violates the Bjorken scaling by introducing dependence of the structure functions on the logarithm of the hard scale Q^2 [1]. The violation of the Bjorken scaling was observed experimentally in 1973.

Taking into account the gluon emission, shown in Fig. 1.3, the structure function takes the following form

$$\frac{F_2(x,Q^2)}{x} = \sum_{q,\bar{q}} e_q^2 \int_x^1 \frac{dy}{y} q(y) \left[\delta(1-\frac{x}{y}) + \frac{\alpha_s}{2\pi} P_{qq}\left(\frac{x}{y}\right) \log\left(\frac{Q^2}{\mu^2}\right) \right], \tag{1.22}$$

where P_{qq} is a splitting function, computed perturbatively in QCD. For $Q^2 \gg \Lambda^2_{QCD}$, i.e. in the deep inelastic regime, the strong coupling constant $\alpha_s(Q^2)$ decreases which allows

to apply perturbative calculations in QCD. Eq. (1.22) can be written as

$$\frac{F_2(x,Q^2)}{x} = \sum_{q,\bar{q}} e_q^2 \left(q(x) + \Delta q(x,Q^2) \right) , \tag{1.23}$$

where a change in the parton densities is given by

$$\Delta q(x,Q^2) \equiv \frac{\alpha_s}{2\pi} \log(\frac{Q^2}{\mu^2}) \int_x^1 \frac{dy}{y} q(y) P_{qq} \left(\frac{x}{y} \right) . \tag{1.24}$$

The gluon emission from quarks implies that with the increase of the hard scale Q^2 a virtual photon starts see a partonic structure of the hadron, composed of point-like quarks and gluons. Defining the quark density distribution in the leading logarithmic limit,

$$q(x,Q^2) = q(x) + \Delta q(x,Q^2) , \tag{1.25}$$

the following integro-differential equation can be obtained

$$\frac{d}{d\log Q^2} q(x,Q^2) = \frac{\alpha_s}{2\pi} \int_x^1 \frac{dy}{y} q(y,Q^2) P_{qq} \left(\frac{x}{y} \right) . \tag{1.26}$$

The above equation is known as the DGLAP (Dokshitzer-Gribov-Lipatov-Altarelli-Parisi) evolution equation [3, 4, 5] (for nonsinglet quark distributions). It implies that quark carrying momentum fraction x could have come from a parent quark with a larger momentum, $y > x$, which has radiated a gluon. The probability of this process per unit of $\log Q^2$ is proportional to $\alpha_s P_{qq}(x/y)$. The full description of the PDFs also includes the evolution of the gluon distribution function together with the distributions of sea quarks (quark-antiquark pairs created from vacuum). Although these components of the proton do not provide its quantum numbers, they constitute more than 50% of proton's momentum.

The DGLAP evolution equations are widely used in global determinations of parton distribution functions which also include the distribution of gluons. Thus, QCD predicts the violation of the Bjorken scaling and allows to calculate the dependence of the structure function $F_2(x,Q^2)$ on the hard scale Q^2,

$$F_2(x,Q^2) = \sum_{q,\bar{q}} e_q^2 x q(x,Q^2) , \tag{1.27}$$

where the quark/antiquark distribution functions acquired dependence on the hard scale Q^2 at which the proton is probed by the virtual photon emitted by the incident electron. The experimental results on the structure function $F_2(x,Q^2)$, obtained by the H1 Collaboration, are shown in Fig. 1.4. For $x \approx 0.25$, the structure function is found to scale and does not depend on Q^2 at this particular value of x. However, for other values of x, the structure function increases (for $x < 0.25$) or decreases (for $x > 0.25$) with Q^2. This behavior can be explained by the DGLAP evolution equations once the initial conditions for

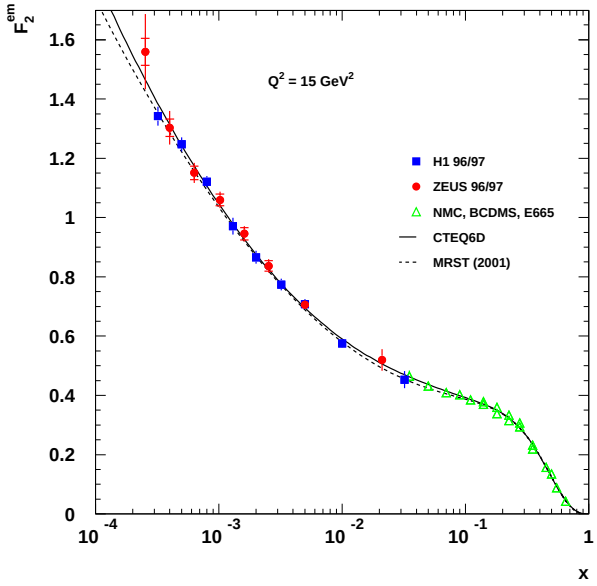

Figure 1.5: The F_2 data from the H1 and ZEUS collaborations. The proton structure function strongly increases with the decreasing Bjorken variable x.

them are determined from fits to the data (see solid lines in Fig. 1.4).

1.6 Parton saturation

The essential observation at the theoretical progress in the physics of hadron interactions at high energy is the fact that the proton structure function, in the region of the small Bjorken variable $x \ll 1$, strongly increases with decreasing x for fixed values of Q^2,

$$F_2(x,Q^2) \sim x^{-\lambda}\,, \tag{1.28}$$

with $\lambda = 0.2 \div 0.3$. The experimental confirmation of this result is shown in Fig. 1.5. This strong rise, however, cannot go on indefinitely and eventually saturates due to the fact that the structure of hadron at small-x limit is dominated by dense field of low momentum gluons. This phenomena of increasing parton densities (sea quarks and gluons) at high energy is known as *parton saturation*.

Measurements conducted by many experiments on deep inelastic scattering allowed to determine the distributions of quarks and gluons. The results of the H1 and ZEUS experiments, presented in Fig. 1.6, clearly show the dominance of the gluon distributions $xg(x,Q^2)$ in the small-x limit while for the larger values of $x \to 1$ - the contribution of valence quarks is significant. Thus, it is the gluon distribution which should saturate first

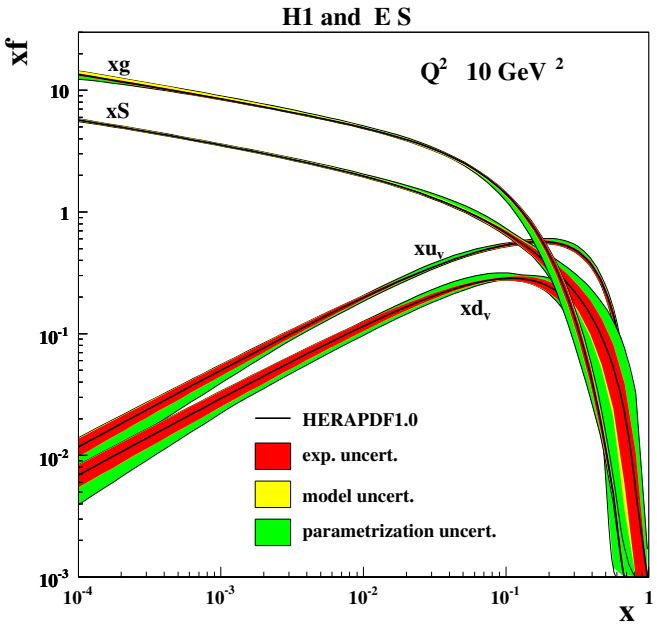

Figure 1.6: The quark and gluon distributions from H1 and ZEUS experiments [6] . At the small-x limit, the contribution of the sea quarks and gluons is significant.

at small x since it grows faster then the quark density. Thus, is the driving force towards saturation.

Saturation effects introduce into the measured cross sections an internal momentum scale, known as *saturation scale* Q_s. It is given in terms of the gluon distribution,

$$Q_s^2 = \alpha_s(Q_s) N_c \frac{1}{\pi R^2} xg(x, Q_s^2) , \tag{1.29}$$

where the variable R is the hadron radius and $\alpha_s N_c$ is the color charge squared of a single gluon. The saturation scale grows with the center-of-mass energy, $\sqrt{s}$, i.e. with the decreasing Bjorken variable x,

$$Q_s^2 \sim s^{\lambda} \sim x^{-\lambda} . \tag{1.30}$$

Therefore, for high energy hadron collisions, the saturation scale becomes large

$$Q_s^2(s) \gg \Lambda_{QCD}^2 , \tag{1.31}$$

which leads to small values of the QCD coupling constant,

$$\alpha_s(Q_s^2) \ll 1 . \tag{1.32}$$

As a result, the computation of saturation effects in QCD can be approached from the

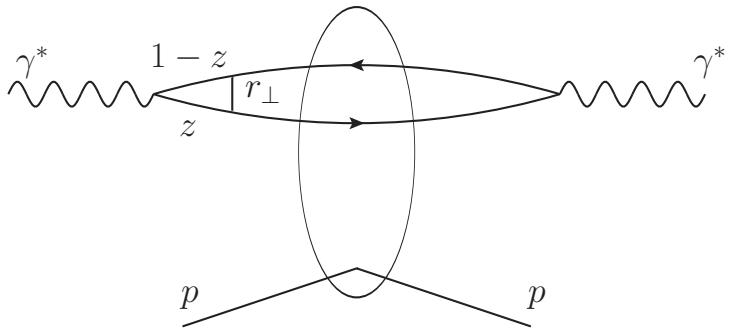

Figure 1.7: Dipole model of the DIS process at small-x limit.

perturbative side. The most physically appealing description of saturation effects in DIS at small x is provided by color dipole models.

1.7 Color dipole models of DIS

The main assumption of the color dipole models concerns the decay of photon into $q\bar{q}$ pair due to gluon exchange, see Fig. 1.7 for a graphical illustration of this process. The proton still carries most of the total energy, while the virtual photon has just enough energy to dissociate long before the scattering into a quark-antiquark dipole. In the kinematic range of small-x, the virtual photon - proton cross section factorizes into a convolution of the photon light-cone wave functions $\Psi_{T,L}$ and the dipole cross section $\sigma_{q\bar{q}}$, describing the interaction of the incoming quark-antiquark pair with strong gluon fields of the target hadron. Both quantities are functions of transverse separation $r_\perp$ of the $q\bar{q}$ pair.

The proton structure function can be given in terms of the virtual photon-proton cross sections [7, 8, 9, 10]

$$F_2(x,Q^2) = F_T(x,Q^2) + F_L(x,Q^2)\,, \tag{1.33}$$

with

$$F_{T,L}(x,Q^2) = \frac{Q^2}{4\pi^2\alpha_{em}}\sigma_{T,L}(x,Q^2)\,, \tag{1.34}$$

where $\sigma_{T,L}$ are the $\gamma^* p$ cross sections which depend on the transverse dipole size $r_\perp$ and the longitudinal momentum fraction z of the photon's longitudinal momentum carried by the quark with flavor f. They are given by the formula

$$\sigma_{T,L}(x,Q^2) = \int d^2 r_\perp \int_0^1 dz |\Psi_{T,L}(r_\perp,z,Q^2)|^2\, \sigma_{q\bar{q}}(x,r_\perp)\,, \tag{1.35}$$

where the wave functions $\Psi_{T,L}$ for the transversely (T) and longitudinally (L) polarized

photons can be interpreted as probabilities for γ^* to fluctuate into the $q\bar{q}$ dipole,

$$|\Psi_T(r_\perp,z,Q^2)|^2 = \frac{6\alpha_{em}}{4\pi^2}\sum_f e_f^2\Big\{[z^2+(1-z)^2]\mu^2K_1^2(\mu r)+m_f^2K_0^2(\mu r)\Big\}, \quad (1.36)$$

$$|\Psi_L(r_\perp,z,Q^2)|^2 = \frac{6\alpha_{em}}{4\pi^2}\sum_f e_f^2\Big\{4Q^2z^2(1-z)^2K_0^2(\mu r)\Big\}, \quad (1.37)$$

in which $\mu^2 = z(1-z)Q^2+m_f^2$ and $K_{0,1}$ are the Mc Donald-Bessel functions.

The dipole cross section $\sigma_{q\bar{q}}$ in eq. (1.35) characterizes the interaction of the quark-antiquark dipole with the proton through gluon exchanges dominating in the small-x region. It encodes all the information about hadronic interactions and can be computed from the dipole-proton scattering amplitude $A(x,r_\perp,\Delta)$ as follows

$$\sigma_{q\bar{q}}(x,r_\perp) = 2\,\mathrm{Im}\,A(x,r_\perp,\Delta=0) = 2\int d^2b_\perp N(x,r_\perp,b_\perp)\,. \quad (1.38)$$

The imaginary part of the forward dipole-proton scattering amplitude, $N(x,r_\perp,b_\perp)$, is interpreted as the probability for the $q\bar{q}$ dipole to scatter off the proton and can be given in terms of the gluon distribution at the scale $Q^2\sim 1/r_\perp^2 \gg \Lambda^2_{QCD}$,

$$N(x,r_\perp,b_\perp) \sim \alpha_s r_\perp^2\, xg(x,1/r_\perp^2)\,. \quad (1.39)$$

For larger values of dipole sizes, the dipole-proton scattering amplitude can be modeled using ideas of parton saturation hoping that more precise QCD based calculations will support the general picture encoded in the models of parton saturation.

Several models with gluon saturation effects have been proposed. In the historically first Golec-Biernat - Wuesthoff (GBW) model [7], the dipole cross section is assumed in the form

$$\sigma_{q\bar{q}}(x,r_\perp) = \sigma_0\,(1-\mathrm{e}^{-\hat{r}^2})\,, \quad (1.40)$$

where $\hat{r} = r_\perp/2R_0(x)$. The quantity R_0, called in [7] saturation radius, plays the role of the saturation scale, $R_0(x) = 1/Q_s(x)$, and is assumed in the form

$$R_0(x) = (x/x_0)^{\lambda/2} \quad (1.41)$$

in units of GeV^{-1}. The parameters of the model, $\sigma_0 = 23$ mb, $\lambda = 0.29$ and $x_0 = 3\cdot 10^{-4}$ have been determined from the fit to HERA data on F_2 for $x<0.01$. At the limit of the small Q^2, saturation in the $\sigma_{q\bar{q}}$ sets in for $r_\perp \sim 2R_0$, $\sigma_{q\bar{q}}\sim\sigma_0$, which allows a good description of the structure function F_2 in the small Q^2 regime. In this regime, the photon-proton cross sections (1.35) for the transverse polarized (T) photons gives $\sigma_T\sim\sigma_0$. For large Q^2, the dominant contribution reflects small dipole configurations with $r_\perp\sim 2/Q \ll$

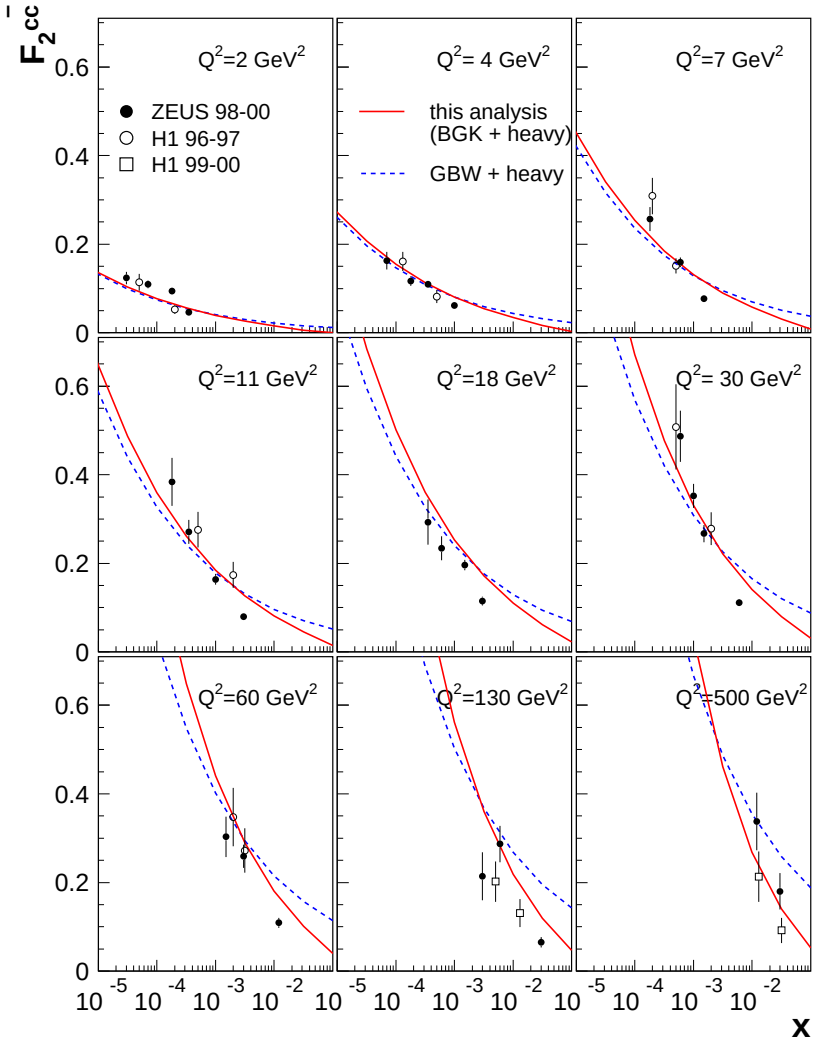

Figure 1.8: Predictions for the structure function $F_2^{c\bar{c}}$ in the BGKS saturation model (BGK model + heavy quarks) (from [11]).

R_0, due to the relation $\sigma_T \sim 1/Q^2$, which leads to the Bjorken scaling for F_2 for the contribution from the small dipoles.

Along with obtaining more precise experimental data it has been observed that the GBW model characterizes the region of the photon virtuality $Q^2 < 20$ GeV^2 only. For larger values of the photon virtuality one should take into account the gluon distributions that satisfy the DGLAP evolution equations. These improvements, altogether with the contribution of heavy quarks c and b, have been included in Bartels - Golec-Biernat - Kowalski (BGK) [12, 13] and Golec-Biernat - Sapeta (GS) [11] models. In these models the dipole cross section was assumed in the form

$$\sigma_{qq}(x, r_\perp) = \sigma_0 \Big\{ 1 - \exp(-\pi^2 r_\perp^2 \alpha_s(\mu^2) x g(x, \mu^2)/3\sigma_0) \Big\}, \tag{1.42}$$

with the scale

$$\mu^2 = \frac{C}{r_\perp^2} + \mu_0^2 , \tag{1.43}$$

where the parameters C, μ_0^2 and σ_0 were determined from a fit to DIS data. The gluon density $g(x,\mu^2)$ is evolved with the leading order DGLAP evolution equation in which quarks are neglected due to the gluon dominance in the small-x limit. At the initial scale $Q_0^2 = 1$ GeV^2, the gluon density is given by

$$xg(x,Q_0^2) = A_g x^{-\lambda_g}(1-x)^{5.6} , \tag{1.44}$$

with parameters A_g and λ_g determined from the fit to the HERA DIS data at $x < 0.01$. The exponent 5.6 is taken from parametrizations of the parton distribution functions for large values of x. The main motivation for the form (1.42) of the dipole cross section is its proper limit (1.39) for small transverse sizes of color dipoles, $r_\perp \ll 1/Q$,

$$\sigma_{qq}(x,r_\perp) \simeq \frac{\pi^2}{3} r_\perp^2 \alpha_s x g(x,\mu^2) . \tag{1.45}$$

On other hand, for large dipoles, $r_\perp \gg 1/Q$, the dipole cross section saturates to a constant value σ_0. In contrast to the GBW dipole cross section, the rise in $1/x$ has become dependent on $r_\perp$ and, in consequence, the DGLAP evolution strengthens the rise in $1/x$ with increasing Q^2, which is necessary to describe the small-x data for large values of Q^2.

To summarize, the GBW model describes well the structure function F_2 at small values of the photon virtuality (< 20 GeV^2), while the BGK model improves these results and the small-$r_\perp$ part of the dipole cross section by incorporating the DGLAP evolution equations. The final improvement of both discussed saturation models has been provided by the GBS model [11] by adding the heavy quark (charm and beauty) contributions in the theoretical formula for F_2. It can be clearly seen in Fig. 1.8 that predictions of the GBS model are consistent with the H1 and ZEUS experimental data.

1.8 The Balitsky-Kovchegov equation

The calculation of the color dipole scattering amplitude can be also attempted directly from QCD by solving the Balitsky-Kovchegov (BK) evolution equation [14, 15, 16]. At the high energies and small values of the Bjorken x, the increase of the gluon distribution leads to a major complication with computing tools of perturbation theory. The QCD applies well to the events with small parton distributions, however in the parton saturation regime, the non-perturbative features occurs and only weak coupling methods can be used. In order to organize the calculations of processes in this region, a new effective

theory has been developed known as the color glass condensate (CGC) [10, 17].

The CGC theory is based on the division of partons in a hadron into fast and slow ones. The high energy kinematics, which is used in CGC, simplify the description of the fast partons by exploiting the fact that their dynamics is slowed down by Lorentz time dilation and thus they can be viewed as static. Partons with momenta larger than the separation scale $\lambda^+ = xP^+$ (given by the fixed hadron light-cone momentum P^+) are fast, while partons with small momenta $k^+ < \lambda^+$ are slow. The fast partons are nearly frozen in light-cone time x^+, and can be treated as static gluon color sources $\rho^a(x^-, x_\perp)$ for slow partons. An average over color sources can be calculated by using 2-point equal time correlation function [18]

$$\Big\langle A_\mu(x^+, x_\perp) A_\nu(x^+, y_\perp) \Big\rangle_x = \int \mathscr{D}\rho W_x[\rho] A_\mu[\rho] A_\nu[\rho] \,, \tag{1.46}$$

in which the low x gluons are described by gauge fields $A^a_\mu[\rho]$ and a weight $W_x[\rho]$ depends on the separation scale λ^+. The basic relation of the CGC reflects a renormalization group equation for the weight $W_x[\rho]$ and is known as the JIMWLK equation [18]

$$\frac{\partial W_x[\rho]}{\partial Y} = \tfrac{1}{2} \int_{x_\perp, y_\perp} \frac{\delta}{\delta \rho^a(x_\perp)} \chi_{ab}(x_\perp, y_\perp) \frac{\delta}{\delta \rho^b(y_\perp)} W_x[\rho] \,, \tag{1.47}$$

where $Y = \ln(1/x)$ is rapidity and χ_{ab} is a positive definite kernel depending on the color sources via the Wilson line,

$$V(x_\perp) = P \exp\Big\{ ig \int dx^- A^+_a(x^-, x_\perp) \Big\} \,, \tag{1.48}$$

in which $A^+[\rho]$ is a solution of the Yang-Mills equation in the covariant gauge,

$$\nabla^2_\perp A^+ = -\rho \,, \tag{1.49}$$

with ρ being the color charge density. In the CGC formalism, the saturated gluons form a collective state described by strong classical color fields, $A^a \sim 1/g$, leading to highly nonlinear phenomena. This is the reason why it is very difficult to find a general solution to the JIMWLK equation and various approximations have to be developed.

In one of them, the BK equation has been derived. This is an evolution equation for the the S-matrix element for the color dipole-proton scattering $S(x, r_\perp, b_\perp)$, defined as as an average of the path ordered exponentials (1.48) over classical gluon fields in the proton that form the CGC,

$$S(Y, x_\perp, y_\perp) \equiv \frac{1}{N_c} \Big\langle \mathrm{Tr}\Big(V^\dagger(x_\perp) V(y_\perp) \Big) \Big\rangle_Y \,, \tag{1.50}$$

where the trace is performed over color indices. The dipole scattering amplitude from the

previous section, $N(x, r_\perp, b_\perp)$, can be written through the S-matrix element as

$$N(x, r_\perp, b_\perp) \equiv 1 - S(Y, x_\perp, y_\perp)\,, \tag{1.51}$$

where $(x_\perp, y_\perp)$ are two-dimensional vectors of the transverse position of the dipole ends. Thus, the dipole transverse size $r_\perp = x_\perp - y_\perp$, the impact parameter $b_\perp = (x_\perp + y_\perp)/2$ and the dipole cross section

$$\sigma_{q\bar{q}}(x, r_\perp) = 2 \int d^2 b_\perp \left(1 - S(Y, x_\perp, y_\perp)\right). \tag{1.52}$$

The S-matrix element obeys the non-linear evolution equation in rapidity Y [14, 15, 16], called the BK equation,

$$\begin{aligned} \frac{\partial}{\partial Y} S(Y, x_\perp, y_\perp) &= -\bar{\alpha}_s \int \frac{d^2 z_\perp}{2\pi} \frac{(x_\perp - y_\perp)^2}{(x_\perp - z_\perp)^2 (y_\perp - z_\perp)^2} \\ &\times \Big(S(Y, x_\perp - y_\perp) - S(Y, x_\perp - z_\perp) S(Y, z_\perp - y_\perp) \Big)\,, \end{aligned} \tag{1.53}$$

where the strong coupling $\bar{\alpha}_s = (N_c \alpha_s)/\pi$ is fixed in the original derivation. The BK has been formulated in the leading $\ln(1/x)$ and large N_c approximations. The kernel of the this equation has the property of conformal symmetry and is invariant with respect to scale change, translations, rotations and inversions. Due to its simplicity, the BK equation is well suited for numerical and analytic studies of the evolution in the parton saturation regime.

Based on the solutions to the BK equation, the following parametrization of the dipole cross section has been proposed by Iancu, Itakura and Munier (IIM model) [10, 17],

$$\sigma_{q\bar{q}}(x, r_\perp) = 2\pi R^2 \times \begin{cases} N_0 \left(\frac{r_\perp Q_s}{2} \right)^{2\left(\gamma_s + \frac{1}{\kappa \lambda Y} \ln \frac{2}{r_\perp Q_s}\right)} & \text{for} \quad r_\perp Q_s \le 2\,, \\ 1 - e^{-a \ln^2 (b r_\perp Q_s)} & \text{for} \quad r_\perp Q_s > 2\,, \end{cases} \tag{1.54}$$

where the saturation scale

$$Q_s = Q_s(x) = (x_0/x)^{\lambda/2}\ \text{GeV}\,. \tag{1.55}$$

The parameters $R = 0.572$ fm, $\lambda = 0.22$, $x_0 = 1.63 \cdot 10^{-5}$, $a = 0.615$, $b = 1.006$, $N_0 = 0.7$, $\kappa = 9.9$ and $\gamma_s = 0.7376$ and were obtained from the fit to the small x DIS data.

1.9 Geometric scaling

The GBW model of deep inelastic scattering at small-x limit predicts a geometric scaling of the total photon-proton cross section. At this regime, the dipole cross sec-

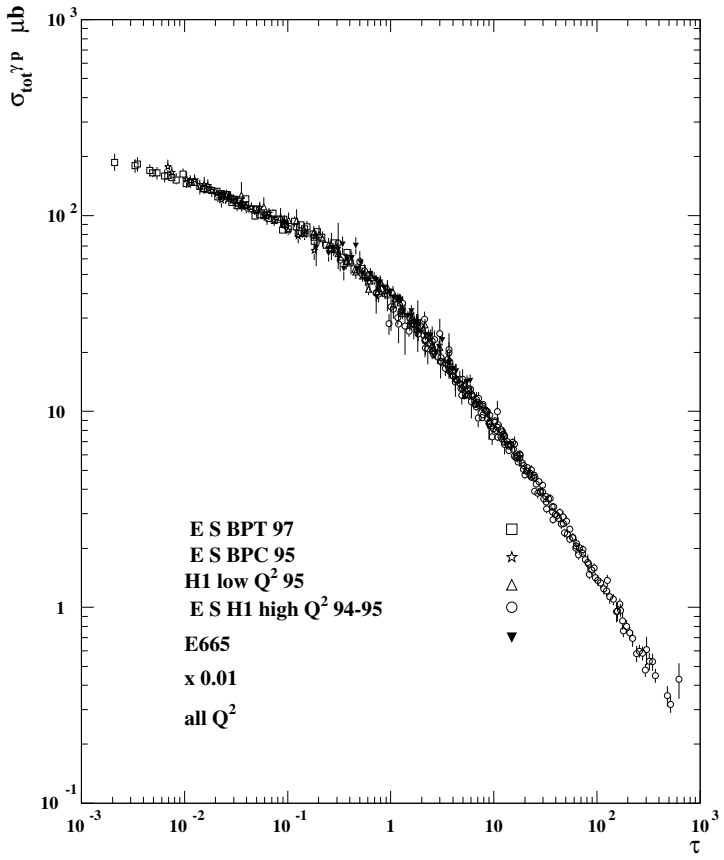

Figure 1.9: Experimental data on the total photon-proton cross section as a function of the scaling variable $\tau = Q^2/Q_s^2(x)$, [19].

tion $\sigma_{q\bar{q}}$ depends only on the dimensionless quantity $r_\perp Q_s(x)$, where the saturation scale $Q_s(x) = 1/R_0(x)$,

$$\sigma_{q\bar{q}}(x, r_\perp) = \sigma_{q\bar{q}}(r_\perp Q_s(x)) \,. \tag{1.56}$$

As a result, $\gamma^* p$ cross section is a function of the ratio Q^2/Q_s^2,

$$\sigma_{T,L}(x, Q^2) = \sigma_{T,L}\left(\frac{Q^2}{Q_s^2(x)}\right). \tag{1.57}$$

This behavior is called *geometric scaling*. The implications of geometric scaling have been confronted with experimental data in [19] and are shown in Fig. 1.9. It is clearly seen that the data exhibit geometric scaling over a very broad region of Q^2.

The BK equation also predicts geometric scaling. It can be solved at large transverse distance, $r_\perp \gg Q_s(Y)$, where the scaling property was found

$$S(Y, r_\perp) = f(r_\perp Q_s(Y)) \,. \tag{1.58}$$

Furthermore, the scaling in the BK evolution equation implies the following dependence of the saturation scale on rapidity

$$Q_s^2(Y) = \Lambda^2 \, \mathrm{e}^{c\bar{\alpha}_s Y} \,, \tag{1.59}$$

where c is a constant and $\Lambda \sim \Lambda_{QCD}$. Parametrization (1.54) takes these facts into account. In the saturation regime, $Q^2 \ll Q_s^2$, there is only one intrinsic scale - the saturation momentum and all physical quantities should be expressed as a dimensionless function of Q^2/Q_s^2 times some power of Q_s^2 giving the right dimension. Moreover, $1/Q_s$ is the typical transverse size of the saturated gluons. Thus, geometric scaling is a phenomenon resulting from parton saturation.

Chapter 2

Drell-Yan processes

In 1970, S. D. Drell and T.-M. Yan [20], showed that parton model assumptions based on deep inelastic scattering also apply to certain processes in hadron-hadron collisions. An example of such a process is a production of lepton pair l^+l^- with annihilation of quark-antiquark pair $q\bar{q}$, also known as the Drell-Yan process.

The production of the Drell-Yan lepton pair is one of the most important processes of high-energy physics which allows the description of the hadron collisions in terms of the parton model. The analysis of the Drell-Yan process provide data about the structure of hadrons and parton distributions. These functions are essential for calculations of the cross sections for many processes occurring at hadron collisions. This chapter contains an analysis of the Drell-Yan process in two approaches - based on the collinear factorization and on the dipole model formalism. Particularly important is the comparison of the obtained results from the point of view of parton saturation, encoded in the form of the dipole cross section in the dipole approach. We show that the Drell-Yan cross section in the dipole approach is significant smaller than that in the collinear approach.

2.1 Lepton pair production in the collinear approach

The parton model assumes that a cross section for the Drell-Yan process can be presented in terms of parton distribution functions for quarks $q_f(x)$ and antiquarks $\overline{q}_f(x)$ obtained from the deep inelastic scattering. In this notation, the lowest order cross section σ^{DY} of the Drell-Yan process with a large invariant mass squared M^2,

$$M^2 = (p_{l^+} + p_{l^-})^2 \gg 1 \text{ GeV}^2 , \tag{2.1}$$

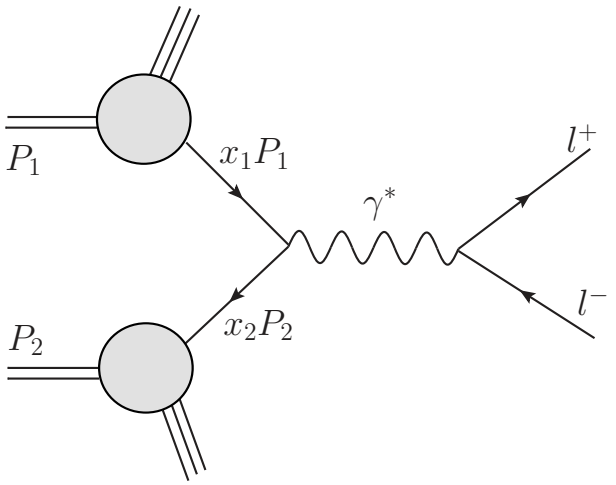

Figure 2.1: Drell-Yan process - quark-antiquark annihilation into lepton pair.

is given as follows

$$\sigma^{DY} = \sum_f \int dx_1 dx_2 q_f(x_1) \overline{q}_f(x_2) \hat{\sigma}_{q\overline{q}\to l^+l^-}\,, \tag{2.2}$$

where x_1 and x_2 are parton longitudinal momentum fractions. $\hat{\sigma}_{q\overline{q}\to l^+l^-}$ is a subprocess cross section which characterizes annihilation of quark-antiquark pair into lepton pair with emission of virtual photon γ^* with virtuality $Q^2 = M^2 > 0$,

$$q\bar{q} \to \gamma^* \to l^+l^-\,. \tag{2.3}$$

In analogy to deep inelastic scattering and Bjorken limit (sec. 1.3), cross section (2.2) is valid for the domain of the asymptotic scaling: $M^2, s \to \infty$ with $\dfrac{M^2}{s}$ fixed. The graphical illustration of the Drell-Yan process is shown in Fig. 2.1.

The conducted measurements of the Drell-Yan cross sections showed the compatibility of the experimental data with theoretical predictions based on eq. (2.2). This confirmed the validity of the parton model, which also holds for gluon corrections imposed by quantum chromodynamics. The collinear singularities occurring in corrections for Drell-Yan cross section can be absorbed into renormalized parton distributions. After taking into consideration the leading corrections, cross section (2.2) can be rewritten in formalism of the scale-dependent parton distributions $q_f(x,M^2)$, $\overline{q}_f(x,M^2)$:

$$\begin{aligned}\sigma^{DY} &= \sum_f \int dx_1 dx_2 q_f(x_1,M^2) \overline{q}_f(x_2,M^2) \hat{\sigma}_{q\overline{q}\to l^+l^-} \\ &= \sum_f \int dx_1 dx_2 q_f(x_1,M^2) \overline{q}_f(x_2,M^2) \times \left[\hat{\sigma}_0 + a\hat{\sigma}_1 + a^2\hat{\sigma}_2 + ...\right]_{q\overline{q}\to l^+l^-}\,,\end{aligned} \tag{2.4}$$

in which the factor $a = \dfrac{\alpha_s(M^2)}{2\pi}$.

As it has been shown in [2], the cross section for $q\bar{q}$ annihilation into lepton pair of mass M can be given in the lowest order as

$$\frac{d\hat{\sigma}(q\bar{q} \to l^+l^-)}{dM^2} = \frac{\sigma_0}{N_c}\, e_f^2\, \delta(\hat{s} - M^2)\,, \tag{2.5}$$

with $\sigma_0 = \dfrac{4\pi\alpha^2}{3M^2}$ in which $\alpha^{-1} = 137.036$ is the fine structure coupling constant. Factor N_c in eq. (2.5) is the number of quark colors, e_f is the quark charge, while $\sqrt{\hat{s}}$ is the $q\bar{q}$ collision energy given by four-momenta p_1 and p_2 of the incoming partons and the center-of-mass energy $\sqrt{s}$ of the hadron-hadron collision:

$$\begin{aligned} \hat{s} &= (p_1 + p_2)^2 = x_1 x_2 s, \\ p_1 = \frac{\sqrt{s}}{2}(x_1, 0, 0, x_1), &\quad p_2 = \frac{\sqrt{s}}{2}(x_2, 0, 0, -x_2). \end{aligned} \tag{2.6}$$

Substituting eq. (2.5) into (2.4), we find the following formula of the Drell-Yan cross section in the parton model approach, [2]:

$$\begin{aligned} \frac{d\sigma^{DY}}{dM^2} &= \int_0^1 dx_1 dx_2 \sum_f \{q_f(x_1)\overline{q}_f(x_2) + (q \leftrightarrow \bar{q})\} \times \frac{d\hat{\sigma}(q\bar{q} \to l^+l^-)}{dM^2} \\ &= \frac{\sigma_0}{N_c} \int_0^1 dx_1 dx_2 \delta(x_1 x_2 s - M^2) \times \left[\sum_f e_f^2 \{q_f(x_1)\overline{q}_f(x_2) + (q \leftrightarrow \bar{q})\} \right]. \end{aligned} \tag{2.7}$$

The parton momentum fractions x_1 and x_2 are expressed with the help of the rapidity y of the lepton pair

$$x_1 = \sqrt{\frac{M^2}{s}} \exp(y), \qquad x_2 = \sqrt{\frac{M^2}{s}} \exp(-y)\,. \tag{2.8}$$

In this notation, relation (2.7) can be rewritten as a double-differential cross section

$$\frac{d^2\sigma^{DY}}{dM^2 dy} = \frac{\sigma_0}{N_c s} \left[\sum_f e_f^2 \{q_f(x_1)\overline{q}_f(x_2) + (q \leftrightarrow \bar{q})\} \right], \tag{2.9}$$

which allows the direct measurement of the quark and antiquark distribution functions of the colliding hadrons.

According to the naïve parton model, distribution functions $q_f(x)$ and $\overline{q}_f(x)$ are independent of the invariant mass M^2. Thus, the Drell-Yan cross section (2.7) (multiplied

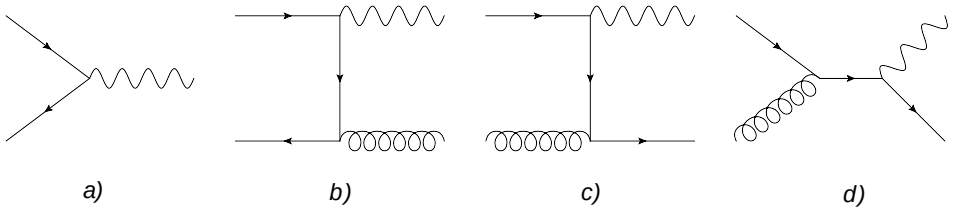

Figure 2.2: Leading order (a) and next-to-leading order (b-d) diagrams of the Drell-Yan process.

by M^4) scales with respect to the variable M^2/s:

$$M^4 \frac{d\sigma^{DY}}{dM^2} = \frac{4\pi\alpha^2}{3N_c s} M^2 \int_0^1 dx_1 dx_2 \delta(x_1 x_2 - \frac{M^2}{s}) \times \left[\sum_f e_f^2 \{ q_f(x_1)\overline{q}_f(x_2) + (q \leftrightarrow \bar{q}) \} \right]$$
$$= \frac{4\pi\alpha^2}{3N_c} \frac{M^2}{s} F\left(\frac{M^2}{s}\right), \tag{2.10}$$

which formula exhibit scaling analogous to the Bjorken scaling of the DIS structure functions.

2.2 Perturbative corrections to the Drell-Yan cross section

As it has already been mentioned, effects of the quantum chromodynamics impose perturbative corrections $\mathcal{O}(\alpha_s)$ to the parton model cross section of the Drell-Yan process. The calculation of $\mathcal{O}(\alpha_s)$ is analogous to the corresponding corrections to the structure function F_2. In particular, the key point here is to consider:

- corrections to the leading order (LO) contribution (shown in Fig. 2.2) from virtual gluons,
- next-to-leading (NLO) corrections obtained from real gluons in scattering process $q + \overline{q} \to \gamma^* + g$ (see Fig. 2.2 b,c),
- and NLO corrections from quark(antiquark)-gluon scattering $q + g \to \gamma^* + q$ (see Fig. 2.2 d).

In the case of perturbation corrections to higher orders, e.g. $\mathcal{O}(\alpha_s^2)$, one should also take into account the dependence on the type of the colliding objects. In general, those corrections should be much smaller than $\mathcal{O}(\alpha_s)$. After taking into account the leading order QCD corrections to the Drell-Yan cross section, eq. (2.10) can be rewritten in the

following form [2]:

$$
\begin{aligned}
M^4\frac{d\sigma^{DY}}{dM^2} &= \frac{4\pi\alpha^2}{3Ns}M^2\int_0^1 dx_1dx_2dz\,\delta(x_1x_2z-\frac{M^2}{s}) \\
&\times \left[\sum_f e_f^2\{q_f(x_1,M^2)\overline{q}_f(x_2,M^2)+(q\leftrightarrow\overline{q})\}\left(\delta(1-z)+\frac{\alpha_s(M^2)}{2\pi}D_q(z)\right)\right. \\
&+ \left.\sum_f e_f^2\{g(x_1,M^2)(q_f(x_2,M^2)+\overline{q}_f(x_2,M^2))+(q,\overline{q}\leftrightarrow g)\}\times\frac{\alpha_s(M^2)}{2\pi}D_g(z)\right],
\end{aligned}
\tag{2.11}
$$

where $g(x,M^2)$ is the gluon distribution and the coefficient functions D_q and D_g are given by the relations [21, 22, 23, 24]

$$
\begin{aligned}
D_q(z) &= C_F\left[4(1+z^2)\left(\frac{\ln(1-z)}{1-z}\right)-2\frac{1+z^2}{1-z}\ln z+\delta(1-z)\left(\frac{2\pi^2}{3}-8\right)\right], \\
D_g(z) &= T_R\left[(z^2+(1-z)^2)\ln\frac{(1-z)^2}{z}+\frac{1}{2}+3z-\frac{7}{2}z^2\right],
\end{aligned}
\tag{2.12}
$$

where $C_F=4/3$ and $T_R=1/2$.

Experiments on the Drell-Yan process are mainly based on the measurement of the double differential cross section $d^2\sigma/dM^2dy$ in a limited range of rapidity, as well as the cross section $d^2\sigma/dM^2dx_F$ which depends on the longitudinal momentum fraction of the lepton pair x_F. The variable x_F is known as the *Feynman's variable* and can be expressed by the parton momentum fractions x_1 and x_2 as follows

$$
x_F=\frac{2}{\sqrt{s}}(p_{l^+}+p_{l^-})\approx x_1-x_2. \tag{2.13}
$$

In the lowest approximation, the energy-momentum conservation $(x_1p_{l^+}+x_2p_{l^-})^2=M^2$ leads to relation

$$
x_1x_2=\frac{M^2}{s}. \tag{2.14}
$$

Using relations (2.13) and (2.14), the LO Drell-Yan cross section can be written in the following way

$$
\frac{d^2\sigma^{LO}}{dM^2dx_F}=\frac{4\pi\alpha^2}{3NM^4}\frac{x_1x_2}{(x_1+x_2)}\sum_f e_f^2\left[q_f(x_1,M^2)\bar{q}_f(x_2,M^2)+\bar{q}_f(x_1,M^2)q_f(x_2,M^2)\right] \tag{2.15}
$$

with the parton momentum fractions given by the kinematic variables x_F, M^2 and s

$$
x_1=\frac{1}{2}\left(\sqrt{x_F^2+4(M^2/s)}+x_F\right),\quad x_2=\frac{1}{2}\left(\sqrt{x_F^2+4(M^2/s)}-x_F\right). \tag{2.16}
$$

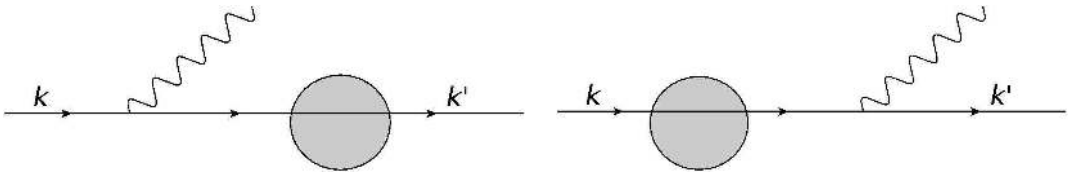

Figure 2.3: The Drell-Yan process in the framework of the dipole model.

In the NLO approximation, additional emission of a parton into the final state has to be taken into account. Thus, the energy momentum conservation includes fraction $z < 1$ of the original parton momentum carried by quark: $(x_1 p_{l^+} + z x_2 p_{l^-})^2 = M^2$, which leads to the relation

$$x_1 x_2 = \frac{M^2}{zs}\,, \tag{2.17}$$

with parton momentum fractions equal

$$x_1 = \frac{1}{2}(\sqrt{x_F^2 + 4(M^2/zs)} + x_F), \qquad x_2 = \frac{1}{2}(\sqrt{x_F^2 + 4(M^2/zs)} - x_F). \tag{2.18}$$

In this approximation, the Drell-Yan cross section is proportional to the strong coupling constant α_s,

$$\begin{aligned} \frac{d^2\sigma^{NLO}}{dM^2 dx_F} &= \frac{4\pi\alpha^2}{3NM^4}\frac{\alpha_s(M^2)}{2\pi}\int_{z_{min}}^1 dz\,\frac{x_1 x_2}{x_1 + x_2}\sum_f e_f^2 \\ &\times \Big\{ q_f(x_1, M^2)\,\bar{q}_f(x_2, M^2)\,D_q(z) \\ &+ g(x_1, M^2)\,[q_f(x_1, M^2) + \bar{q}_f(x_2, M^2)]\,D_g(z) + (x_1 \leftrightarrow x_2)\Big\}\,, \end{aligned} \tag{2.19}$$

where $z_{min} = M^2/s(1 - x_F)$ and coefficient functions D_q and D_g are given by eqs. (2.12). Thus, the final formula for the Drell-Yan cross section in the collinear approximation up to order $\mathcal{O}(\alpha_s)$ is given by the following sum

$$\frac{d^2\sigma^{DY}}{dM^2 dx_F} = \frac{d^2\sigma^{LO}}{dM^2 dx_F} + \frac{d^2\sigma^{NLO}}{dM^2 dx_F}\,. \tag{2.20}$$

2.3 Drell-Yan processes in the dipole picture

The Drell-Yan cross section can also be computed in the rest frame of one of the hadrons. This allows the formulation of the Drell-Yan process in the dipole picture. The original description has been proposed in [25, 26] with details of the calculations presented in [27]. This process has also been reexamined in [28] and later on in [29, 30] within the framework of the color glass condensate which well suited to studies of parton

saturation effects in the DY processes. In the dipole picture, the Drell-Yan process can be seen as a scattering of the quark (or antiquark) from the fast moving proton on the target at rest. In this approach, a fast quark interacts with a strong gluon field of the target and emits a virtual photon which later on decays into the lepton pair. The emission of the virtual photon may be treated as a bremsstrahlung and occurs before or after scattering on the target, see Fig. 2.3. As a result, the Drell-Yan cross section is viewed as a product of two quark amplitudes, testing the gluonic field at two different transverse positions, and can be described by the same dipole cross section as in the DIS.

In the target rest frame, the Drell-Yan process is considered in a kinematic regime of the small-x wherein the mass of the lepton pair M is much smaller than the center-of-mass energy $\sqrt{s}$ and larger than the QCD scale Λ_{QCD}:

$$\Lambda^2_{QCD} \ll M^2 \ll s\,.$$

In the small-x limit, in which the momentum fraction carried by the fast incoming parton x_1 is much larger than the second one,

$$x_1 \sim 1, \qquad\qquad x_2 = \frac{M^2}{s\,x_1} \ll 1\,, \tag{2.21}$$

the Drell-Yan cross section can be given in terms of the incoming quark/antiquark distributions in the proton [28]

$$\begin{aligned}\frac{d^2\sigma^{DY}}{dM^2 dx_F} &= \frac{\alpha}{6\pi M^2}\frac{x_1}{x_1+x_2}\sum_f e_f^2 \int_{x_1}^1 \frac{dz}{z^2}\left[q_f(\frac{x_1}{z},M^2)+\overline{q}_f(\frac{x_1}{z},M^2)\right] \\ &\times\ \sigma_f^{T,L}(qp\to\gamma^* X)\,.\end{aligned} \tag{2.22}$$

Using the proton structure function F_2, relation (2.22) can be rewritten as

$$\frac{d^2\sigma^{DY}}{dM^2\,dx_F} = \frac{\alpha_{em}}{6\pi M^2}\frac{1}{x_1+x_2}\int_{x_1}^1 \frac{dz}{z} F_2\left(\frac{x_1}{z},M^2\right)\sigma_f^{T,L}(qp\to\gamma^* X)\,, \tag{2.23}$$

in which factor $\alpha_{em}/6\pi M^2$ characterizes photon decay into lepton pair and

$$F_2\left(\frac{x_1}{z},M^2\right) = \sum_f Q_f^2\,\frac{x_1}{z}\left[q_f(\frac{x_1}{z},M^2)+\overline{q}_f(\frac{x_1}{z},M^2)\right]. \tag{2.24}$$

The cross section $\sigma(qp\to\gamma^* X)$ in eq. (2.23) describes the emission of a virtual photon γ^* with the momentum fraction z of the fast quark and is given in the dipole picture as [28]

$$\sigma_f^{T,L}(qp\to\gamma^* X) = \int d^2r_\perp\, W_f^{T,L}(z,r_\perp,M^2,m_f)\,\sigma_{q\overline{q}}(x_2,zr_\perp), \tag{2.25}$$

where (T,L) refer to the transverse and longitudinal polarization of the virtual photon and

$r_\perp$ is the photon-quark transverse separation. The wave functions for the transverse and longitudinal virtual photon polarization can be calculated in perturbation theory,

$$W_f^T = \frac{\alpha}{\pi^2}\left\{[1+(1-z)^2]\eta^2 K_1^2(\eta r_\perp) + m_f^2 z^4 K_0^2(\eta r_\perp)\right\}, \tag{2.26}$$
$$W_f^L = \frac{2\alpha}{\pi^2} M^2 (1-z)^2 K_0^2(\eta r_\perp),$$

in which $K_{0,1}$ are the Bessel-Mc Donald functions and the auxiliary variable η, depending on the quark mass m_f, is given by

$$\eta^2 = (1-z)M^2 + z^2 m_f^2. \tag{2.27}$$

The dipole cross section, $\sigma_{q\bar{q}}$ in eq. (2.25), is known from the DIS analyses, described in detail in Chapter 1.

2.4 Numerical results

The cross section for the Drell-Yan process has been measurement by many experiments, with a wide choice of targets and energies, and obtained results were compared with theoretical predictions. As an example of such a comparison are the results of an experiment conducted by the E605 collaboration [31] in which they measured the Drell-Yan cross section $d^2\sigma/dM^2dy$ for $pCu \to \mu^+\mu^-$ process at the energy $\sqrt{s} = 38.8$GeV. It has been shown in Fig. 2.4, that there is a excellent agreement between theoretical assumptions obtained from the next-to-leading order MRS(A) parton distributions and experimental data.

In our research, we analyze the Drell-Yan lepton pair production at forward rapidities at the LHC energy $\sqrt{s} = 14$ TeV. In particular, we compare the Drell-Yan cross sections computed in the two approaches described in this chapter,

- the collinear factorization approach in the NLO, see eq. (2.20),
- the dipole approach, see eq. (2.23),

with the intention to study the possibility to see saturation effects in the DY processes, described in the dipole approach by the dipole cross section. In our calculations, we used the following models of dipole cross section, $\sigma_{q\bar{q}}$,

- the GBW model [7, 8], given by eq. (1.40),
- the GS model [11], given by eq. (1.42),
- the IIM model [10, 17], given by eq. (1.54).

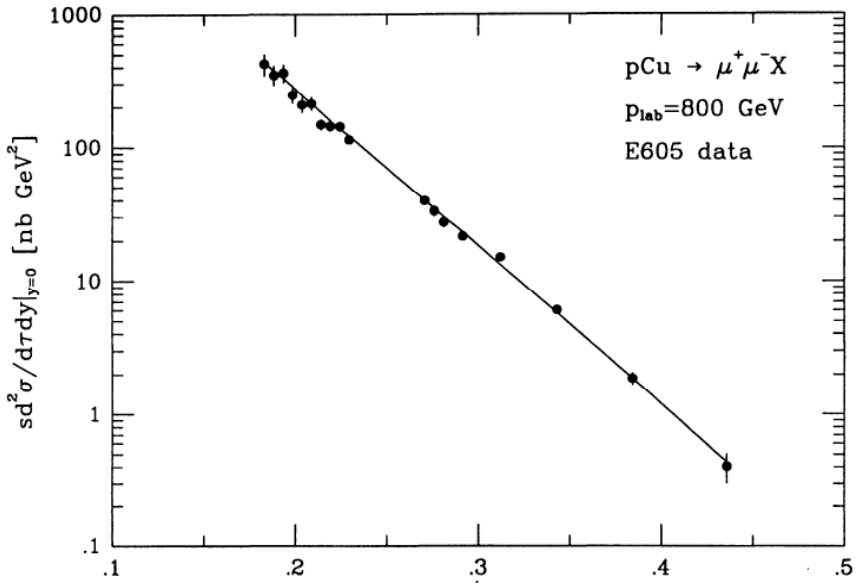

Figure 2.4: The Drell-Yan cross section $d^2\sigma/dM^2dy$ measured by the E605 collaboration [31] at the energy $\sqrt{s} = 38.8$ GeV against the theoretical prediction.

In Fig. 2.5 we present a comparison of the collinear factorization approach with the dipole approach against the existing data from the Fermilab E772 Collaboration [34]. We used the NLO CTEQ6.6M parton distribution functions [35] in the collinear factorization and the GBW model [7] for the dipole cross section. It is clearly seen that for different values of the Feynman variable x_F, the E772 experimental data are above the results from both approaches. A similar result was found for the NLO MSTW08 parton distributions [36]. As far as the dipole approach is concerned, for the energy $\sqrt{s} = 38.8$ GeV and the indicated values of M and x_F, the fraction of the slow parton momentum, $x_2 \approx 0.01 - 0.1$, is slightly beyond the applicability of this approach. Nevertheless, the presented results show that both predictions are in the right ballpark.

In Fig. 2.6 we show the predictions for the Drell-Yan cross section as a function of the center-of-mass energy $\sqrt{s}$ at fixed $x_F = 0.15$ for three values of the lepton pair mass $M = 6, 8, 10$ GeV. At the LHC energy, the GBW dipole model with saturation give results which are significantly below the collinear factorization predictions with the NLO CTEQ6.6M parton distributions. The same results are shown in the linear scale in Fig. 2.7, in which the CTEQ6.6M and MSTW08 parton distributions are used in the collinear factorization approach and the GBW (dipole-GBW) and GS (dipole-GS) dipole cross sections are substituted into the dipole approach formulae. The IIM dipole cross section gives results which are very close to the GBW one. At the LHC energy, the fraction $x_2 \approx 3 \cdot 10^{-6}$ lies in the small x domain which has not been explored experimentally yet for the DY processes and we clearly see that saturation effects encoded in the dipole cross section give results which are systematically below the collinear factorization predictions. These results are awaiting experimental verification at the LHC.

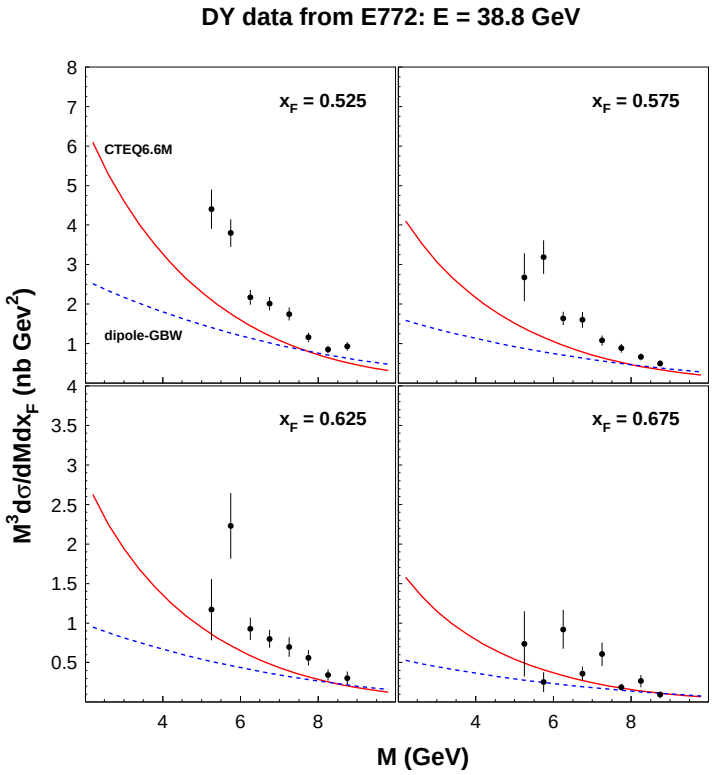

Figure 2.5: The Drell-Yan cross section in the collinear and dipole formulas against the E772 Collaboration data from Tevatron, [32, 33].

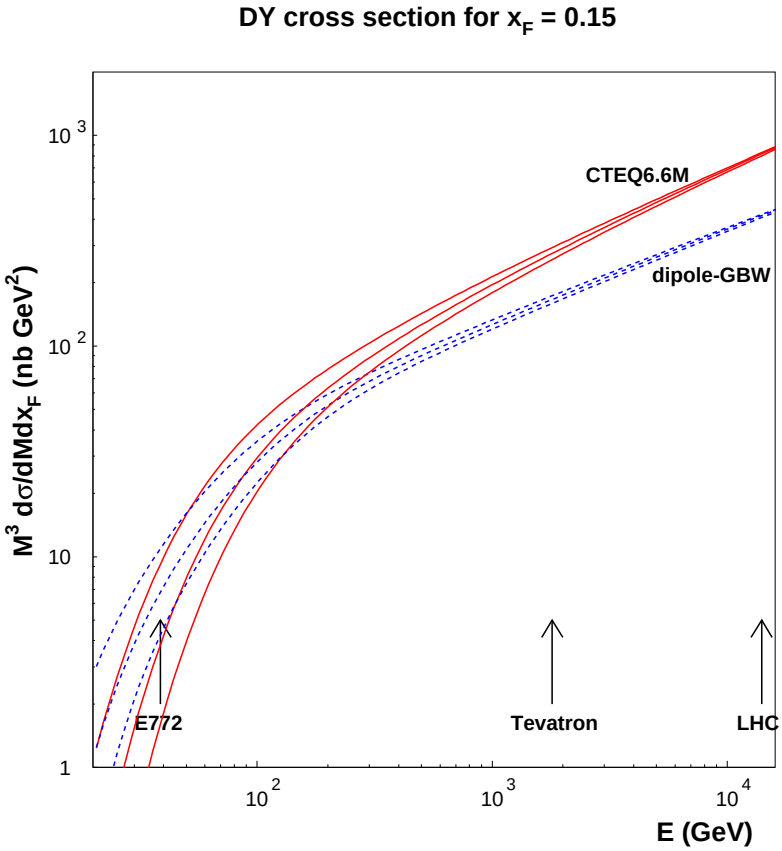

Figure 2.6: The Drell-Yan collinear and dipole cross section predicted for the LHC energies and three values of the lepton pair mass $M = 6, 8, 10$ GeV, [32, 33].

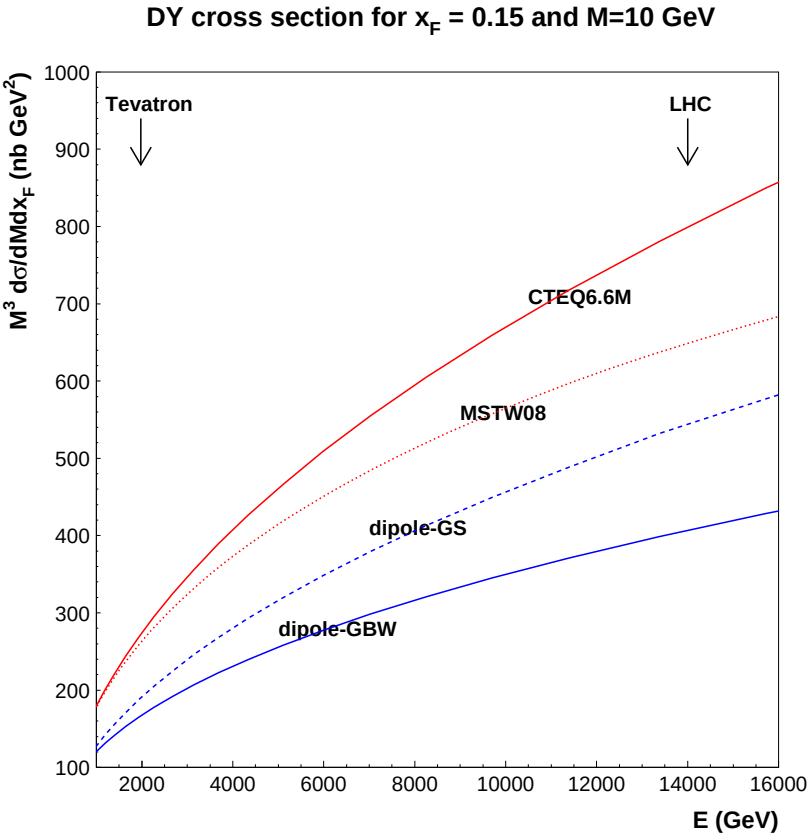

Figure 2.7: The Drell-Yan cross section from the collinear and dipole approaches for fixed $x_F = 0.15$ and lepton pair mass $M = 10$ GeV, [32, 33].

Chapter 3

Double parton scattering

The standard approach of the hard processes usually assumes that only a single parton scattering (SPS) occurs in the hadron collision. However, the experiments at CERN, conducted back in the 80's by the AFS collaboration [37], allowed us to observe a double parton scattering (DPS). This type of scattering is one of the processes of the multi parton interactions (MPI) and occurs when in one hadron-hadron collision two independent hard interactions take place (Fig. 3.1). The multi parton interactions allow us to gain new data about hadron structure and correlations between partons within them. Therefore, they are an important issue for the high energy collisions available on the LHC. The parton scattering processes are described by the corresponding parton distributions:

- *single parton distribution functions* (SPDFs) for the single parton scattering, where the final state of the hadron-hadron collision has been produced from only one hard interaction,
- and *multi parton distributions*, which characterize the multi parton interactions. In this work we will analyze the special case of the MPI: double parton scattering, described by the *double parton distribution functions* (DPDFs).

The double parton scattering has been the subject of numerous theoretical [38, 39, 40, 41, 42, 43, 44, 45, 46, 47, 48, 49, 50] and phenomenological analyses [51, 52, 53, 54,

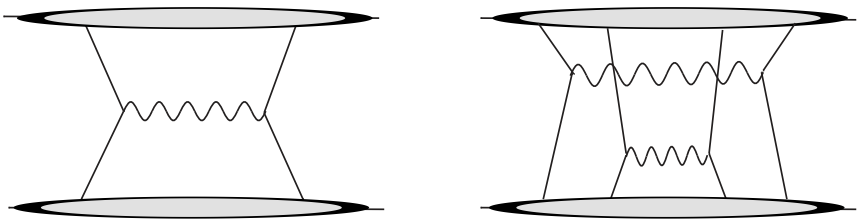

Figure 3.1: In the single parton scattering only one hard subprocess occurs, while in the double scattering - two hard interactions take place.

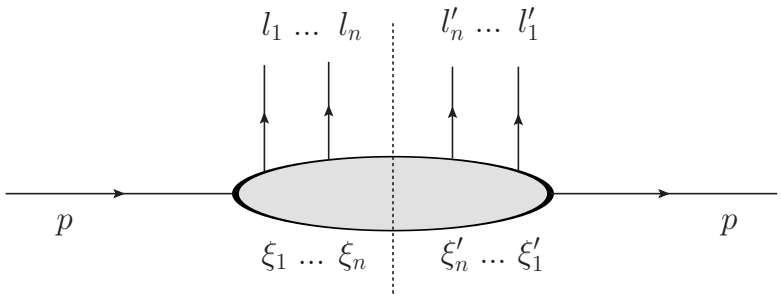

Figure 3.2: Graphical illustration of the n-parton correlation function.

55, 56]. The experimental evidence of the double parton scattering has been presented in [37, 57, 58, 59, 60, 61]. The most important research of the double scattering are the experiments on pp collisions at the energy of $\sqrt{s} = 63$ GeV made by ASF Collaboration, as well as $p\bar{p}$ collisions conducted by CDF [58] and D0 [59] groups at the energies of $\sqrt{s} = 1.8$ TeV and $\sqrt{s} = 1.96$ TeV. Recent research carried out by the ATLAS [60] and CMS [61] Collaborations allow the measurements of double parton scattering at the energy of 7 TeV.

The specific objective of this chapter is the understanding of double parton scattering processes within a rigorous approach based on quantum chromodynamics. More specifically, the key element in this plan are the double parton distributions which undergo QCD evolution equations. These distributions fulfill crucial and highly nontrivial sum rules which have to be built in the solutions of the evolution equations through initial conditions. From a broader perspective, these studies extend our knowledge on partonic structure of a nucleon, providing information on correlations between partons.

3.1 Parton correlation functions

In order to derive the formula for double parton distributions we have to first define the correlation functions which inform us about the structure of the interactions between partons. In the lowest order analysis of the proton-proton collision, the n-parton correlation function takes the following form in the momentum space [46]

$$\begin{aligned} \tilde{\Phi}(l_1,\ldots,l_n,l'_1,\ldots,l'_n) \;=\; & \prod_{i=1}^{n} \int \frac{d^4\xi_i}{(2\pi)^4} \frac{d^4\xi'_i}{(2\pi)^4}\, \mathrm{e}^{i\xi_i l_i - i\xi'_i l'_i} \\ & \times \;\; \langle p|\, \bar{T}[\phi(\xi'_1)...\phi(\xi'_n)]\, T[\phi(\xi_1)...\phi(\xi_n)]\, |p\rangle\,. \end{aligned} \tag{3.1}$$

The letters $T, \bar{T}$ denote time and anti-time ordering of the hermitian parton fields ϕ while ξ_i, ξ'_i and l_i, l'_i are parton positions and four-momenta, see Fig. 3.2. From translation invariance, we can shift the variables in the matrix element and obtain parton correlation

function with the position argument of the first field to be equal zero, $\xi_1' = 0$,

$$\begin{aligned}\tilde{\Phi}(l_1,\ldots,l_n,l_1',\ldots,l_n') \;=\; & \int \frac{d^4\xi_n'}{(2\pi)^4}\, \mathrm{e}^{i\xi_n'(\sum_{i=1}^{n} l_i - \sum_{i=1}^{n} l_i')} \\ & \prod_{i=1}^{n}\int \frac{d^4\xi_i}{(2\pi)^4}\, \mathrm{e}^{i\xi_i l_i} \prod_{i=1}^{n-1}\int \frac{d^4\xi_i'}{(2\pi)^4}\, \mathrm{e}^{-i\xi_i' l_i'} \\ & \times\; \langle p|\, \bar{T}[\phi(0)...\phi(\xi_{n-1}')]\, T[\phi(\xi_1)...\phi(\xi_n)]\, |p\rangle\ .\end{aligned} \tag{3.2}$$

The Dirac delta function, obtained in the first term of eq. (3.2), imposes the momentum conservation

$$\sum_{i=1}^{n} l_i = \sum_{i=1}^{n} l_i'\,, \tag{3.3}$$

which reduce the number of independent momenta. Thus, the final form of the n-parton correlation function is given by relation

$$\begin{aligned}\Phi(l_1,\ldots,l_n,l_1',\ldots,l_{n-1}') \;=\; & \prod_{i=1}^{n}\int \frac{d^4\xi_i}{(2\pi)^4}\, \mathrm{e}^{i\xi_i l_i} \prod_{i=1}^{n-1}\int \frac{d^4\xi_i'}{(2\pi)^4}\, \mathrm{e}^{-i\xi_i' l_i'} \\ & \times\; \langle p|\, \bar{T}[\phi(0)...\phi(\xi_{n-1}')]\, T[\phi(\xi_1)...\phi(\xi_n)]\, |p\rangle\ .\end{aligned} \tag{3.4}$$

From the formula for n partons, the double parton correlation function for $n = 2$ can be found

$$\begin{aligned}\Phi(l_1,l_2,l_1') \;=\; & \int \frac{d^4\xi_1}{(2\pi)^4}\,\frac{d^4\xi_2}{(2\pi)^4}\,\frac{d^4\xi_1'}{(2\pi)^4}\; \mathrm{e}^{i\xi_1 l_1 - i\xi_1' l_1'}\, \mathrm{e}^{i\xi_2 l_2} \\ & \times\; \langle p|\, \bar{T}[\phi(0)\phi(\xi_1')]\, T[\phi(\xi_1)\phi(\xi_2)]\, |p\rangle.\end{aligned} \tag{3.5}$$

Let us reparametrize the parton four-momenta

$$l_1 = k_1 - \frac{q_1}{2}\,, \qquad l_2 = k_2 - \frac{q_2}{2}\,, \qquad l_1' = k_1 + \frac{q_1}{2}\,, \qquad l_2' = k_2 + \frac{q_2}{2}\,, \tag{3.6}$$

where the momentum conservation (3.3) gives

$$q_1 = -q_2 \equiv q\,. \tag{3.7}$$

Now, we have

$$\begin{aligned}\Phi(k_1,k_2,q) \;=\; & \int \frac{d^4\xi_1}{(2\pi)^4}\,\frac{d^4\xi_2}{(2\pi)^4}\,\frac{d^4\xi_1'}{(2\pi)^4}\; \mathrm{e}^{i(\xi_1-\xi_1')k_1 - i(\xi_1+\xi')\frac{1}{2}q}\, \mathrm{e}^{i\xi_2(k_2+\frac{1}{2}q)} \\ & \times\; \langle p|\, \bar{T}[\phi(-\tfrac{1}{2}\xi_2)\phi(\xi_1'-\tfrac{1}{2}\xi_2)]\, T[\phi(\xi_1-\tfrac{1}{2}\xi_2)\phi(\tfrac{1}{2}\xi_2)]\, |p\rangle\,,\end{aligned} \tag{3.8}$$

where, from translation invariance, we shift arguments in the matrix element by $-\xi_2/2$.

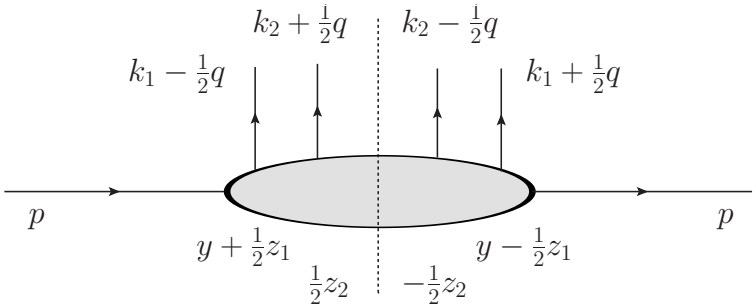

Figure 3.3: Position and momentum arguments in the double parton correlation function.

Introducing new position variables

$$y-\tfrac{1}{2}z_1=\xi_1'-\tfrac{1}{2}\xi_2\,,\qquad y+\tfrac{1}{2}z_1=\xi_1-\tfrac{1}{2}\xi_2\,,\qquad z_2=\xi_2\,, \tag{3.9}$$

we finally obtain

$$\begin{aligned}\Phi(k_1,k_2,q) \;=\; & \int\frac{d^4z_1}{(2\pi)^4}\frac{d^4z_2}{(2\pi)^4}\frac{d^4y}{(2\pi)^4}\,\mathrm{e}^{iz_1k_1}\,\mathrm{e}^{iz_2k_2}\,\mathrm{e}^{-iyq} \\ & \times\;\langle p|\,\bar{T}[\phi(-\tfrac{1}{2}z_2)\phi(y-\tfrac{1}{2}z_1)]\;T[\phi(y+\tfrac{1}{2}z_1)\phi(\tfrac{1}{2}z_2)]\;|p\rangle\;.\end{aligned} \tag{3.10}$$

The graphical illustration of the assignment of position and momentum arguments in the double parton correlation function is shown in Fig. 3.3.

3.2 Double parton distributions

The correlation function (3.10) is a starting point for a definition of double parton distributions of hadrons. Let us introduce a frame in which the colliding hadrons are collinear and move very fast. The plane perpendicular to the collision axis defines transverse directions which allow to introduce the light cone coordinates for parton momenta

$$k_i=(k_i^+,k_i^-,\mathbf{k}_i)\,,\qquad q=(q^+,q^-,\mathbf{q})\,, \tag{3.11}$$

where $k_i^\pm=k_i^0\pm k_i^3$, $q^\pm=q^0\pm q^3$ and $\mathbf{k}_i$ and $\mathbf{q}$ are two dimensional transverse vectors. We define the double parton distribution by integrating out the minus components of parton momenta in correlation function (3.10),

$$F(x_1,x_2,\mathbf{k}_1,\mathbf{k}_2,\mathbf{q})=(2\pi)^3p^+k_1^+k_2^+\int dk_1^-\,dk_2^-\,dq^-\,\Phi(k_1,k_2,q)\Big|_{k_i^+=x_ip^+,q^+=0}. \tag{3.12}$$

Notice that we introduced parton plus-momentum fractions x_i with respect to the large incoming hadron momentum p^+ and set the plus component of q to zero. Thus, the double parton distribution depends on two momentum fractions, x_1 and x_2, and three transverse

momenta, $\mathbf{k}_1$, $\mathbf{k}_2$ and $\mathbf{q}$.

In order to better understand this definition, let us rewrite correlation function (3.10) in the light cone notation. For the right-moving partons, we obtain

$$\begin{aligned}\Phi(k_1,k_2,q) \;=\; & \int \frac{dy^+dy^-d^2\mathbf{y}}{(2\pi)^4}\; \mathrm{e}^{-i(y^+q^-+y^-q^+-\mathbf{y}\cdot\mathbf{q})} \\ & \times \int \frac{dz_1^+dz_1^-d^2\mathbf{z}_1}{(2\pi)^4}\;\frac{dz_2^+dz_2^-d^2\mathbf{z}_2}{(2\pi)^4}\; \mathrm{e}^{i(z_1^+k_1^-+z_1^-k_1^+-\mathbf{z}_1\cdot\mathbf{k}_1)}\; \mathrm{e}^{i(z_2^+k_2^-+z_2^-k_2^+-\mathbf{z}_2\cdot\mathbf{k}_2)} \\ & \times \langle p|\, \bar{T}[\phi(-\tfrac{1}{2}z_2)\phi(y-\tfrac{1}{2}z_1)]\, T[\phi(y+\tfrac{1}{2}z_1)\phi(\tfrac{1}{2}z_2)]\,|p\rangle\,. \end{aligned} \tag{3.13}$$

Substituting this form into eq. (3.12), integrating over $dk_1^-dk_2^-$ and executing all of the delta functions, we find the following expression

$$\begin{aligned}F(x_1,x_2,\mathbf{k}_1,\mathbf{k}_2,\mathbf{q}) \;=\; & 2p^+k_1^+k_2^+\int dy^-d^2\mathbf{y}\,\mathrm{e}^{i\mathbf{y}\cdot\mathbf{q}} \\ & \times \int \frac{dz_1^-}{2\pi}\frac{dz_2^-}{2\pi}\,\mathrm{e}^{ix_1z_1^-p^+}\,\mathrm{e}^{ix_2z_2^-p^+}\int\frac{d^2\mathbf{z}_1}{(2\pi)^2}\frac{d^2\mathbf{z}_2}{(2\pi)^2}\,\mathrm{e}^{-i\mathbf{z}_1\cdot\mathbf{k}_1}\,\mathrm{e}^{-i\mathbf{z}_2\cdot\mathbf{k}_2} \\ & \times \langle p|\,\bar{T}[\phi(-\tfrac{1}{2}z_2)\phi(y-\tfrac{1}{2}z_1)]\,T[\phi(\tfrac{1}{2}z_2)\phi(y+\tfrac{1}{2}z_1)]\,|p\rangle\,, \end{aligned} \tag{3.14}$$

where the spatial plus-components in the matrix element vanish, $z_1^+=z_2^+=y^+=0$. With vanishing plus-components the fields in the matrix element are space-like separated so they commute and may be written in any order. Therefore, eq. (3.14) can be written as

$$\begin{aligned}F(x_1,x_2,\mathbf{k}_1,\mathbf{k}_2,\mathbf{q}) \;=\; & 2p^+\int dy^-d^2\mathbf{y}\,\mathrm{e}^{i\mathbf{y}\cdot\mathbf{q}} \\ & \times \int \frac{dz_1^-}{2\pi}\frac{dz_2^-}{2\pi}\,\mathrm{e}^{ix_1z_1^-p^+}\,\mathrm{e}^{ix_2z_2^-p^+}\int\frac{d^2\mathbf{z}_1}{(2\pi)^2}\frac{d^2\mathbf{z}_2}{(2\pi)^2}\,\mathrm{e}^{-i\mathbf{z}_1\cdot\mathbf{k}_1}\,\mathrm{e}^{-i\mathbf{z}_2\cdot\mathbf{k}_2} \\ & \times \langle p|\,\mathscr{O}(0,z_2)\,\mathscr{O}(y,z_1)\,|p\rangle\,, \end{aligned} \tag{3.15}$$

where $\mathscr{O}$ are bilinear parton operators

$$\mathscr{O}(y,z)=\phi(y-\tfrac{1}{2}z)\,\tfrac{i}{2}(\overrightarrow{\partial}^+-\overleftarrow{\partial}^+)\,\phi(y+\tfrac{1}{2}z)\Big|_{y^+=z^+=0}. \tag{3.16}$$

Integrating over transverse momenta $\mathbf{k}_1$ and $\mathbf{k}_2$, we find the quasi-collinear double parton distribution

$$\begin{aligned}F(x_1,x_2,\mathbf{q}) \;=\; & \int d^2\mathbf{k}_1d^2\mathbf{k}_2\,F(x_1,x_2,\mathbf{k}_1,\mathbf{k}_2,\mathbf{q}) \\ \;=\; & 2p^+\int dy^-d^2\mathbf{y}\,\mathrm{e}^{i\mathbf{y}\cdot\mathbf{q}}\int\frac{dz_1^-}{2\pi}\frac{dz_2^-}{2\pi}\,\mathrm{e}^{ix_1z_1^-p^+}\,\mathrm{e}^{ix_2z_2^-p^+}\,\langle p|\,\mathscr{O}(0,z_2)\mathscr{O}(y,z_1)\,|p\rangle, \end{aligned} \tag{3.17}$$

where $\mathbf{z}_1=\mathbf{z}_2=\mathbf{0}$ (but $\mathbf{y}\neq 0$) for spatial arguments of the bilinear operators. This distribution enters the DPS cross section formula in the collinear approximation, discussed in the next section.

It is interesting to notice that for a single parton ($n = 1$), relation (3.17) reduces to the standard definition of the collinear parton distribution function

$$F(x) = 2p^+ \int \frac{dz^-}{2\pi}\, \mathrm{e}^{ixz^-p^+} \langle p|\, \mathscr{O}(0,z^-)\, |p\rangle\,, \tag{3.18}$$

where now $\mathscr{O}(0,z^-)$ is the light-cone operator.

It has also been proposed in [46] to introduce the double parton distribution that depends on the transverse momenta variables, $\mathbf{k}_{1,2}$, and $\mathbf{x}$ being the Fourier conjugate variable to the transverse momentum $\mathbf{q}$,

$$\begin{aligned} F(x_1,x_2,\mathbf{k}_1,\mathbf{k}_2,\mathbf{x}) \;&=\; \int \frac{d^2\mathbf{q}}{(2\pi)^2}\, \mathrm{e}^{-i\mathbf{x}\cdot\mathbf{q}}\, F(x_1,x_2,\mathbf{k}_1,\mathbf{k}_2,\mathbf{q}) \\ &=\; \int \frac{dz_1^-}{2\pi}\, \frac{dz_2^-}{2\pi}\, \mathrm{e}^{ix_1 z_1^- p^+}\, \mathrm{e}^{ix_2 z_2^- p^+} \int \frac{d^2\mathbf{z}_1}{(2\pi)^2}\, \frac{d^2\mathbf{z}_2}{(2\pi)^2}\, \mathrm{e}^{-i\mathbf{z}_1\cdot\mathbf{k}_1}\, \mathrm{e}^{-i\mathbf{z}_2\cdot\mathbf{k}_2} \\ &\times\; 2p^+ \int dy^- \langle p|\, \mathscr{O}(0,z_2)\, \mathscr{O}(y,z_1)\, |p\rangle\,. \end{aligned} \tag{3.19}$$

This distribution has features of a Wigner function. Namely, integrating over $\mathbf{k}_1$ and $\mathbf{k}_2$, we obtain

$$F(x_1,x_2,\mathbf{x}) = \int d^2\mathbf{k}_1 d^2\mathbf{k}_2\, F(x_1,x_2,\mathbf{k}_1,\mathbf{k}_2,\mathbf{x})\,, \tag{3.20}$$

which is a probability to find two partons in a hadron with plus-momentum fractions $x_{1,2}$, separated by a transverse vector $\mathbf{x}$. Similarly, after integrating over $\mathbf{x}$, the distribution

$$F(x_1,x_2,\mathbf{k}_1,\mathbf{k}_2) = \int d^2\mathbf{x}\, F(x_1,x_2,\mathbf{k}_1,\mathbf{k}_2,\mathbf{x}) \tag{3.21}$$

is a probability to find two partons with the momentum fractions $x_{1,2}$ and transverse momenta $\mathbf{k}_{1,2}$.

For simplicity of presentation, the definitions of the parton distributions were provided in the simplest possible case where partons are scalar particles with no internal quantum numbers. In the case of quantum chromodynamics with quark and gluon color fields everything gets more complicated. Such issues like spin, color or gauge invariance have to be carefully examined. For details, we refer the reader to review [46] where more references can also be found.

3.3 Double parton scattering cross sections

The double parton distributions presented in the previous section can be used to evaluate a cross section for the double parton scattering in hadron-hadron collisions. The relevant graph for the computation with assignment of particle momenta is shown in

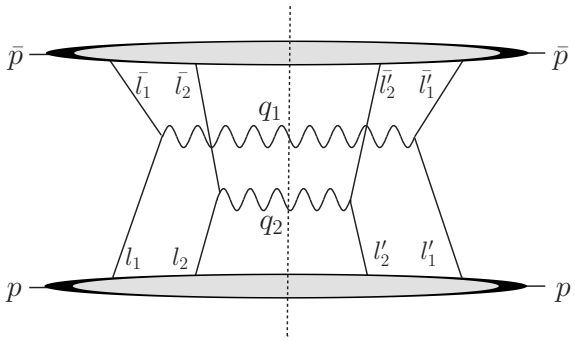

Figure 3.4: The cross section for double hard scattering of two pairs of partons.

Fig. 3.4. The wavy lines denote two final state particle produced in double scattering of two pairs of partons. Their momenta, $q_{1,2}$, are on mass shell which is denoted by the final-state cut line. The lower blob is associated with the right-moving hadron (with momentum p) while the upper blob with the left-moving hadron (with momentum $\bar{p}$) while the scattering partons are denoted by the solid lines. The assignment of parton momenta corresponds to that in Fig. 3.2 for $n = 2$. Notice that the four-momentum conservation is imposed at each vertex. Thus

$$l_i + \bar{l}_i = q_i = l'_i + \bar{l}'_i\,, \qquad i = 1,2\,. \tag{3.22}$$

In addition, the global momentum conservation for all final state particles holds,

$$p + \bar{p} = q_1 + q_2 + \sum_{j=1}^{m} p_{X,j} + \sum_{j=1}^{\bar{m}} p_{\bar{X},j}\,. \tag{3.23}$$

The cross section computation is performed in a kinematic frame, where the colliding hadrons are moving fast to the right (p) and to the left ($\bar{p}$) with transverse momenta $\mathbf{p} = \bar{\mathbf{p}} = \mathbf{0}$. Thus, each momentum is given in light-cone coordinates, see eq. (3.11). In addition, the parton momenta, $l_i, l'_i, \bar{l}_i, \bar{l}'_i$, are reparametrized as in Fig. 3.3,

$$l_1 = k_1 - \tfrac{1}{2}q\,, \quad l_2 = k_2 + \tfrac{1}{2}q\,, \quad l'_2 = k_2 - \tfrac{1}{2}q\,, \quad l'_1 = k_1 + \tfrac{1}{2}q \tag{3.24}$$

and similarly for the upper parton momenta. So we have two sets of momenta, (k_1, k_2, q) for the lower blob partons and $(\bar{k}_1, \bar{k}_2, \bar{q})$ for the upper blob partons. From the momentum conservation (3.22),

$$q + \bar{q} = 0\,. \tag{3.25}$$

The plus-components of k momenta are parametrized with momentum fractions

$$k_i^+ = x_i\, p^+\,, \qquad \bar{k}_i = \bar{x}_i\, (\bar{p})^-\,, \qquad i = 1,2\,, \tag{3.26}$$

where p^+ is a large component of the right-moving hadron momentum while $\bar{p}^-$ is a large component of the left-moving hadron momentum. The derivation of the DPS cross section is rather lengthy, and we refer the reader to review [46] for details. We emphasize here only the most important points.

In order to obtain a formula in a collinear factorization form, which is convolution of two hard scattering partonic cross sections and two double parton distributions, several kinematic assumptions have to be made. Thus, we assume the following.

- The largest scale (or scales) in the process is a hard scale Q which of the order of final state particle masses, $Q^2 \sim q_i^2$, while the hadronic scale (of the order of hadronic mass M), which characterizes non-perturbative interactions, is much smaller than the hard scale, $\Lambda \ll Q$.

- All transverse momenta are of the order of the hadronic scale,

$$|\mathbf{k}_i| \sim |\bar{\mathbf{k}}_i| \sim |\mathbf{q}_i| \sim |\mathbf{q}| \sim \Lambda\,. \tag{3.27}$$

  From this we have for the longitudinal components of the produced particles

$$q_i^+ \sim q_i^- \sim Q\,, \tag{3.28}$$

  and for the fast moving incoming hadrons

$$p^+ \sim (\bar{p})^- \sim Q\,, \qquad\qquad p^- \sim (\bar{p})^+ \sim \Lambda^2/Q\,. \tag{3.29}$$

- The scattering partons have small virtualities of the order of Λ^2. To achieve this for the parton momentum fractions $x_i, \bar{x}_i \sim 1$, we have to assume the following

$$k_i^+ \sim Q\,, \qquad k_i^- \sim q^- \sim \Lambda^2/Q\,, \tag{3.30}$$

$$(\bar{k})_i^- \sim Q\,, \qquad (\bar{k})_i^+ \sim q^+ \sim \Lambda^2/Q\,. \tag{3.31}$$

  We see that $q^\pm$ are small components.

Using these approximations, we can arrive at the following collinear factorization formula with the momentum dependent parton distributions $F(x_i, \mathbf{k}_i, \mathbf{q})$ and $F(\bar{x}_i, \bar{\mathbf{k}}_i, -\mathbf{q})$ [46],

$$\begin{aligned}\frac{d\sigma}{dx_1 dx_2\, d\bar{x}_1 d\bar{x}_2\, d^2\mathbf{q}_1 d^2\mathbf{q}_2} &= \frac{N}{2}\;\hat{\sigma}_1(x_1\bar{x}_1 s)\,\hat{\sigma}_2(x_2\bar{x}_2 s) \\ &\times \int d^2\mathbf{k}_1\, d^2\bar{\mathbf{k}}_1\, \delta^{(2)}(\mathbf{q}_1 - \mathbf{k}_1 - \bar{\mathbf{k}}_1) \int d^2\mathbf{k}_2\, d^2\bar{\mathbf{k}}_2\, \delta^{(2)}(\mathbf{q}_2 - \mathbf{k}_2 - \bar{\mathbf{k}}_2) \\ &\times \int \frac{d^2\mathbf{q}}{(2\pi)^2} F(x_1, x_2, \mathbf{k}_1, \mathbf{k}_2, \mathbf{q})\, F(\bar{x}_1, \bar{x}_2, \bar{\mathbf{k}}_1, \bar{\mathbf{k}}_2, -\mathbf{q})\,,\end{aligned} \tag{3.32}$$

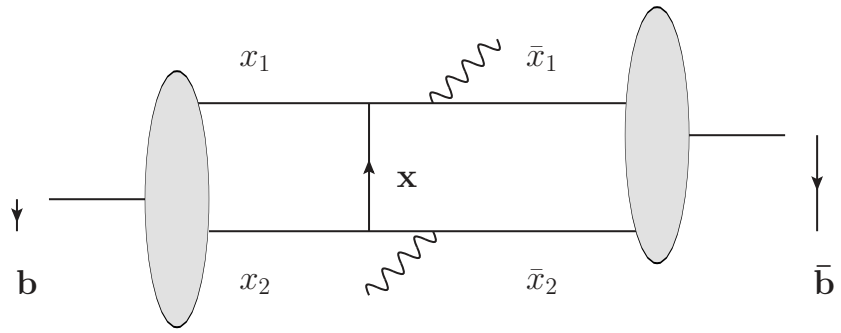

Figure 3.5: The graphical illustration of the cross section (3.36).

where N is a symmetry factor (equal 1 if two hard scattering final state particles are identical or 2 otherwise) and $\hat{\sigma}_{1,2}$ are hard scattering cross sections.

Integrating eq. (3.32) over transverse momenta $\mathbf{q}_{1,2}$, we perform two Dirac delta functions, which allows to integrate the double parton distributions over $\mathbf{k}$ transverse momenta. In this way, we obtain the cross section with the quasi-collinear double parton distributions (3.17),

$$\begin{aligned}\frac{d\sigma}{dx_1 dx_2 d\bar{x}_1 d\bar{x}_2} &= \frac{N}{2}\,\hat{\sigma}_1(x_1\bar{x}_1 s)\,\hat{\sigma}_2(x_2\bar{x}_2 s) \\ &\times \int d^2\mathbf{q}\, F(x_1,x_2,\mathbf{q})\, F(\bar{x}_1,\bar{x}_2,-\mathbf{q})\,. \end{aligned} \tag{3.33}$$

Formula (3.32) can be also be written with the parton distribution functions, $F(x_i,\mathbf{k}_i,\mathbf{x})$ and $F(\bar{x}_i,\bar{\mathbf{k}}_i,\mathbf{x})$, provided the Fourier transform (3.19) exists,

$$\begin{aligned}\frac{d\sigma}{dx_1 dx_2 d\bar{x}_1 d\bar{x}_2 d^2\mathbf{q}_1 d^2\mathbf{q}_2} &= \frac{m}{2}\,\hat{\sigma}_1(x_1\bar{x}_1 s)\,\hat{\sigma}_2(x_2\bar{x}_2 s) \\ &\times \int d^2\mathbf{k}_1\, d^2\bar{\mathbf{k}}_1\, \delta^{(2)}(\mathbf{q}_1-\mathbf{k}_1-\bar{\mathbf{k}}_1) \int d^2\mathbf{k}_2\, d^2\bar{\mathbf{k}}_2\, \delta^{(2)}(\mathbf{q}_2-\mathbf{k}_2-\bar{\mathbf{k}}_2) \\ &\times \int d^2\mathbf{x}\, F(x_1,x_2,\mathbf{k}_1,\mathbf{k}_2,\mathbf{x})\, F(\bar{x}_1,\bar{x}_2,\bar{\mathbf{k}}_1,\bar{\mathbf{k}}_2,\mathbf{x})\,. \end{aligned} \tag{3.34}$$

Integration over transverse momenta $\mathbf{q}_{1,2}$ leads to the following cross section in the collinear approach

$$\begin{aligned}\frac{d\sigma}{dx_1 dx_2 d\bar{x}_1 d\bar{x}_2} &= \frac{N}{2}\,\hat{\sigma}_1(x_1\bar{x}_1 s)\,\hat{\sigma}_2(x_2\bar{x}_2 s) \\ &\times \int d^2\mathbf{x}\, F(x_1,x_2,\mathbf{x})\, F(\bar{x}_1,\bar{x}_2,\mathbf{x})\,, \end{aligned} \tag{3.35}$$

in which the quasi-collinear double parton distributions, $F(x_i,\mathbf{x})$, are defined by eq. (3.20).

The cross section (3.35) has a simple geometric interpretation in impact parameter space if we additionally introduce an impact parameter $\mathbf{b}$ into the distributions $F(x_i,\mathbf{x})$,

see [46] for details of this procedure. In such a case

$$\frac{d\sigma}{dx_1 dx_2\, d\bar{x}_1 d\bar{x}_2} = \frac{N}{2}\,\hat{\sigma}_1(x_1\bar{x}_1 s)\,\hat{\sigma}_2(x_2\bar{x}_2 s) \times \int d^2\mathbf{x} \int d^2\mathbf{b}\, d^2\bar{\mathbf{b}}\, F(x_1,x_2,\mathbf{x},\mathbf{b})\, F(\bar{x}_1,\bar{x}_2,\mathbf{x},\bar{\mathbf{b}})\,, \tag{3.36}$$

and the variable $\mathbf{x}$ can be treated as the average distance between the two scattering partons, while $\mathbf{b}$ and $\bar{\mathbf{b}}$ are the average distances between the parton and the right-moving or left-moving hadron respectively. The graphical visualization of the cross section (3.36) is shown in Fig. 3.5.

The presented formulas correspond to the naïve Feynman parton model. In particular, the double parton distributions do not depend on hard scales. This is the consequences of the assumption that transverse momenta of the final state particles, $|\mathbf{q}_i|$, are of the order of the hadronic scale Λ. If we allow for perturbatively large transverse momenta,

$$\Lambda \ll |\mathbf{q}_i| \ll Q\,, \tag{3.37}$$

a new domain of phase space opens which allows for emissions of quarks or gluons from parton lines. The perturbative resummation of such emissions, in which large logarithms $\log(|\mathbf{q}|/\Lambda)$ are involved, can be done with QCD evolution equations. In this case, parton distributions acquire the dependence on a hard scale (or scales) which is governed by the evolution equations. We refer the reader to paper [46] for the details of their derivation.

In the next chapter we introduce the evolution equations for single and double parton distributions in a way which is most suited from the point of view of phenomenological applications presented in Chapter 5.

Chapter 4

QCD evolution of parton distributions

4.1 QCD evolution of single parton distributions

The detailed analysis of the single parton distribution functions (SPDFs) provides important data on the structure of hadrons and allows to better understand processes occurring in high-energy collisions. The behavior of the SPDFs is determined using appropriate QCD evolution equations. A general formula of the QCD evolution equations can be given as follows

$$\partial_t D_f(x,t) = \sum_{f'} \int_0^1 du\, \mathscr{K}_{ff'}(x,u,t) D_{f'}(u,t)\,, \tag{4.1}$$

where function $D_f(x,t)$ denotes the single parton distributions both for quarks and antiquarks of flavor $f = q_i, \overline{q}_i$ and for gluons $f = G$. The variables x and u, in eq. (4.1), are parton longitudinal momentum fractions with respect to the total nucleon momentum and t is an evolution parameter, $t = \ln(Q^2/Q_0^2)$.

The kernels $\mathscr{K}_{ff'}$ characterize a real and virtual parton emission (see Fig. 4.1) and can be computed perturbatively as a series in powers of the strong coupling constant $\alpha_s = \alpha_s(t)$,

$$\mathscr{K}_{ff'} = \alpha_s\, \mathscr{K}_{ff'}^{(0)} + \alpha_s^2\, \mathscr{K}_{ff'}^{(1)} + \ldots\,. \tag{4.2}$$

A general form of $\mathscr{K}_{ff'}$ is known in QCD as

$$\mathscr{K}_{ff'}(x,u,t) = \mathscr{K}_{ff'}^{R}(x,u,t) - \delta(u-x)\, \delta_{ff'}\, \mathscr{K}_f^V(x,t)\,, \tag{4.3}$$

with the real part $\mathscr{K}_{ff'}^R$ which characterizes a real parton emission with the change of the flavor: $f' \to f$ and the change of the longitudinal momentum fraction: $u \to x$ with $u \geq x$,

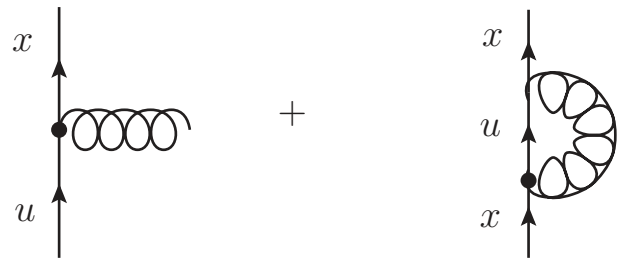

Figure 4.1: The graphical illustration of integral kernels in eq. (4.3), which characterize a real and virtual parton emission.

see the left plot in Fig. 4.1. Thus

$$\mathscr{K}^R_{ff'}(x,u,t) = 0 \qquad \text{for} \qquad u < x\,. \tag{4.4}$$

The function $\mathscr{K}^V_f$ in eq. (4.3) describes a virtual emission, see the right plot in Fig. 4.1, and is computed from the momentum sum rule, valid for all values of t,

$$\sum_f \int_0^1 dx x D_f(x,t) = 1\,. \tag{4.5}$$

The normalization to unity means that partons carry all nucleon momentum. Condition (4.5) is equivalent to the following relation

$$\sum_f \int_0^1 dx x \mathscr{K}_{ff'}(x,u,t) = 0\,. \tag{4.6}$$

After substituting eq. (4.3) into eq. (4.6), we obtain for the virtual part of the kernel (4.3)

$$u\,\mathscr{K}^V_{f'}(u,t) = \sum_f \int_0^1 dx x \mathscr{K}^R_{ff'}(x,u,t)\,, \tag{4.7}$$

or changing the notation: $x \leftrightarrow u$ and $f \leftrightarrow f'$,

$$x\,\mathscr{K}^V_f(x,t) = \sum_{f'} \int_0^1 du u \mathscr{K}^R_{f'f}(u,x,t)\,. \tag{4.8}$$

In this way we arrive at

$$\begin{aligned} \partial_t D_f(x,t) &= \sum_{f'} \int_0^1 du \left\{ \mathscr{K}^R_{ff'}(x,u,t) - \delta(u-x)\,\delta_{ff'}\,\mathscr{K}^V_f(x,t) \right\} D_{f'}(u,t) \qquad (4.9) \\ &= \sum_{f'} \int_0^1 du\, \mathscr{K}^R_{ff'}(x,u,t)\, D_{f'}(u,t) - D_f(x,t) \sum_{f'} \int_0^1 \frac{du}{x}\, u\, \mathscr{K}^R_{f'f}(u,x,t)\,. \end{aligned}$$

Using relation (4.3), we write the most general form of the evolution equations which obey the momentum sum rule (4.5)

$$\partial_t D_f(x,t) = \sum_{f'} \left\{ \int_x^1 du\, \mathcal{K}^R_{ff'}(x,u,t)\, D_{f'}(u,t) - D_f(x,t) \int_0^x \frac{du}{x}\, u\, \mathcal{K}^R_{f'f}(u,x,t) \right\}. \quad (4.10)$$

The QCD evolution equations can be interpreted as master equations for the Markov stochastic processes. Let us assume that $D_f(x,t)$ is a probability distribution to find a parton f with a momentum fraction x at a scale t. An infinitesimal change of the scale, $t \to t+\delta t$, allows the parton (f,x) to be produced from a decay of the partons (f',u). And thus, the following master equation can be written

$$D_f(x,t+\delta t) = \delta t \sum_{f'} \int_0^1 du\, \mathcal{K}^R_{ff'}(x,u,t) D_{f'}(u,t)\,, \quad (4.11)$$

where $\delta t\, \mathcal{K}^R_{ff'}(x,u,t)$ is a conditional probability of the parton transition $(f',u) \to (f,x)$ in the time interval δt. We should add to this equation the term

$$\left(1 - \delta t\, \mathcal{K}^V_f(x,t)\right) D_f(x,t)\,, \quad (4.12)$$

where $\delta t\, \mathcal{K}^V_f(x,t)$ is the transition probability that the parent parton (f,x) will decay to any parton state when the scale is changed by δt. The above term describes the probability that nothing will happen with the parton (f,x) after the change of the scale by δt. We finally obtain the following master equation

$$D_f(x,t+\delta t) = \delta t \sum_{f'} \int_0^1 du\, \mathcal{K}^R_{ff'}(x,u,t) D_{f'}(u,t) + \left(1 - \delta t\, \mathcal{K}^V_f(x,t)\right) D_f(x,t)\,. \quad (4.13)$$

After taking the limit $\delta t \to 0$ the above equation can be written as a differential equation

$$\partial_t D_f(x,t) = \sum_{f'} \int_0^1 du \left\{ \mathcal{K}^R_{ff'}(x,u,t) - \delta(u-x)\, \delta_{ff'} \mathcal{K}^V_f(x,t) \right\} D_{f'}(u,t)\,, \quad (4.14)$$

which is the evolution equation (4.1) with the kernel (4.3).

The general form of the evolution equations (4.10) can be examined in the case of the DGLAP equations (see eq. 1.26). The evolution variable is related to the parton transverse momentum, which is ordered along the chain of partons in subsequent emissions. The real emission kernels have the following form

$$\mathcal{K}^R_{ff'}(x,u,t) = \frac{1}{u} P_{ff'}\left(\frac{x}{u}, t\right) \Theta(x<u)\,, \quad (4.15)$$

where $P_{ff'}$ are called splitting functions and the theta function results from conservation

of the parton longitudinal momentum. After substituting eq. (4.15) in eq. (4.10) we obtain

$$\partial_t D_f(x,t) = \sum_{f'} \int_x^1 \frac{du}{u} P_{ff'}\left(\frac{x}{u},t\right) D_{f'}(u,t) - D_f(x,t) \sum_{f'} \int_0^x \frac{du}{x}\frac{u}{x} P_{f'f}\left(\frac{u}{x},t\right). \quad (4.16)$$

Changing the variables $z = x/u$ in the first integral and $z = u/x$ in the second one, we arrived at the equations

$$\partial_t D_f(x,t) = \sum_{f'} \int_x^1 \frac{dz}{z} P_{ff'}(z,t) D_{f'}\left(\frac{x}{z},t\right) - D_f(x,t) \sum_{f'} \int_0^1 dz z P_{f'f}(z,t). \quad (4.17)$$

The diagonal splitting functions $P_{ff}(z,t)$ have a simple pole at $z = 1$. This singularity is removed by the virtual term and the final form of the evolution equations reads

$$\begin{aligned} \partial_t D_f(x,t) &= \int_x^1 \frac{dz}{z} P_{ff}(z,t) \left\{ D_f\left(\frac{x}{z},t\right) - z^2 D_f(x,t) \right\} - D_f(x,t) \int_0^x dz z P_{ff}(z,t) \\ &+ \sum_{f' \neq f} \left\{ \int_x^1 \frac{dz}{z} P_{ff'}(z,t) D_{f'}\left(\frac{x}{z},t\right) - D_f(x,t) \int_0^1 dz z P_{f'f}(z,t) \right\}. \quad (4.18) \end{aligned}$$

The combination of the parton distributions in the first integral (equal to zero for $z = 1$) cures the splitting function singularity.

The splitting functions are computed perturbatively in QCD and are given as a series in powers of the strong coupling constant α_s,

$$P_{ff'}(z,t) = \frac{\alpha_s(t)}{2\pi} P^{(0)}_{ff'}(z) + \left(\frac{\alpha_s(t)}{2\pi}\right)^2 P^{(1)}_{ff'}(z) + \ldots, \quad (4.19)$$

where $t = \ln(\mu^2/\mu_0^2)$, and μ is a factorization scale which separates long-distance QCD effects from short-distance ones. In addition, the splitting functions are quark flavor independent and the following relations are valid for $f, f' \in \{q_i, \overline{q}_i, G\}_{i=1,\ldots n_f}$

$$\begin{aligned} P_{q_i q_j} &= P_{\overline{q}_i \overline{q}_j} \equiv \delta_{ij} P^V_{qq} + P^S_{qq}, \\ P_{q_i \overline{q}_j} &= P_{\overline{q}_i q_j} \equiv \delta_{ij} P^V_{q\overline{q}} + P^S_{q\overline{q}}, \\ P_{q_i G} &= P_{\overline{q}_i G} \equiv P_{qG}, \\ P_{G q_i} &= P_{G \overline{q}_i} \equiv P_{Gq}. \end{aligned} \quad (4.20)$$

There is also $P_{GG}(z)$ splitting function for the gluon-to-gluon transition.

In the leading logarithmic approximation (LLA) we keep the first term in expansion (4.19),

$$P_{ff'}(z,t) = \frac{\alpha_s(t)}{2\pi} P^{(0)}_{ff'}(z), \quad (4.21)$$

and additionally

$$P^V_{qq} = P^V_{q\overline{q}}\,, \qquad\qquad P^S_{qq} = P^S_{q\overline{q}} = 0\,. \tag{4.22}$$

Thus, the non-zero splitting functions read

$$P^{(0)}_{qq}(z) \;=\; C_F\,\frac{1+z^2}{1-z} = P^V_{qq}(z)\,, \tag{4.23}$$

$$P^{(0)}_{Gq}(z) \;=\; C_F\,\frac{1+(1-z)^2}{z} = P^{(0)}_{qq}(1-z)\,, \tag{4.24}$$

$$P^{(0)}_{qG}(z) \;=\; T_R\,[z^2+(1-z)^2] = P^{(0)}_{qG}(1-z)\,, \tag{4.25}$$

$$P^{(0)}_{GG}(z) \;=\; 2C_A\left[\frac{z}{1-z}+\frac{1-z}{z}+z(1-z)\right] = P^{(0)}_{GG}(1-z)\,, \tag{4.26}$$

where the $SU(N_c)$ gauge group coefficients read

$$C_F = \frac{N_c^2-1}{2N_c}\,, \qquad C_A = N_c\,, \qquad T_R = \frac{1}{2}\,. \tag{4.27}$$

The strong coupling constant $\alpha_s(t)$ can be absorbed into the definition of a new evolution parameter

$$t = \frac{6}{33-2n_f}\ln\frac{\ln(\mu^2/\Lambda^2_{QCD})}{\ln(\mu_0^2/\Lambda^2_{QCD})}\,, \tag{4.28}$$

where n_f in the number of active quark flavors and Λ_{QCD} is the basic dimensionfull parameter of QCD.

Thus eqs. (4.18) take the following form for quark/antiquark and gluon distributions (we omit the superscript (0))

$$\begin{aligned}
\partial_t\, q_i(x,t) \;&=\; \int_x^1 \frac{dz}{z}\left\{P_{qq}(z)\,q_i\left(\frac{x}{z},t\right)+P_{qG}(z)\,G\left(\frac{x}{z},t\right)\right\} \\
&-\; q_i(x,t)\int_0^1 dz z\big[P_{qq}(z)+P_{Gq}(z)\big]\,, \\
\partial_t\, G(x,t) \;&=\; \int_x^1 \frac{dz}{z}\left\{P_{GG}(z)\,G\left(\frac{x}{z},t\right)+P_{Gq}(z)\,\Sigma\left(\frac{x}{z},t\right)\right\} \\
&-\; G(x,t)\int_0^1 dz z\big[P_{GG}(z)+2n_f P_{qG}(z)\big]\,,
\end{aligned} \tag{4.29}$$

where $i = 1,2,\ldots 2n_f$ denotes quark flavor (including antiflavor: $q_{n_f+i} \equiv \overline{q}_i$). We also

introduced a short hand notation for the singlet quark distribution

$$\Sigma(x,t) = \sum_{i=1}^{n_f} \{q_i(x,t) + \overline{q}_i(x,t)\} \,. \tag{4.30}$$

The singularity at $z = 1$ in the splitting functions P_{qq} and P_{GG} in the real emission terms are cured as in eq. (4.18)

$$\begin{aligned}
\partial_t q_i(x,t) &= \int_x^1 \frac{dz}{z} P_{qq}(z) \left\{ q_i\left(\frac{x}{z},t\right) - z^2 q_i(x,t) \right\} - q_i(x,t) \int_0^x dz z P_{qq}(z) \\
&+ \int_x^1 \frac{dz}{z} P_{qG}(z)\, G\left(\frac{x}{z},t\right) - q_i(x,t) \int_0^1 dz z P_{Gq}(z)\,, \\
\partial_t G(x,t) &= \int_x^1 \frac{dz}{z} P_{GG}(z) \left\{ G\left(\frac{x}{z},t\right) - z^2 G(x,t) \right\} - G(x,t) \int_0^x dz z P_{GG}(z) \\
&+ \int_x^1 \frac{dz}{z} P_{Gq}(z)\, \Sigma\left(\frac{x}{z},t\right) - G(x,t) \int_0^1 dz z 2n_f P_{qG}(z)\,.
\end{aligned} \tag{4.31}$$

4.2 Evolution equations for double parton distributions

The main objects in the description of double parton scattering in the collinear approximation are the parton distribution functions (DPDFs), $D_{f_1 f_2}(x_1, x_2, Q_1, Q_2, \mathbf{q})$, introduced in Chapter 3. They provide new information on correlations between partons in a hadron. In the discussion of their evolution with hard scales, Q_1 and Q_2, we set the relative transverse momentum $\mathbf{q} = 0$, postponing the discussion on the $\mathbf{q}$ dependence of the DPDFs until Chapter 5. Thus, our basic object for a discussion is the set of functions

$$D_{f_1 f_2}(x_1, x_2, Q_1, Q_2) \equiv D_{f_1 f_2}(x_1, x_2, Q_1, Q_2, \mathbf{q} = 0)\,, \tag{4.32}$$

where the parton flavors f_1, f_2 include both quarks and gluons.The DPDFs depend on the collinear variables - the parton longitudinal momentum fractions x_1, x_2, which sum cannot exceed the total momentum of the hadron:

$$x_1 + x_2 \leq 1\,. \tag{4.33}$$

For $x_1 + x_2 > 1$, we extend DPDFs into the unphysical domain demanding that

$$D_{f_1 f_2}(x_1, x_2, t_1, t_2) = 0 \qquad \text{for} \qquad x_1 + x_2 > 1\,. \tag{4.34}$$

The DPDFs also depend on two factorization scales, Q_1 and Q_2, fixed by two independent hard processes in which the two partons take part. In the standard, naïve approach, it is

usually assumed that the DPDFs are products of two single PDFs, $D_f(x,Q)$,

$$D_{f_1f_2}(x_1,x_2,Q_1,Q_2) = D_{f_1}(x_1,Q_1)\,D_{f_2}(x_2,Q_2)\,\Theta(1-x_1-x_2). \tag{4.35}$$

It is important to emphasize that this factorized form cannot be generally true, since the correlation imposed by condition (4.33) is usually not built in eq. (4.35). Thus, this approximation is sufficient only for small values of parton momentum fractions. This issue will be discussed in Section 4.5.

The QCD evolution of the double parton distribution functions is a two step process:

- the DPDFs with equal scales are evolved from the initial scale Q_0 up to the smaller scale Q_1, treating both momentum fractions symmetric:

$$D_{f_1f_2}(x_1,x_2,Q_0,Q_0) \quad\to\quad D_{f_1f_2}(x_1,x_2,Q_1,Q_1), \tag{4.36}$$

- the evolution from Q_1 to Q_2 is preformed with respect to the momentum fraction x_2 while keeping x_1 fixed:

$$D_{f_1f_2}(x_1,x_2,Q_1,Q_1) \quad\to\quad D_{f_1f_2}(x_1=\text{fixed},x_2,Q_1,Q_2)\,. \tag{4.37}$$

We start with the evolution equation for the first step (4.36) by introducing evolution parameter $t=\ln(Q^2/Q_0^2)$. In this notation, the QCD evolution equations for the DPDFs in the leading logarithmic approximation (LLA) are given by

$$\begin{aligned}
\partial_t D_{f_1f_2}(x_1,x_2,t) &= \sum_{f'}\int_0^{1-x_2} du\,\mathscr{K}_{f_1f'}(x_1,u,t)\,D_{f'f_2}(u,x_2,t) \\
&+ \sum_{f'}\int_0^{1-x_1} du\,\mathscr{K}_{f_2f'}(x_2,u,t)\,D_{f_1f'}(x_1,u,t) \\
&+ \sum_{f'}\mathscr{K}^R_{f'\to f_1f_2}(x_1,x_1+x_2,t)D_{f'}(x_1+x_2,t)\,.
\end{aligned} \tag{4.38}$$

A graphical illustration of the three terms in eq. (4.38) is shown in Fig. 4.2. The kernels $\mathscr{K}_{ff'}$ in the first two integrals are the single parton distribution evolution kernels (4.3). The real emission part of kernel (4.3) is given in terms of the LLA *splitting functions*

$$\mathscr{K}^R_{ff'}(x,u,t) = \frac{\alpha_s(t)}{2\pi}\frac{1}{u}P^{(0)}_{ff'}\left(\frac{x}{u}\right)\Theta(x<u)\,. \tag{4.39}$$

The third term in eq. (4.38) characterizes the parton splitting

$$(f',x_1+x_2)\to(f_1,x_1)+(f_2,x_2)\,, \tag{4.40}$$

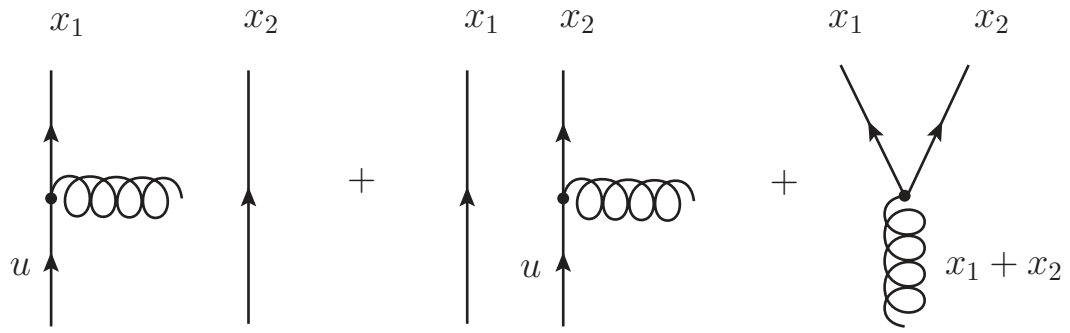

Figure 4.2: An example of the graphical illustration of the three terms in the evolution equation (4.38).

thus, it contains the SPDFs which obeys the DGLAP evolution equation in the LLA

$$\partial_t D_f(x,t) = \sum_{f'} \int_0^1 du\, \mathscr{K}_{ff'}(x,u,t) D_{f'}(u,t)\,. \tag{4.41}$$

In this way, the evolution equations for the single and double parton distributions form a closed set of equations, given by eqs. (4.38) and (4.41). The last term in eq. (4.38), which will be called from now on as *splitting term*, is also symmetric with respect to the interchange $x_1 \leftrightarrow x_2$,

$$\sum_{f'} \mathscr{K}^R_{f'\to f_1 f_2}(x_1, x_1+x_2, t) D_{f'}(x_1+x_2,t) = \sum_{f'} \mathscr{K}^R_{f'\to f_1 f_2}(x_2, x_1+x_2, t) D_{f'}(x_1+x_2,t)\,, \tag{4.42}$$

in which the real emission splitting functions obey the following relations

$$\sum_{f_1} \mathscr{K}^R_{f'\to f_1 f_2} = \mathscr{K}^R_{f_2 f'}\,, \qquad\qquad \sum_{f_2} \mathscr{K}^R_{f'\to f_1 f_2} = \mathscr{K}^R_{f_1 f'}\,. \tag{4.43}$$

Let us finally notice that the upper integration limits in eq. (4.38) reflect condition (4.33) for the parton momentum fractions, saying that the sum of two partons momenta cannot exceed the total momentum of a hadron.

The second evolution step (4.37) is realized by the DGLAP type evolution equations with respect to the second variable x_2, while keeping the momentum fraction x_1 and the evolution parameter $t_1 = t$ fixed:

$$\partial_{t_2} D_{f_1 f_2}(x_1, x_2, t, t_2) = \sum_{f'} \int_0^{1-x_1} du\, \mathscr{K}_{f_2 f'}(x_2, u, t)\, D_{f_1 f'}(x_1, u, t, t_2)\,. \tag{4.44}$$

To derive the explicit form of the evolution equations for the DPDFs, we substitute

the LLA form (4.39) of the DGLAP kernels into the evolution equations (4.38):

$$\partial_t D_{f_1 f_2}(x_1,x_2,t) =$$

$$\sum_{f'}\Bigg\{\int_{x_1}^{1-x_2}\frac{du}{u}P^{(0)}_{f_1 f'}\left(\frac{x_1}{u}\right)D_{f' f_2}(u,x_2,t) - D_{f_1 f_2}(x_1,x_2,t)\int_0^{x_1}\frac{du}{x_1}\frac{u}{x_1}P^{(0)}_{f' f_1}\left(\frac{u}{x_1}\right)$$

$$+\int_{x_2}^{1-x_1}\frac{du}{u}P^{(0)}_{f_2 f'}\left(\frac{x_2}{u}\right)D_{f_1 f'}(x_1,u,t) - D_{f_1 f_2}(x_1,x_2,t)\int_0^{x_2}\frac{du}{x_2}\frac{u}{x_2}P^{(0)}_{f' f_2}\left(\frac{u}{x_2}\right)\Bigg\}$$

$$+\sum_{f'}\frac{1}{x_1+x_2}P_{f'\to f_1 f_2}\left(\frac{x_1}{x_1+x_2}\right)D_{f'}(x_1+x_2,t)\,, \tag{4.45}$$

where the strong coupling constant $\alpha_s(t)$ is absorbed into the definition of the evolution parameter (4.28). Changing the integration variables, $z = x_{1,2}/u$ in the real emission integrals and $z = u/x_{1,2}$ in the virtual emission integrals, we finally find

$$\partial_t D_{f_1 f_2}(x_1,x_2,t) =$$

$$\sum_{f'}\Bigg\{\int_{\frac{x_1}{1-x_2}}^1\frac{dz}{z}P^{(0)}_{f_1 f'}(z)D_{f' f_2}\left(\frac{x_1}{z},x_2,t\right) - D_{f_1 f_2}(x_1,x_2,t)\int_0^1 dz z P^{(0)}_{f' f_1}(z)$$

$$+\int_{\frac{x_2}{1-x_1}}^1\frac{dz}{z}P^{(0)}_{f_2 f'}(z)D_{f_1 f'}\left(x_1,\frac{x_2}{z},t\right) - D_{f_1 f_2}(x_1,x_2,t)\int_0^1 dz z P^{(0)}_{f' f_2}(z)\Bigg\}$$

$$+\sum_{f'}\frac{1}{x_1+x_2}P_{f'\to f_1 f_2}\left(\frac{x_1}{x_1+x_2}\right)D_{f'}(x_1+x_2,t)\,. \tag{4.46}$$

The evolution equations for the SPDFs in the third term above, $D_f(x,t)$, are given by

$$\partial_t D_f(x,t) = \sum_{f'}\int_x^1\frac{dz}{z}P^{(0)}_{f f'}(z)D_{f'}\left(\frac{x}{z},t\right) - D_f(x,t)\sum_{f'}\int_0^1 dz z P^{(0)}_{f' f}(z)\,. \tag{4.47}$$

The simple pole singularity at $z = 1$ in the diagonal splitting functions $P^{(0)}_{ff}$ is regularized by the virtual emission terms in the same way as in the DGLAP evolution equations for the SPDFs, see the previous section for more details.

The presented formulae form a basis for the construction of the numerical program which solves the evolution equations for the DPDFs and SPDFs. We did it using the method with an expansion in Chebyshev polynomials, described in detail in Appendix A.

4.3 Momentum sum rule for double parton distributions

It is well known that the single parton distributions obey momentum and valence quark number sum rules which are conserved under the DGLAP evolution. Corresponding sum rules also exist for the double parton distributions.

The momentum sum rule for double parton distribution functions is given by the following formula

$$\sum_{f_1} \int_0^{1-x_2} dx_1\, x_1 D_{f_1 f_2}(x_1, x_2, t) = (1-x_2) D_{f_2}(x_2, t), \tag{4.48}$$

where $D_{f_2}(x_2,t)$ is a single PDF. The physical interpretation of eq. (4.48) is motivated by the observation that fixing parton (f_2, x_2) leads to the conditional probability to find parton (f_1, x_1) in the colliding hadron,

$$D_{f_1}(x_1|x_2;t) = \frac{D_{f_1 f_2}(x_1, x_2, t)}{D_{f_2}(x_2, t)}\,. \tag{4.49}$$

Thus, after dividing both sides of eq. (4.48) by $D_{f_2}(x_2,t)$, we obtain the relation which says that partons (f_1, x_1) carry only the fraction $(1-x_2)$ of the total nucleon momentum while the missing fraction x_2 is carried by the known second parton. It is important to notice that after imposing the parton exchange symmetry,

$$D_{f_1 f_2}(x_1, x_2) = D_{f_2 f_1}(x_2, x_1)\,, \tag{4.50}$$

the same rule applies to the opposite situation when the parton (f_1, x_1) is fixed,

$$\sum_{f_2} \int_0^{1-x_1} dx_2\, x_2 D_{f_1 f_2}(x_1, x_2, t) = (1-x_1) D_{f_1}(x_1, t)\,. \tag{4.51}$$

Both the conditions, (4.48) and (4.51), are consistent with the QCD evolution equations (4.38) in the LLA form (4.46), once they are imposed on the initial conditions for these equations at some scale t_0.

Let us multiply both sides of eq. (4.48) by $x_2/(1-x_2)$. Then, after summing over all flavors f_2 and integrating over x_2, we find

$$\sum_{f_1, f_2} \int_0^1 dx_2 \int_0^{1-x_2} dx_1\, \frac{x_1 x_2}{1-x_2} D_{f_1 f_2}(x_1, x_2, t) = \sum_{f_2} \int_0^1 dx_2\, x_2 D_{f_2}(x_2, t)\,. \tag{4.52}$$

From the momentum sum rule for the SPDFs (4.5), the last integral equals 1. Thus, the

momentum sum rule for the DPDFs reads

$$\sum_{f_1,f_2}\int_0^1 dx_2\int_0^{1-x_2} dx_1\,\frac{x_1x_2}{1-x_2}D_{f_1f_2}(x_1,x_2,t)=1 \tag{4.53}$$

and, from eq. (4.51), similarly for the variable x_1,

$$\sum_{f_1,f_2}\int_0^1 dx_1\int_0^{1-x_1} dx_1\,\frac{x_1x_2}{1-x_1}D_{f_1f_2}(x_1,x_2,t)=1\,. \tag{4.54}$$

In order to prove the momentum sum rule (4.48) we will show that the function $D_{f_2}(x_2,t)$ on the r.h.s of this relation is indeed the SPDF which obeys the evolution equation (4.14). To this end, let us differentiate both sides of eq. (4.48) over t,

$$(1-x_2)\,\partial_t D_{f_2}(x_2,t)=\sum_{f_1}\int_0^1 dx_1x_1\,\partial_t D_{f_1f_2}(x_1,x_2,t)\,, \tag{4.55}$$

where we set the upper integration limit to 1 by extending the DPDFs into the non-physical domain through condition (4.34). Using eq. (4.38), we find the following relation

$$\begin{aligned}(1-x_2)\,\partial_t D_{f_2}(x_2,t) &= \sum_{f_1}\int_0^1 dx_1x_1\Bigg\{\sum_{f'}\int_0^1 du\,\mathscr{K}_{f_1f'}(x_1,u)D_{f'f_2}(u,x_2,t)\\ &\qquad +\sum_{f'}\int_0^1 du\,\mathscr{K}_{f_2f'}(x_2,u)D_{f_1f'}(x_1,u,t)\Bigg\}\\ &+\sum_{f_1}\int_0^1 dx_1x_1\sum_{f'}\mathscr{K}_{f'\to f_1f_2}(x_1,x_2)D_{f'}(x_1+x_2,t)\,.\end{aligned} \tag{4.56}$$

Changing the order of integrations and summations in the first integral over x_1, we obtain

$$\begin{aligned}(1-x_2)\,\partial_t D_{f_2}(x_2,t) &= \sum_{f'}\int_0^1 du\Bigg\{\sum_{f_1}\int_0^1 dx_1x_1\mathscr{K}_{f_1f'}(x_1,u)\Bigg\}D_{f'f_2}(u,x_2,t)\\ &+\sum_{f'}\int_0^1 du\,\mathscr{K}_{f_2f'}(x_2,u)\Bigg\{\sum_{f_1}\int_0^1 dx_1x_1\,D_{f_1f'}(x_1,u,t)\Bigg\}\\ &+\sum_{f'}\int_0^1 dx_1x_1\sum_{f_1}\mathscr{K}_{f'\to f_1f_2}(x_1,x_2)\,D_{f'}(x_1+x_2,t)\,.\end{aligned} \tag{4.57}$$

The integral in the first line vanishes from eq. (4.6). Using the sum rule (4.48) in the second line and relations (4.43) in the third one, we rewrite the above equation in the

following form

$$(1-x_2)\,\partial_t D_{f_2}(x_2,t) = \sum_{f'}\int_0^1 du\,(1-u)\,\mathscr{K}_{f_2f'}(x_2,u,t)\,D_{f'}(u,t) + \sum_{f'}\int_0^1 dx_1\,x_1\,\mathscr{K}^R_{f_2f'}(x_2,x_1+x_2,t)\,D_{f'}(x_1+x_2,t)\,. \quad (4.58)$$

Substituting kernel (4.3) in the first integral and changing the integration variable, $u \to x_1 = u - x_2$, in the second one, we find after dividing both sides by $(1-x_2)$,

$$\partial_t D_{f_2}(x_2,t) = \sum_{f'}\int_0^1 du\,\frac{1-u}{1-x_2}\left\{\mathscr{K}^R_{f_2f'}(x_2,u,t) - \delta(u-x_2)\,\delta_{f_2f'}\,\mathscr{K}^V_{f_2}(x_2)\right\}D_{f'}(u,t) + \sum_{f'}\int_{x_2}^1 du\,\frac{u-x_2}{1-x_2}\,\mathscr{K}^R_{f_2f'}(x_1,u,t)\,D_{f'}(u,t)\,. \quad (4.59)$$

From the relation

$$\mathscr{K}^R_{ff'}(x,u,t) = 0 \quad \text{for} \quad u < x \quad (4.60)$$

we find, that the lower integration limit in the second integral can be set to zero. Thus, after a simple algebra, we obtain the evolution equation (4.14) for the single parton distributions

$$\partial_t D_{f_2}(x_2,t) = \sum_{f'}\int_0^1 du\left\{\mathscr{K}^R_{f_2f'}(x_2,u,t) - \delta(u-x_2)\,\delta_{f_2f'}\,\mathscr{K}^V_{f_2}(x_2)\right\}D_{f'}(u,t)\,. \quad (4.61)$$

4.4 Valence quark number sum rules

The DPDFs also obey valence quark number sum rules which are more complicated than those for the SPDFs:

$$\int_0^1 dx\left\{D_{q_i}(x,t) - D_{\bar{q}_i}(x,t)\right\} = N_i\,. \quad (4.62)$$

The analogous sum rule depends on the second parton flavor f_2 [41, 62],

$$\int_0^{1-x_2} dx_1\left\{D_{q_if_2}(x_1,x_2,t) - D_{\bar{q}_if_2}(x_1,x_2,t)\right\} = \begin{cases} N_i D_{f_2}(x_2,t) & \text{for} \quad f_2 \neq q_i,\bar{q}_i \\ (N_i-1)\,D_{f_2}(x_2,t) & \text{for} \quad f_2 = q_i \\ (N_i+1)\,D_{f_2}(x_2,t) & \text{for} \quad f_2 = \bar{q}_i\,. \end{cases} \quad (4.63)$$

A similar relation holds true with respect to the first parton, (f_1, x_1),

$$\int_0^{1-x_1} dx_2 \Big\{ D_{f_1 q_i}(x_1,x_2,t) - D_{f_1 \bar{q}_i}(x_1,x_2,t) \Big\} = \begin{cases} N_i D_{f_1}(x_1,t) & \text{for} \quad f_1 \neq q_i, \bar{q}_i \\ (N_i - 1) D_{f_1}(x_1,t) & \text{for} \quad f_1 = q_i \\ (N_i + 1) D_{f_1}(x_1,t) & \text{for} \quad f_1 = \bar{q}_i \,. \end{cases} \tag{4.64}$$

The valence quark number sum rules for DPDFs can be simply derived now. For example, for $f_2 \neq q_j, \bar{q}_j$, we find from the first relation (4.63):

$$\begin{aligned} \int_0^1 dx_2 \int_0^{1-x_2} dx_1 \Big\{ & D_{q_i q_j}(x_1,x_2,t) - D_{\bar{q}_i q_j}(x_1,x_2,t) - D_{q_i \bar{q}_j}(x_1,x_2,t) + D_{\bar{q}_i \bar{q}_j}(x_1,x_2,t) \Big\} \\ & = \; N_i \int_0^1 dx_2 \Big\{ D_{q_j}(x_2,t) - D_{\bar{q}_j}(x_2,t) \Big\} = N_i N_j \,, \end{aligned} \tag{4.65}$$

where we used the sum rule (4.62) in the last equality. A similar relation can be found from the two last relations (4.63) for $N_i \neq 1$:

$$\begin{aligned} \int_0^1 dx_2 \int_0^{1-x_2} dx_1 \Big\{ & \frac{D_{q_i q_i}(x_1,x_2,t) - D_{\bar{q}_i q_i}(x_1,x_2,t)}{N_i - 1} - \frac{D_{q_i \bar{q}_i}(x_1,x_2,t) - D_{\bar{q}_i \bar{q}_i}(x_1,x_2,t)}{N_i + 1} \Big\} \\ & = \; \int_0^1 dx_2 \Big\{ D_{q_i}(x_2,t) - D_{\bar{q}_i}(x_2,t) \Big\} = N_i \,. \end{aligned} \tag{4.66}$$

Let us stress again that the valence quark number sum rules (4.62) and (4.63) are conserved by the DPDFs and SPDFs evolution equations once they are imposed on the initial conditions at some scale t_0.

4.5 Specification of initial conditions

In order to solve the evolution equations for the DPDFs (4.38), both initial distributions: $D_{f_1 f_2}(x_1,x_2,t_0)$ and $D_f(x,t_0)$, have to be specified at some initial value t_0. In view of the importance of the momentum and valence quark number sum rules, the natural question arises how to provide initial conditions which obey these rules. One of the solution is to specify DPDFs and then generate SPDFs in accordance with eqs. (4.48) and (4.63). However, this is not practical since at present the DPDFs are not constrained by experimental data, in contrast to the SPDFs which are very well known from global fit analyses done by many groups. Therefore, we reverse the logic and will try to build the initial DPDFs from the known SPDFs.

In the literature, the following *symmetric* ansatz is often discussed [40, 41]

$$D_{f_1 f_2}(x_1,x_2,t_0) = D_{f_1}(x_1,t_0) D_{f_2}(x_2,t_0) \frac{(1-x_1-x_2)^2}{(1-x_1)^{2+n_1}(1-x_2)^{2+n_2}} \tag{4.67}$$

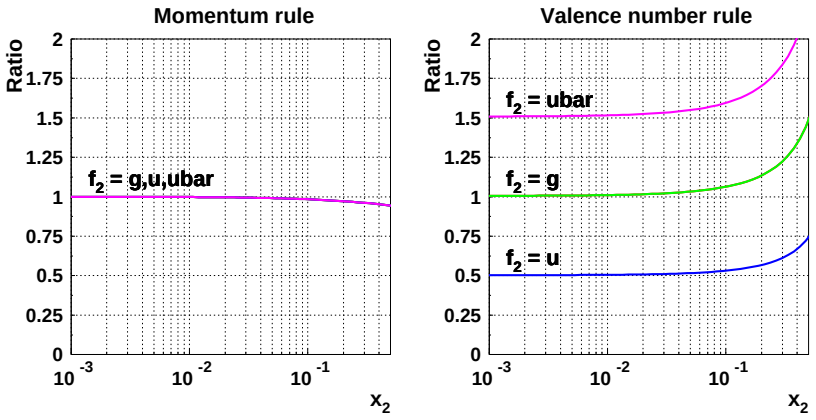

Figure 4.3: The ratio of the r.h.s to the l.h.s of eq. (4.48) (left) and of eq. (4.63) (right) for the input distributions (4.67) as a function x_2 for $f_2 = g, d, u, \bar{u}$. The violation of the sum rules is indicated by the departure of the ratios from 1.

with $n_{1,2} = 0.5$ for valence parton distributions. Although the form (4.67) is parton exchange symmetric and positive definite, it does not fulfill the sum rule relations (4.48) and (4.63). We illustrate this effect in Fig. 4.3 by showing the ratio of the r.h.s to l.h.s of eq. (4.48) (left panel) and of eq. (4.63) (right panel) as the function of x_2 for the flavors $f_2 = g, d, u, \bar{u}$. If the sum rule relations hold true these ratios should be equal to 1 for all values of x_2. This is almost the case for the momentum sum rule but the valence quark number rule is strongly violated for such an ansatz. The valence number ratios for $f_2 = u, \bar{u}$ at small x_2 can be explained by the values $(N_u - 1)/N_u = 0.5$ and $(N_u + 1)/N_u = 1.5$ (with $N_u = 2$), respectively, obtained for the symmetric ansatz.

Now, the question arises whether it is possible to construct initial conditions for QCD evolution of the DPDFs which exactly fulfill the momentum and quark number sum rules and are built out of the known SPDFs. It is easy to check that the following ansatz, proposed in [63, 64], satisfies eq. (4.48) and the first relation in eq. (4.63)

$$D_{f_1 f_2}(x_1, x_2, t_0) = \frac{1}{1 - x_2} D_{f_1}\left(\frac{x_1}{1 - x_2}, t_0\right) D_{f_2}(x_2, t_0)\,, \tag{4.68}$$

where the condition $x_1 + x_2 \leq 1$ is implicit. However, the last two valence quark relations (4.63) are not satisfied. In order to fulfill them, we have to correct ansatz (4.68) for the same quark flavors or antiflavors, $f_2 = q_i$ or $f_2 = \overline{q}_i$,

$$D_{f_1 f_1}(x_1, x_2, t_0) = \frac{1}{1 - x_2}\left(D_{f_1}\left(\frac{x_1}{1 - x_2}, t_0\right) - \frac{1}{2}\right) D_{f_1}(x_2, t_0)\,, \tag{4.69}$$

$$D_{f_1 \bar{f}_1}(x_1, x_2, t_0) = \frac{1}{1 - x_2}\left(D_{f_1}\left(\frac{x_1}{1 - x_2}, t_0\right) + \frac{1}{2}\right) D_{\bar{f}_1}(x_2, t_0)\,. \tag{4.70}$$

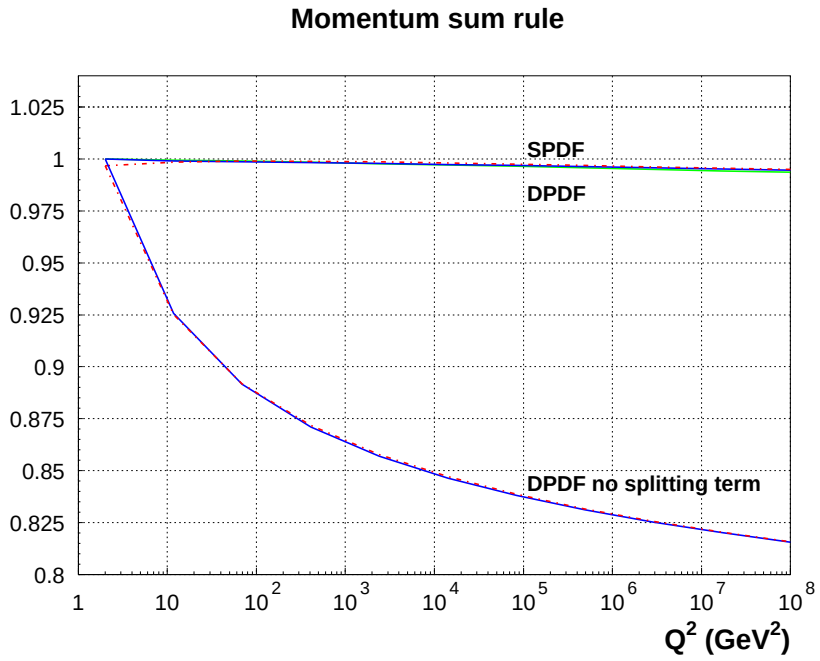

Figure 4.4: The momentum sum rule (4.48) as a function of the evolution scale for input (4.68). The momentum sum rule for SPDFs is also shown. The lowest curve illustrates the importance of the third (splitting) term in evolution equations (4.38).

The additional factors with $\pm 1/2$ account for the factors with ± 1 on the r.h.s of eqs. (4.63) and do not spoil the already fulfilled momentum sum rule (4.48). However, the proposed ansatz is not symmetric with respect to the exchange of partons,

$$D_{f_1 f_2}(x_1, x_2, t_0) \neq D_{f_2 f_1}(x_2, x_1, t_0)\,. \tag{4.71}$$

In addition, the quark distributions $D_{q_i q_i}(x_1, x_2)$ and $D_{\bar{q}_i \bar{q}_i}(x_1, x_2)$ are not positive definite in the whole physical domain: $x_1 + x_2 \leq 1$. This situation is summarized in Table 4.1.

Properties	Symmetric ansatz	Our ansatz
Parton symmetry	yes	no
Positivity	yes	no
Sum rules	no	yes

Table 4.1: Properties of the two discussed in the text initial conditions.

In Fig. 4.4 we show how the momentum sum rule (4.53) is preserved by our numerical program. The 1% deviation from unity results from numerical inaccuracies. We also show the momentum sum rule for the SPDFs. The lowest curve illustrates the role of the splitting terms in the evolution equations (4.38). Without this terms, the momentum sum rule for the DPDFs is strongly violated.

In Fig. 4.5 we show the graphical comparison of the two inputs as functions of x_1

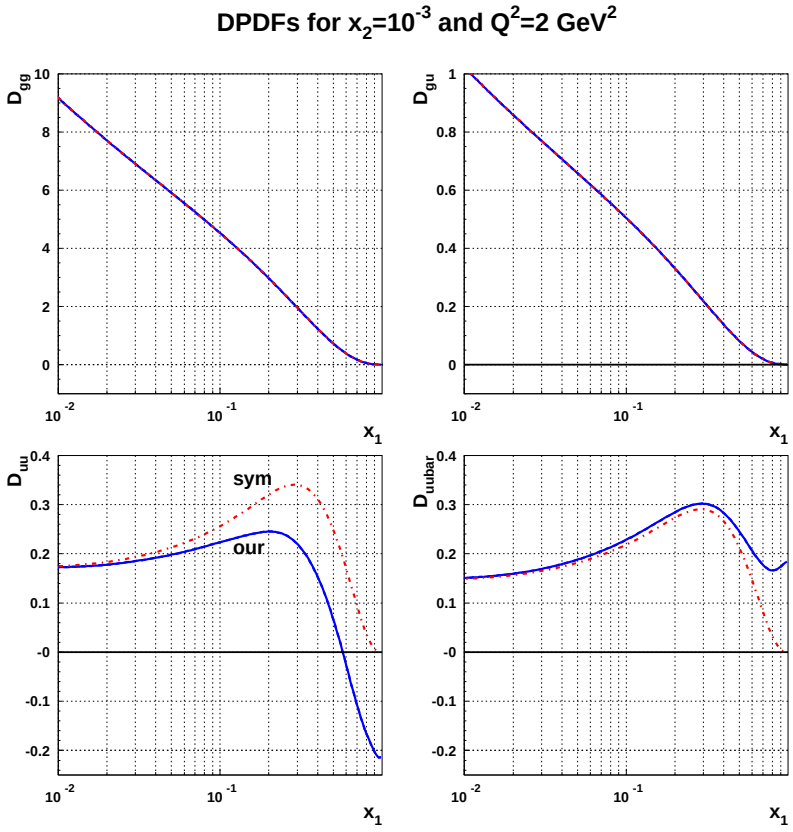

Figure 4.5: The initial DPDFs, $x_1x_2D_{f_1f_2}(x_1,x_2)$, as functions of x_1 for fixed $x_2 = 10^{-3}$ and the input scale $Q_0^2 = 2$ GeV^2. The two input distributions (4.67) (sym) and (4.68) (our) are plotted.

with fixed $x_2 = 10^{-3}$, using the MSTW08 LO [36] parametrization of the SPDFs taken at the scale $Q_0^2 = 2$ GeV^2. For such a small x_2, both ansatze give practically the same distributions with gluons, D_{gg} and D_{gu}. However, this is not the case for the pure quark distributions, D_{uu} and $D_{u\bar{u}}$, which are significantly different in the large x_1 region. As expected, D_{uu} from eq. (4.69) is negative for $x_1 > 0.6$. Notice also that the modifications given by eqs. (4.69) and (4.70) lead to non-zero values of the distributions $D_{f_if_i}$ and $D_{f_i\bar{f}_i}$ at the kinematic boundary: $x_1 + x_2 = 1$.

4.6 Effects of QCD evolution of the DPDFs

In order to study evolution of the DPDFs we use the constructed numerical program based on the Chebyshev polynomial expansion, described in detail in Appendix A. We solve simultaneously eqs. (4.31) and (4.46), starting from the two initial conditions specified in the previous section. In Fig. 4.6 we show the DPDFs from Fig. 4.5, evolved up to the scale $Q^2 = 100$ GeV^2, while in Fig. 4.7 we present a graphical comparison of

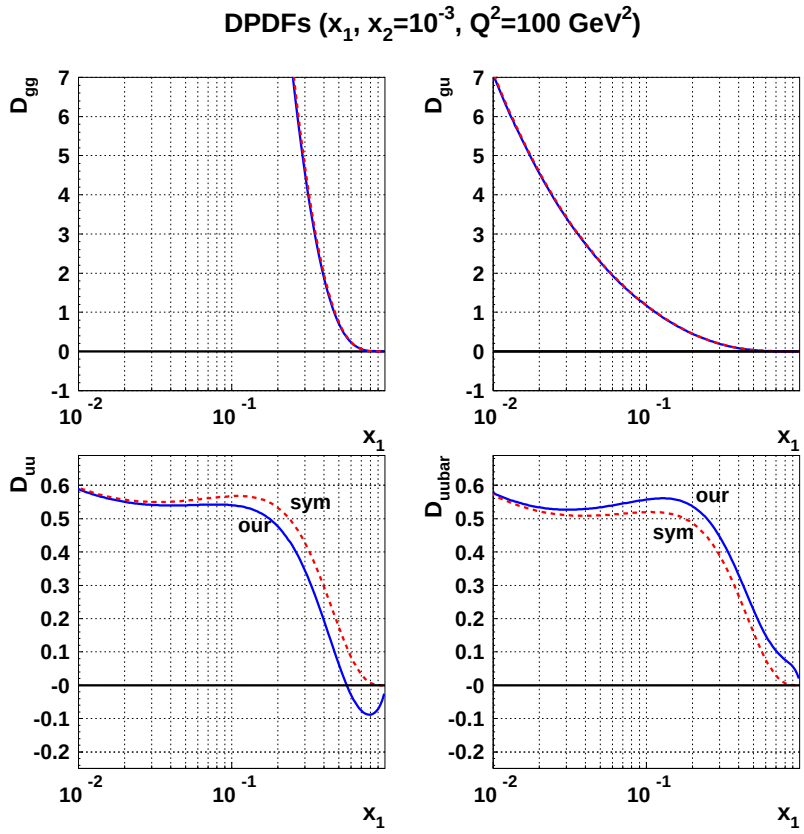

Figure 4.6: The DPDFs as in Fig. 4.5 but evolved to $Q^2 = 100$ GeV^2.

the initial and evolved double parton distributions, shown on previous plots. We clearly see that the evolved distributions D_{gg} and D_{gu} give exactly the same results in the whole domain of x_1 while the distributions D_{uu} and $D_{u\bar{u}}$ are different for large values of x_1. As expected, D_{uu} from our input stays negative for $x_1 > 0.6$. On the other hand, for small values of parton momentum fractions, $x_1, x_2 \ll 1$, both distributions tend to the same, factorized form

$$D_{f_1 f_2}(x_1, x_2, Q) \approx D_{f_1}(x_1, Q) D_{f_2}(x_2, Q)\,. \tag{4.72}$$

To study the question of the factorization (4.72) in more detail, we plot in Fig. 4.8 the ratio

$$R_{f_1 f_2} = \frac{D_{f_1 f_2}(x_1, x_2, Q^2)}{D_{f_1}(x_1, Q^2) D_{f_2}(x_2, Q^2)} \tag{4.73}$$

as a function of x_1 for fixed $x_2 = 10^{-3}$ and $Q^2 = 100$ GeV^2. As we can see, the effect of the violation of factorization for small values of x_1 and x_2 is only seen for the distribution $D_{u\bar{u}}$. This is due to the third term in the evolution equations (4.38) which characterize parton splitting. In particular, the violation is significant only for the splitting $g \to q\bar{q}$, due to

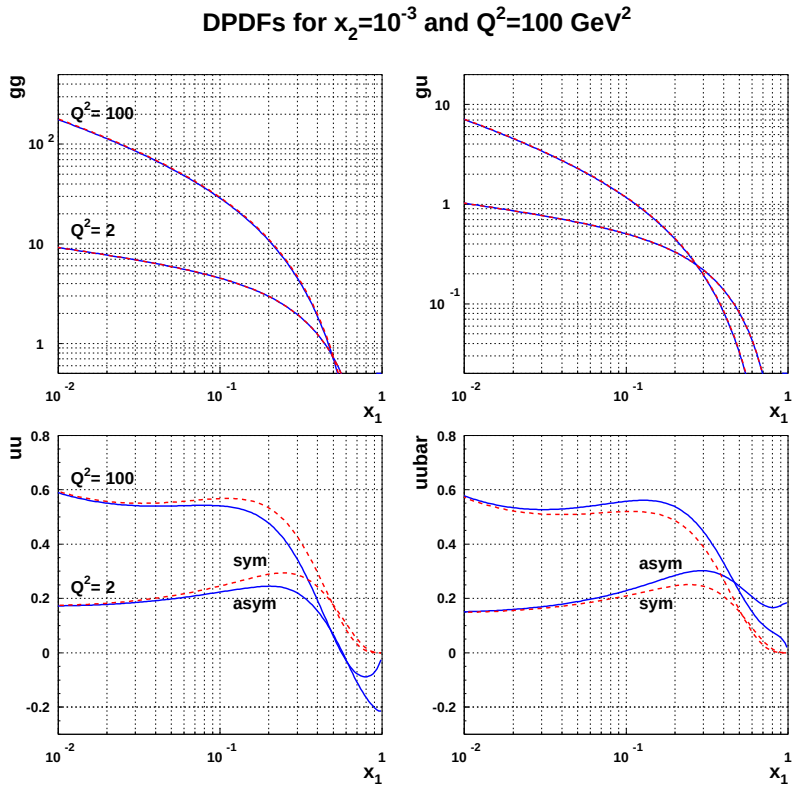

Figure 4.7: Comparison of the initial and evolved DPDFs for the symmetric (dashed curves) and our (asymmetric) (solid curves) inputs.

a large value of the gluon distribution $g(x)$ at small x. For the distributions D_{gg}, D_{gu}, D_{uu}, the factorization holds very well once one of the parton momentum fractions (or both) are small. The same conclusions are valid for the others quark flavors.

To summarize, our goal to construct the DPDFs initial distributions which are built out of the existing SPDFs and fulfill the new sum rules to reduce arbitrariness in the DPDFs evolution is not fully successful. The lack of the parton exchange symmetry and the negative values for some of them for large values of the parton momentum fractions make them rather unsatisfactory for practical purposes.

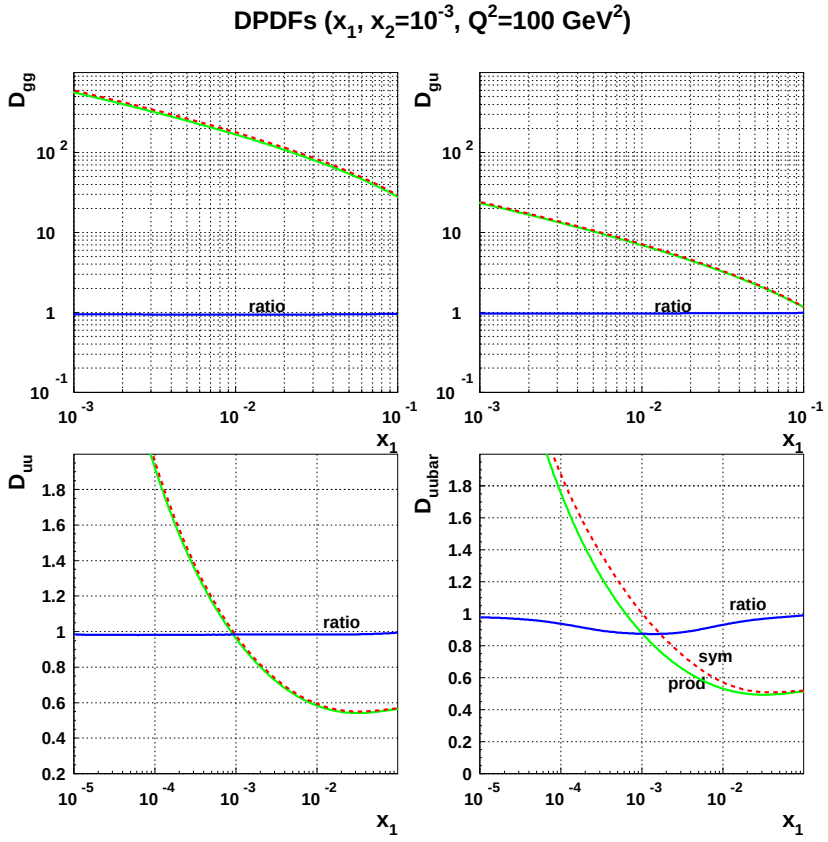

Figure 4.8: The ratio (4.73) for the symmetric (4.67) (dashed line) and our (4.68) (solid line) inputs evolved to $Q^2 = 100$ GeV^2 as functions of x_1 for fixed $x_2 = 10^{-3}$.

Chapter 5

Electroweak bosons production in double parton scattering

A crucial prediction of the Standard Model is the existence of vector bosons W and Z mediating in the weak interactions. In 1983, experiments of the UA1 [65] and UA2 [66] Collaborations, conducted at the CERN $p\bar{p}$ collider SPS, allow to experimentally confirm theoretical predictions concerning them with high accuracy. The electroweak W and Z boson production is one of the most valuable processes in the particle physics which allows to determine the important data on the hadronic structure.

For better understanding of this process, we analyze in this chapter the W^+W^- and Z^0Z^0 electroweak boson production in terms of the simplest multi-parton process - the double parton scattering. We study the vector boson production in DPS by using the QCD evolution equations for the DPDFs. In particular, we analyze the role of the splitting terms in these evolution equations and show their significance for the computed cross sections.

5.1 W and Z bosons production

The vector bosons $W^{\pm}$ and Z^0 can be produced from annihilation of two quarks in a hadronic collision. They have particular small decay widths: $\Gamma_W = 2.085$ GeV and $\Gamma_Z = 2.4952$ GeV, in comparison to their masses

$$M_W = 80.385\ \text{GeV}, \tag{5.1}$$

$$M_Z = 91.1876\ \text{GeV}. \tag{5.2}$$

The lowest-order diagrams for the $W^{\pm}$ and Z^0 boson production in the single parton scattering are shown in Fig. 5.1.

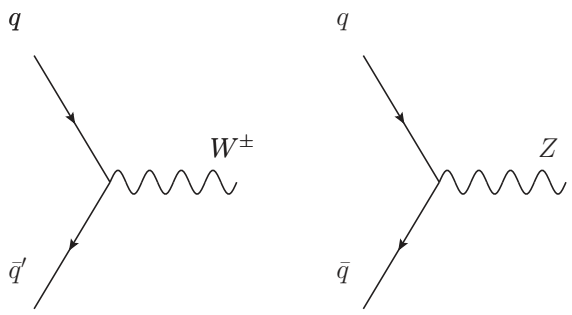

Figure 5.1: Lowest order diagrams for the production of the vector bosons $W^{\pm}$ and Z^0.

In the collinear approximation, the cross section of the elementary process,

$$q\bar{q}' \to W/Z \to lX\,,$$

is given by the parton distribution functions q_f and $\overline{q}_f$, known from Feynman's parton model (see Section 1.4),

$$\sigma = \sum_f \int dx\,dz\,q_f(x)\,\overline{q}'_f(z)\,\hat{\sigma}_{q\bar{q}'\to W/Z}\,. \tag{5.3}$$

In addition,

$$x = \frac{M_{W/Z}}{\sqrt{s}}\mathrm{e}^{y}\,, \qquad z = \frac{M_{W/Z}}{\sqrt{s}}\mathrm{e}^{-y}\,, \tag{5.4}$$

are the parton longitudinal momentum fractions given in terms of the boson rapidity y. The subprocess cross sections $\hat{\sigma}_{q\bar{q}'\to W/Z}$ has the following form [2]

$$\hat{\sigma}_{q\bar{q}'\to W} = \frac{\pi}{3}\sqrt{2}\,G_F\,M_W^2\,|V_{qq'}|^2\,\delta(\hat{s}-M_W^2)\,, \tag{5.5}$$

$$\hat{\sigma}_{q\bar{q}'\to Z} = \frac{\pi}{3}\sqrt{2}\,G_F\,M_Z^2\,(V_q^2+A_q^2)\,\delta(\hat{s}-M_Z^2)\,, \tag{5.6}$$

where G_F is the Fermi constant (1.13), $V_{qq'}$ is an appropriate element of the Cabibbo-Kobayashi-Masakawa (CKM) matrix [67, 68],

$$V = \begin{pmatrix} V_{ud} & V_{us} & V_{ub} \\ V_{cd} & V_{cs} & V_{cb} \\ V_{td} & V_{ts} & V_{tb} \end{pmatrix}\,, \tag{5.7}$$

and V_q, A_q are the couplings of the fermions to the Z boson, given by [2]

$$V_{u,c,t} = +0.191\,, \quad A_{u,c,t} = +\tfrac{1}{2}\,, \tag{5.8}$$

$$V_{d,s,b} = -0.345\,, \quad A_{d,s,b} = -\tfrac{1}{2}\,. \tag{5.9}$$

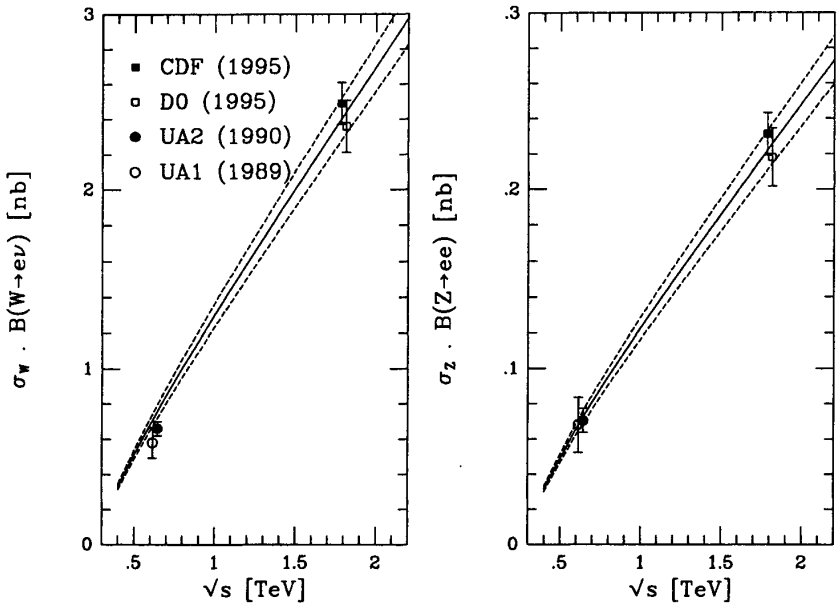

Figure 5.2: The theoretical predictions for the W and Z cross sections compared with the UA1, UA2, D0 and CDF experimental data [2].

The cross section of the electroweak bosons production has been measured by many experiments and collaborations. Fig. 5.2 shows a comparison of the W and Z cross section (multiplied by branching ratios $\sigma_{W/Z} \cdot BR$) , measured in $p\bar{p}$ collisions by UA1 [69], UA2 [70], D0 [71] and CDF [72] Collaborations, with theoretical predictions. The leptonic branching ratios are known from the Standard Model and are equal to

$$BR(W \to l\nu) = 0.1084\,, \tag{5.10}$$

$$BR(Z \to l^+ l^-) = 0.0336\,, \tag{5.11}$$

while the parton distribution functions are from the MRS(A') set [73] with the factorization scale $\mu = M_{W,Z}$. It is clearly seen that the agreement between theoretical predictions and experimental data is very good.

The production of the electroweak bosons $W^{\pm}$ and Z^0 can be characterizes by the differential cross section in rapidity, $y = \frac{1}{2}\ln(x_1/x_2)$. In this case, the cross section for the $W^{\pm}$ boson production is given in terms of the convolution of the elementary cross section (5.5) and the parton distribution functions

$$\frac{d\sigma_{W^{\pm}}}{dy} = \sigma_0^W \sum_{qq'} |V_{qq'}|^2 \left\{ q(x_1,\mu)\bar{q}'(x_2,\mu) + \bar{q}(x_1,\mu)q'(x_2,\mu) \right\}\,, \tag{5.12}$$

with the factorization scale $\mu = M_W$ and

$$\sigma_0^W = \frac{2\pi G_F}{3\sqrt{2}} \frac{M_W^2}{s}\,. \tag{5.13}$$

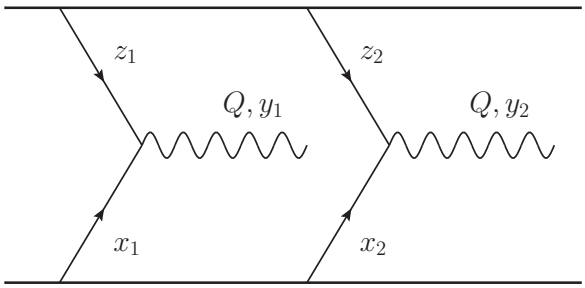

Figure 5.3: Production of the electroweak bosons in double parton scattering.

For the Z boson production, the cross section is obtained from eq. (5.12) by replacing

$$|V_{qq'}|^2 \to \delta_{qq'}(V_q^2 + A_q^2)\,, \tag{5.14}$$

and changing the mass $M_W \to M_Z$.

5.2 Simplified DPS cross section

The production of the $W^{\pm}$ and Z^0 bosons can be also analyzed for the double parton scattering. The graphical illustration of the electroweak bosons production in DPS is shown in Fig. 5.3. The hard scale Q in such a case is equal to the boson mass $Q = M_{W,Z}$, while the parton longitudinal momentum fractions x_1, x_2 and z_1, z_2 can be related in the collinear approach to the produced boson rapidities, y_1, y_2, as follows

$$x_{1,2} = \frac{Q}{\sqrt{s}}\,\mathrm{e}^{y_{1,2}}\,, \qquad z_{1,2} = \frac{Q}{\sqrt{s}}\,\mathrm{e}^{-y_{1,2}}\,. \tag{5.15}$$

Using relation (5.15) and the following conditions for the momentum fractions

$$x_{1,2} \leq 1\,, \qquad z_{1,2} \leq 1\,, \tag{5.16}$$

$$(x_1 + x_2) \leq 1\,, \qquad (z_1 + z_2) \leq 1\,, \tag{5.17}$$

the allowed values of rapidities can be specified

$$-\ln\frac{\sqrt{s}}{Q} \leq y_{max} \leq \ln\frac{\sqrt{s}}{Q}\,. \tag{5.18}$$

We consider the W^+W^- and Z^0Z^0 boson production in the proton-proton scattering at the LHC center-of-mass energy $\sqrt{s} = 14$ TeV. In Fig. 5.4 (left), we show the rapidity plane for the W^+W^- boson production, where the solid lines correspond to constant values of (5.17) while the dashed lines represent the constant ratios $x_2/x_1 = z_1/z_2$. The middle point corresponds to fully symmetric momentum fractions $x_i = z_i \approx 0.5 \cdot 10^{-2}$.

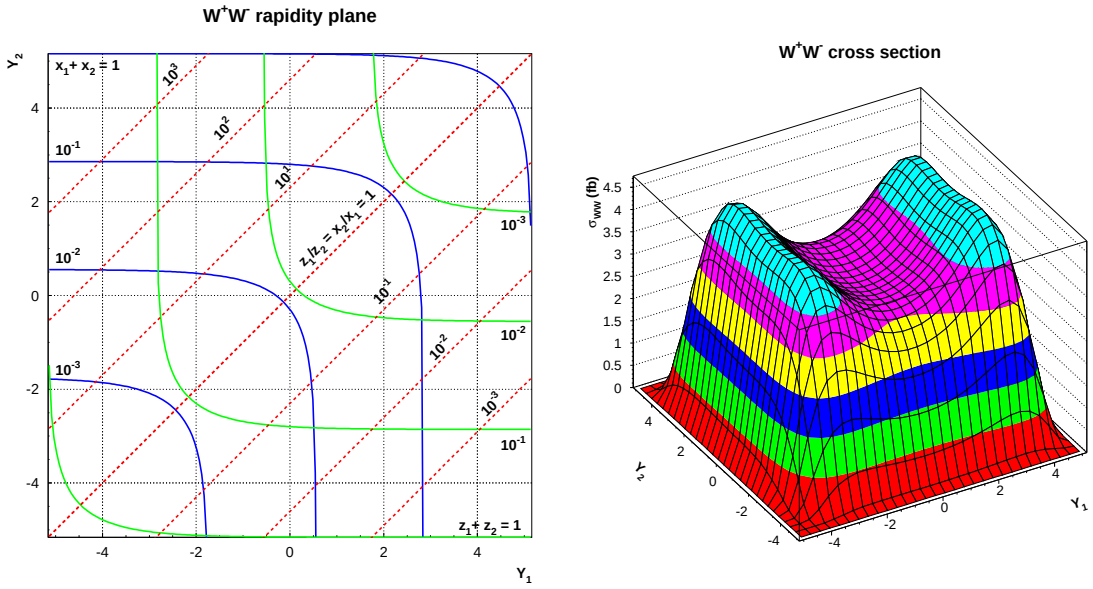

Figure 5.4: Kinematic plane for W^+W^- production in DPS at the LHC energy 14 TeV (left) and cross section (5.20) for this process (right).

In the standard approach, the estimation of the DPS cross section σ_{AB} is usually factorized into a product of the two single parton scattering cross sections σ_A and σ_B

$$\sigma_{AB} = \frac{N}{2}\frac{\sigma_A \sigma_B}{\sigma_{eff}}, \tag{5.19}$$

with a symmetry factor N equal 1 for $A = B$ and 2 otherwise, and an effective cross section, $\sigma_{eff} \approx 15$ mb, estimated by the CDF and D0 Collaborations from the DPS data [57, 58, 59]. In this approach, the DPS cross section for the W^+W^- bosons production can be computed using the single scattering cross sections (5.12)

$$\frac{\sigma_{W^+W^-}}{dy_1 dy_2} = \frac{1}{\sigma_{eff}}\frac{d\sigma_{W^+}}{dy_1}\frac{d\sigma_{W^-}}{dy_2}. \tag{5.20}$$

The results of such a computation are shown in Fig. 5.4 (right) where we present the DPS cross section (5.20) obtained using three quark flavors u, d, s and the MSTW08(LO) parametrization of the single PDFs [36].

Formula (5.19) is only an approximation. A full description of DPS cross sections in the collinear approximation with the double parton distributions is presented in the next section.

5.3 DPS cross section with DPDFs

The double parton scattering allows to gain information on parton correlations by measuring the double parton scattering cross section in high energy collisions of two hadrons. The inclusive DPS cross section in the collinear approximation is given by the following formula with the DPDFs [46, 44], see also eq. (3.33) for scalar partons,

$$\sigma_{AB} = \frac{N}{2} \sum_{f_1 f_2 f_1' f_2'} \int dx_1 dx_2 dx_1' dx_2' \; \hat{\sigma}^A_{f_1 f_1'}(x_1, x_1', Q_1) \; \hat{\sigma}^B_{f_2 f_2'}(x_2, x_2', Q_2) \qquad (5.21)$$
$$\times \int \frac{d^2\mathbf{q}}{(2\pi)^2} \, D_{f_1 f_2}(x_1, x_2, Q_1, Q_2, \mathbf{q})) \, D_{f_1' f_2'}(x_1', x_2', Q_1, Q_2, -\mathbf{q}) \,,$$

where A and B denote the two hard parton states, N is a symmetry factor (equal 1 for $A = B$ and 2 otherwise) and $\mathbf{q}$ is the relative transverse momentum discussed in Sec. 5.3.2.

For equal hard scales, $Q_1 = Q_2 \equiv Q$, the DPDFs evolve with a hard scale Q according to the evolution equations (4.46) and (4.47). Using the results of Chapter 4 and our numerical program which solves the evolution equations, we are ready to analyze the DPS production of electroweak boson pairs in detail. Two related questions are particularly interesting:

- how the simplified cross section (5.19) compares with more accurate formula (5.21),
- how important are the splitting terms in the evolution equations (4.46) for the obtained results.

In order to answer the latter question it is useful to reformulate the evolution equations for DPDFs in the double Mellin moment space. This will allow to easily separate two contributions to the DPDFs, shown in a simplified form in Fig. 4.2. The first contribution comes from partonic emissions from one of the two partons while the remaining one acts as a spectator. The second contribution is the splitting contribution in which parton emissions come from two partons originating from a single one. This is the contribution which is described by the splitting terms in the evolution equations (4.46).

5.3.1 Evolution equations for Mellin momens of DPDFs

We rewrite evolution equations (4.46) for equal scales with the help of the double Mellin moments of the DPDFs,

$$\tilde{D}_{f_1 f_2}(n_1, n_2, t) = \int_0^1 dx_1 \int_0^1 dx_2 \; x_1^{n_1} x_2^{n_2} \, \theta(1 - x_1 - x_2) \, D_{f_1 f_2}(x_1, x_2, t) \,, \qquad (5.22)$$

where the theta function imposes the basic momentum fraction constraint (4.33). Notice that we keep $\mathbf{q} = 0$ for the DPDFs. Neglecting for simplicity of the notation the nega-

tive virtual correction terms in eqs. (4.46), we can write these equations in the following equivalent form

$$\begin{aligned}\partial_t D(x_1,x_2,t) \;=\; & \int_0^1 dy \int_0^1 dz\, \delta(x_1-yz)\,\theta(1-z-x_2)\,P(y)\,D(z,x_2,t) \\ & + \int_0^1 dy \int_0^1 dz\; \delta(x_2-yz)\;\theta(1-x_1-z)\,P(y)\,D(x_1,z,t) \\ & + \frac{1}{x_1+x_2} P\left(\frac{x_1}{x_1+x_2}\right) D(x_1+x_2,t)\,, \end{aligned} \tag{5.23}$$

where we used a matrix notation in flavors, e.g. $(D)_{f_1 f_2} = D_{f_1 f_2}$. Integrating both sides of this equation as in eq. (5.22), we find the equation with two homogeneous terms and one non-homogeneous term

$$\partial_t \tilde{D}(n_1,n_2,t) = A_1 + A_2 + B\,. \tag{5.24}$$

The first homogeneous term, A_1, is given by

$$\begin{aligned} A_1 \;=\; & \int_0^1 dx_1 \int_0^1 dx_2 \int_0^1 dy \int_0^1 dz\; \delta(x_1-yz)\,\theta(1-z-x_2)\theta(1-x_1-x_2) \\ & \qquad\qquad \times x_1^{n_1}\, x_2^{n_2}\, P(y)\,D(z,x_2,t) \\ =\; & \int_0^1 dy \int_0^1 dz \int_0^1 dx_2\; \theta(1-z-x_2)\;\theta(1-yz-x_2)\,(yz)^{n_1}\, x_2^{n_2}\, P(y)\,D(z,x_2,t)\,, \end{aligned}$$

where we performed integration over x_1 with the help of the delta function in the third line. The second theta function does not impose additional constraint and can be skipped. Thus

$$\begin{aligned} A_1 \;=\; & \Big[\int_0^1 dy\, y^{n_1} P(y)\Big] \cdot \Big[\int_0^1 dz \int_0^1 dx_2\, z^{n_1} x_2^{n_2}\,\theta(1-z-x_2)\,D(z,x_2,t)\Big] \\ =\; & \gamma(n_1)\cdot \tilde{D}(n_1,n_2,t)\,, \end{aligned} \tag{5.25}$$

where the known matrix of anomalous dimensions read

$$\gamma(n) = \int_0^1 dx\, x^n\, P(x)\,. \tag{5.26}$$

In the same way we find a similar relation for the second homogeneous term,

$$A_2 = \tilde{D}(n_1,n_2,t)\cdot \gamma^T(n_2)\,. \tag{5.27}$$

The transformation of the non-homogeneous term is slightly more complicated,

$$B = \int_0^1 dx_1 \int_0^1 dx_2\, \theta(1-x_1-x_2)\, x_1^{n_1}\, x_2^{n_2}\, \frac{1}{x_1+x_2}\, P\left(\frac{x_1}{x_1+x_2}\right) D(x_1+x_2,t). \tag{5.28}$$

After changing variables, $x_2 \to z = x_1 + x_2$, we find the following relation

$$\begin{aligned} B &= \int_0^1 dx_1\, x_1^{n_1} \int_{x_1}^1 dz\, (z-x_1)^{n_2}\, \frac{1}{z} P(x_1/z)\, D(z,t) \\ &= \int_0^1 dx_1\, x_1^{n_1} \int_0^1 dy \int_0^1 dz\, \delta(x_1 - yz)\, (z-x_1)^{n_2}\, P(y)\, D(z,t)\,. \end{aligned} \tag{5.29}$$

Preforming the integration over x_1 with the delta function, we find

$$\begin{aligned} B &= \int_0^1 dy \int_0^1 dz\, (yz)^{n_1}\, (z-yz)^{n_2}\, P(y) D(z,t) \\ &= \Big[\int_0^1 dy\, y^{n_1}\, (1-y)^{n_2}\, P(y)\Big] \cdot \Big[\int_0^1 dz\, z^{n_1+n_2} D(z,t)\Big] \\ &= \tilde{\gamma}(n_1,n_2) \cdot \tilde{D}(n_1+n_2,t)\,, \end{aligned} \tag{5.30}$$

where

$$\tilde{\gamma}(n_1,n_2) = \int_0^1 dy\, y^{n_1}\, (1-y)^{n_2}\, P(y)\,. \tag{5.31}$$

From eqs. (5.25), (5.27) and (5.30), we can finally obtain the following form of the evolution equation in the Mellin moments representation

$$\partial_t \tilde{D}(n_1,n_2,t) = \underbrace{\gamma(n_1)\, \tilde{D}(n_1,n_2,t) + \tilde{D}(n_1,n_2,t)\, \gamma^T(n_2)}_{\text{homogeneous terms}} + \underbrace{\tilde{\gamma}(n_1,n_2)\, \tilde{D}(n_1+n_2,t)}_{\text{non-homogeneous term}}. \tag{5.32}$$

Notice that the non-homogeneous term corresponds to the parton splitting contribution to the DPDFs. Let us notice that $\tilde{D}(n_1+n_2,t)$ is a vector of the Mellin moments of the single PDFs,

$$\tilde{D}_f(n,t) = \int_0^1 dx\, x^n\, D_f(x,t)\,. \tag{5.33}$$

The evolution equation for them can be found in a similar way. We obtain the equation

$$\partial_t \tilde{D}(n,t) = \gamma(n)\, \tilde{D}(n,t)\,, \tag{5.34}$$

which has a simple solution

$$\tilde{D}(n,t) = \mathrm{e}^{\gamma(n)\, t}\, \tilde{D}_0(n)\,, \tag{5.35}$$

where $\tilde{D}_0(n)$ is an initial condition.

The general solution to the evolution equation (5.32) is the sum of the general solu-

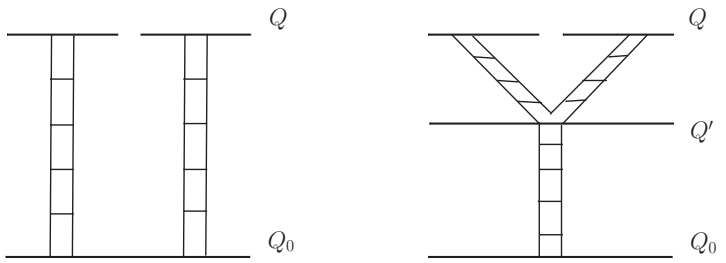

Figure 5.5: Schematic illustration of two contributions in eq. (5.39).

tion to the homogeneous part and a particular solution to the non-homogeneous part. The homogeneous equation has the following general solution

$$\tilde{D}(n_1,n_2,t) = \mathrm{e}^{\gamma(n_1)t} A(n_1,n_2)\,\mathrm{e}^{\gamma^T(n_2)t}. \tag{5.36}$$

A particular solution to the non-homogeneous equation can be found by making $A(n_1,n_2)$ time dependent and substituting such an ansatz to the full equation (5.32). Then, we find the equation

$$\partial_t A(n_1,n_2,t) = \mathrm{e}^{-\gamma(n_1)t}\,\tilde{\gamma}(n_1,n_2)\,\tilde{D}(n_1+n_2,t)\,\mathrm{e}^{-\gamma^T(n_2)t}, \tag{5.37}$$

which can be easily solved

$$A(n_1,n_2,t) = \tilde{D}_0(n_1,n_2) + \int_0^t dt'\,\mathrm{e}^{-\gamma(n_1)t'}\,\tilde{\gamma}(n_1,n_2)\,\tilde{D}(n_1+n_2,t')\,\mathrm{e}^{-\gamma^T(n_2)t'}, \tag{5.38}$$

where $\tilde{D}_0(n_1,n_2)$ is an initial condition for the DPDFs. Substituting (5.38) into (5.36), we obtain the final form of the solution

$$\begin{aligned}\tilde{D}(n_1,n_2,t) &= \mathrm{e}^{\gamma(n_1)t}\,\tilde{D}_0(n_1,n_2)\,\mathrm{e}^{\gamma^T(n_2)t} \\ &+ \int_0^t dt'\,\mathrm{e}^{\gamma(n_1)(t-t')}\,\tilde{\gamma}(n_1,n_2)\,\tilde{D}(n_1+n_2,t')\,\mathrm{e}^{\gamma^T(n_2)(t-t')}.\end{aligned} \tag{5.39}$$

Relation (5.39) is the sum of two contributions. The first term describes two independent DGLAP evolutions up to the scale Q of two partons emerging from a hadron at the initial scale Q_0 ($t=0$). The second term describes the emergence of the two partons from the splitting of a single parton at the scale Q' (corresponding to t') which then independently evolve up to the scale Q. Notice that the splitting occurs at any value of $Q' \in [Q_0, Q]$. The graphical illustration of these two terms is given in Fig. 5.5.

With eq. (5.39) it is easy to compute the two contributions to the solution of the evolution equations for DPDFs. To find the homogeneous part, we solve these equations without the splitting terms for initial conditions imposed at some initial scale. The non-

homogeneous, splitting contribution can be found by solving the full evolution equations for initial conditions which are equal to zero at the same initial scale.

The preformed analysis allows us to present the solution for two different scales, say $Q_1 < Q_2$ ($t_1 < t_2$),

$$\begin{aligned}\tilde{D}(n_1,n_2,t_1,t_2) \;=\; & \mathrm{e}^{\gamma(n_1)t_1}\,\tilde{D}_0(n_1,n_2,\mathbf{q})\,\mathrm{e}^{\gamma^T(n_2)t_2} \\ & + \int\limits_0^{\min\{t_1,t_2\}} dt'\,\mathrm{e}^{\gamma(n_1)(t_1-t')}\,\tilde{\gamma}(n_1,n_2)\,\tilde{D}(n_1+n_2,t')\,\mathrm{e}^{\gamma^T(n_2)(t_2-t')}\,. \qquad (5.40)\end{aligned}$$

The evolution equations which correspond to this case have been derived in [42]. The x-space representation of eqs. (5.39) and (5.40) is obtained from the inverse Mellin transformation and can be found in [44, 74].

5.3.2 Relative momentum dependence

The form (5.39) of the solution is the basis of the proposition of Ryskin and Snigirev [44] regarding the dependence of the DPDFs on the relative momentum $\mathbf{q}$. This dependence is not specified by the evolution equations and is a matter of a physically motivated modeling. The basic idea is that for two partons originating from a nucleon, $\mathbf{q}$ reflects their correlation inside the nucleon, described by a non-perturbative form factor

$$F_{2g}(\mathbf{q}) \;=\; \frac{1}{\left(1+\mathbf{q}^2/m_g^2\right)^2}\,, \qquad (5.41)$$

known as the two-gluon nucleon form factor with $m_g \approx 1.5$ GeV being an effective gluon mass. Therefore, the first term in eq. (5.39) has been postulated in [44] with the factorized $\mathbf{q}$-dependence,

$$\tilde{D}^{(1)}(n_1,n_2,t,\mathbf{q}) \;=\; \mathrm{e}^{\gamma(n_1)t}\,\tilde{D}_0(n_1,n_2)\,\mathrm{e}^{\gamma^T(n_2)t}\,F_{2g}^2(\mathbf{q})\,. \qquad (5.42)$$

In principle, the form factor could depend on parton flavors, however, this dependence is not taken into account.

On the other hand, if the two partons originate from a point-like parton through its splitting, such a correlation (and the form factor) no longer exists. The $\mathbf{q}$-dependence has been introduced in the splitting term in eq. (5.39) through the lower integration limit

$$\tilde{D}^{(2)}(n_1,n_2,t,\mathbf{q}) \;=\; \int_{t_0(\mathbf{q})}^{t} dt'\,\mathrm{e}^{\gamma(n_1)(t-t')}\,\tilde{\gamma}(n_1,n_2)\,\tilde{D}(n_1+n_2,t')\,\mathrm{e}^{\gamma^T(n_2)(t-t')}\,, \qquad (5.43)$$

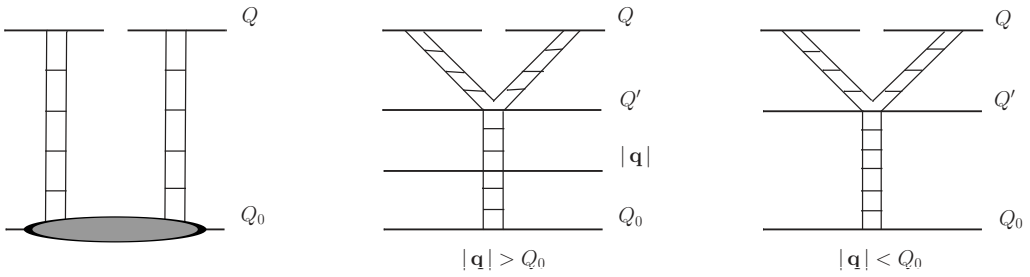

Figure 5.6: Schematic **q**-dependence of the DPDFs according to [44].

where

$$t_0(\mathbf{q}) = \begin{cases} 0 & \text{if } |\mathbf{q}| \leq Q_0 \\ \\ t(\mathbf{q}) & \text{if } Q_0 < |\mathbf{q}| \leq Q \end{cases} \tag{5.44}$$

and $t(\mathbf{q})$ is given by

$$t(\mathbf{q}) \equiv \int_{Q_0^2}^{\mathbf{q}^2} \frac{\alpha_s(\mu^2)}{2\pi} \frac{d\mu^2}{\mu^2} = \frac{1}{b} \ln \frac{\ln(\mathbf{q}^2/\Lambda_{QCD}^2)}{\ln(Q_0^2/\Lambda_{QCD}^2)}, \tag{5.45}$$

with $b = (33 - 2n_f)/6$. Thus, for $|\mathbf{q}| > Q_0$, $|\mathbf{q}|$ is the scale from which the splitting starts, see Fig. 5.6. For $|\mathbf{q}| < Q_0$, the relative loop momentum is small and may be neglected due to strong ordering in transverse parton momenta in the DGLAP approximation. Notice that $|\mathbf{q}| \leq Q$, which means that Q is the largest scale in the problem.

Summarizing, after the transformation into the x-space, the DPDFs can be written as a sum of the two discussed contributions

$$D(x_1, x_2, t, \mathbf{q}) = D^{(1)}(x_1, x_2, t, \mathbf{q}) + D^{(2)}(x_1, x_2, t, \mathbf{q}), \tag{5.46}$$

which in the Mellin moment space are given by eqs. (5.42) and (5.43).

5.3.3 Contributions to the DPS cross section

We are now ready to conclude our analysis of the W^+W^- and Z^0Z^0 production in DPS using the double parton distribution functions [75]. Coming back to cross section (5.21) with AB being the above mentioned boson pairs, we can write it in terms of the two components in eq. (5.46) as the following sum of the three contributions

$$\sigma_{AB} = \sigma_{AB}^{(11)} + \sigma_{AB}^{(12+21)} + \sigma_{AB}^{(22)}, \tag{5.47}$$

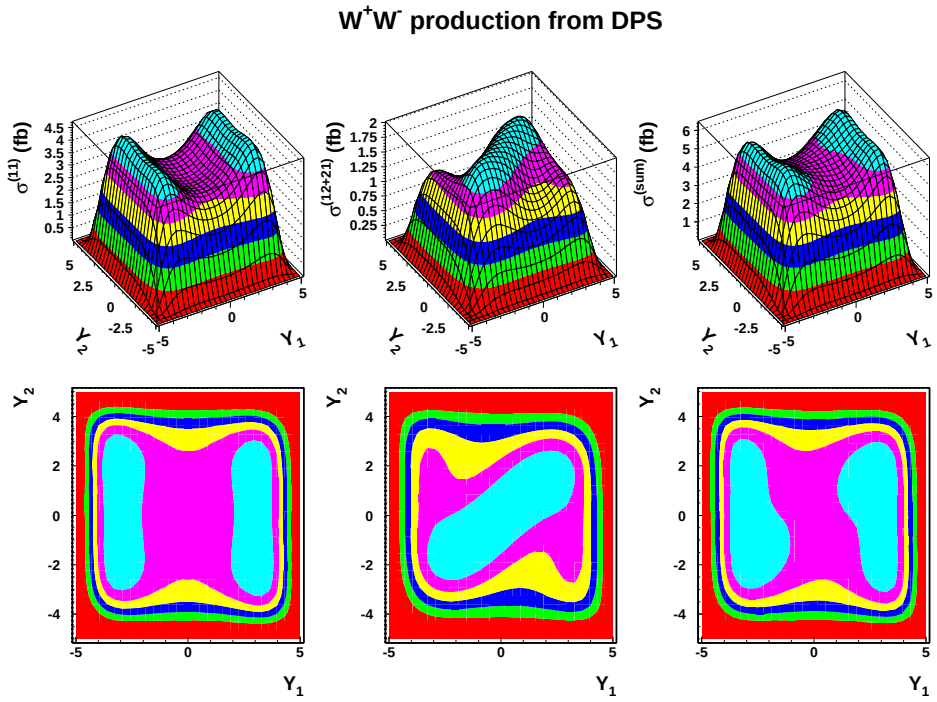

Figure 5.7: The (11) and $(12+21)$ contributions to the W^+W^- production cross section (5.47) and their sum. Contours of constant values are shown below.

where for $i,j \in \{1,2\}$

$$\sigma_{AB}^{(ij)} = \frac{N}{2}\sum_{\text{flav}}\int dx_1 dx_2\, dx_1' dx_2'\; \hat{\sigma}^A_{f_1 f_1'}(x_1,x_1',Q)\,\hat{\sigma}^B_{f_2 f_2'}(x_2,x_2',Q) \times \int \frac{d^2\mathbf{q}}{(2\pi)^2}\, D^{(i)}_{f_1 f_2}(x_1,x_2,t,\mathbf{q})\, D^{(j)}_{f_1' f_2'}(x_1',x_2',t,-\mathbf{q})\,. \tag{5.48}$$

Each term in the above equation has a clear interpretation: $\sigma_{AB}^{(11)}$ is a contribution without parton splitting in the DPDFs evolution equations, the mixed contribution $\sigma_{AB}^{(12+21)}$ has a single parton splitting from only one hadron side while $\sigma_{AB}^{(22)}$ is the double splitting contribution with two parton splittings from both hadrons each.

The double splitting contribution $\sigma_{AB}^{(22)}$ was a matter of intensive debate in past years [45, 43, 76, 46, 77, 78] and was classified rather as the single parton scattering process, entirely characterized by the SPDFs. Since the double splitting contribution needs careful diagrammatic analysis, we do not consider it in our analysis.

In the presented analysis, the differential cross section (5.47) in boson rapidities $Y_{1,2}$ was computed with $A = W^+$ and $B = W^-$. For this purpose, we used our numerical program which solves the evolution equations for DPDFs. For initial conditions, we used prescription (4.67) from [41] in which the DPDFs are products of single parton distributions (from the parametrization [36]) multiplied by a correlation factor in parton momentum fractions $x_{1,2}$. To perform decomposition (5.46), we first found the solution to the

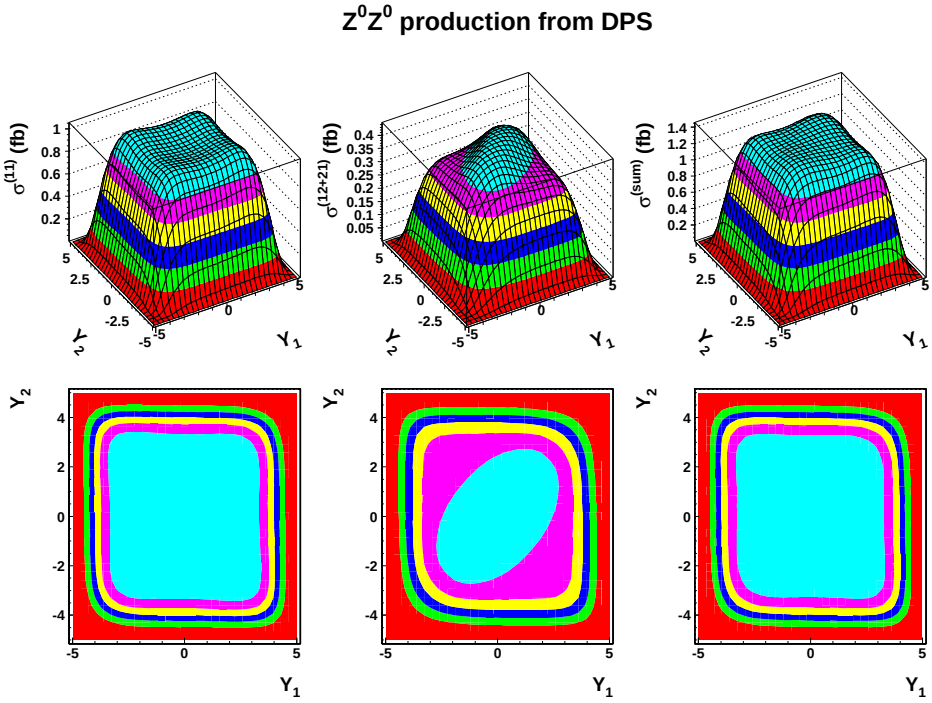

Figure 5.8: The (11) and $(12+21)$ contributions to Z^0Z^0 production cross section (5.47) and their sum. Contours of constant values are shown below.

homogeneous evolution equations with the initial condition form [41], $D^{(hom)}$. Next, we found the solution to the non-homogeneous equation with zero initial conditions, $D^{(nhom)}$. The two components in eq. (5.46) can written with the help of the found solutions

$$D^{(1)}(x_1,x_2,Q,\mathbf{q}) = D^{(hom)}(x_1,x_2,Q)F_{2g}^2(\mathbf{q}), \tag{5.49}$$

$$D^{(2)}(x_1,x_2,Q,\mathbf{q}) = D^{(nhom)}(x_1,x_2,Q) - D^{(nhom)}(x_1,x_2,|\mathbf{q}|), \tag{5.50}$$

where the subtraction in the second equation accounts for the lower integration limit in eq. (5.43). The first two components of the cross section (5.47) are shown in Fig. 5.7. We see that the single splitting contribution, $\sigma_{WW}^{(12+21)}$, is of the same order that the standard contribution, $\sigma_{WW}^{(11)}$. Notice also the change in the correlation pattern in rapidity due to the splitting contribution, shown in the plots with contours of constant values of the cross sections.

We repeat our analysis for the Z^0Z^0 boson production in DPS obtaining qualitatively the same results, see Fig. 5.8. In this case, the splitting contribution is peaked around $y_1 \simeq y_2 \approx 0$, which is due to the configuration with parton momentum fractions $x_1 \simeq x_2 \sim 10^{-2}$ for which the splitting contribution is determined by the strongly rising single gluon distribution, driving the splitting $g \to q\bar{q}$. The relevance of the single splitting contribution is shown in Table 5.1 where values of the total cross sections for the discussed contributions are shown. They were calculated after the integration over the allowed values of bosons rapidities.

in [fb]	$\sigma_{tot}^{(11)}$	$\sigma_{tot}^{(12+21)}$	$\sigma_{tot}^{(12+21)}/\sigma_{tot}^{(11)}$
W^+W^-	256	97	0.38
Z^0Z^0	61	22	0.36

Table 5.1: Components of the DPS cross sections for the electroweak boson production.

5.3.4 Discussion of the splitting contribution

In order to understand to the origin of the significance of the single splitting contribution for the computed cross sections, reflected for example in Table 5.1, we plot the cross section $d\sigma_{W^+W^-}/dy_1dy_2d\mathbf{q}^2$ as a function of $\mathbf{q}^2$ for the standard and splitting contributions at $y_1 = y_2 = 0$, see Fig. 5.9. We see that both contributions are suppressed for large values of q^2 because of the presence of the form factor $F_{2g}(\mathbf{q})$ in the homogeneous part of the DPDFs, see eq. (5.49). The standard contribution, $\sigma^{(11)}$, is stronger suppressed that the single splitting one, $\sigma^{(12+21)}$, because it is proportional to

$$\int \frac{d^2\mathbf{q}}{(2\pi)^2} F_{2g}^4(\mathbf{q}) = \frac{m_g^2}{28\pi}, \tag{5.51}$$

while the single splitting contribution is proportional to

$$\int \frac{d^2\mathbf{q}}{(2\pi)^2} F_{2g}^2(\mathbf{q}) = \frac{m_g^2}{12\pi}. \tag{5.52}$$

We checked that an additional dependence on $\mathbf{q}$ in the non-homogeneous part of the DPDFs is negligible. Thus, from the pure $\mathbf{q}$-dependence, the standard contribution is smaller by the factor

$$12\pi/28\pi \approx 0.43. \tag{5.53}$$

However, the significant enhancement of the single splitting contribution due to weaker q^2-dependence is compensated by a smaller size of the non-homogeneous component of the DPDFs, $D^{(2)}$, in comparison to the homogeneous component, $D^{(1)}$. Roughly speaking, in $\sigma^{(11)}$ the DPDFs are proportional to $(x^{-\lambda})^4$ with $\lambda \sim 0.3 - 0.5$ (at $x < 0.1$) while in $\sigma^{(12+21)}$ they are only proportional to $(x^{-\lambda})^3$. More precisely, the ratio of the DPDFs taken for $y_1 = y_2 = 0$ in the two contributions can be found from the values of the cross sections at $\mathbf{q}^2 \approx 0$ in Fig. 5.9,

$$DPDF^{(11)} : DPDF^{(12+21)} \approx 3.7. \tag{5.54}$$

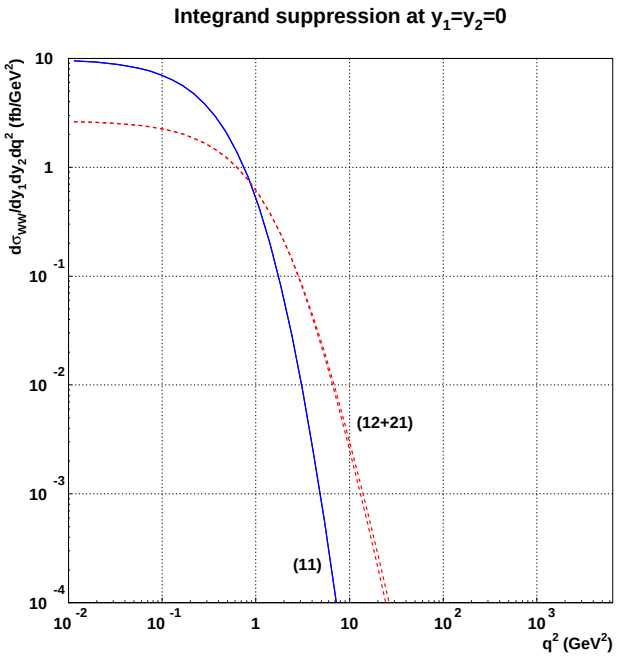

Figure 5.9: The $\mathbf{q}^2$-dependence of $d\sigma_{W^+W^-}/dy_1dy_2d\mathbf{q}^2$ at $y_1 = y_2 = 0$ for the indicated contributions. The upper limit for $\mathbf{q}^2$ equals M_W^2.

From ratios (5.53) and (5.54) we find that for the differential cross sections at $y_1 = y_2 = 0$, we have

$$d\sigma^{(12+21)} : d\sigma^{(11)} = 0.63\,. \tag{5.55}$$

This ratio is bigger than those for the total cross sections in Table 5.1, but it stays in the right ballpark. Thus, the single splitting contribution should be present in all analyses of the DPS processes.

The presented analysis of the DPS electroweak boson production can also be quantified with the help of the effective cross section. Let us recall, that in the simplified analysis with eq. (5.19), $\sigma_{\rm eff}$ is a constant, approximately equal to 15 mb, which sets the right scale for the computed cross sections. In our analysis with the DPDFs, this scale enters through the value of the effective gluon mass in the two-gluon form factor, $m_g \approx 1.5$ GeV. However, formula (5.19) no longer holds. How strongly it is violated can be shown by plotting the effective cross section defined now as the ratio

$$\sigma_{\rm eff} = \frac{N}{2}\frac{(d\sigma_A/dy_1)(d\sigma_B/dy_2)}{d\sigma_{AB}/dy_1dy_2}\,. \tag{5.56}$$

In the simplified case this would a constant equal to 15 mb but in general $\sigma_{\rm eff}$ depends on boson rapidities (y_1, y_2).

We performed the computations for two cases: $\sigma_{AB} = \sigma_{AB}^{(11)}$ and $\sigma_{AB} = \sigma_{AB}^{(11)} + \sigma_{AB}^{(12+21)}$ for the W^+W^- and Z^0Z^0 production at the LHC. The results are shown in

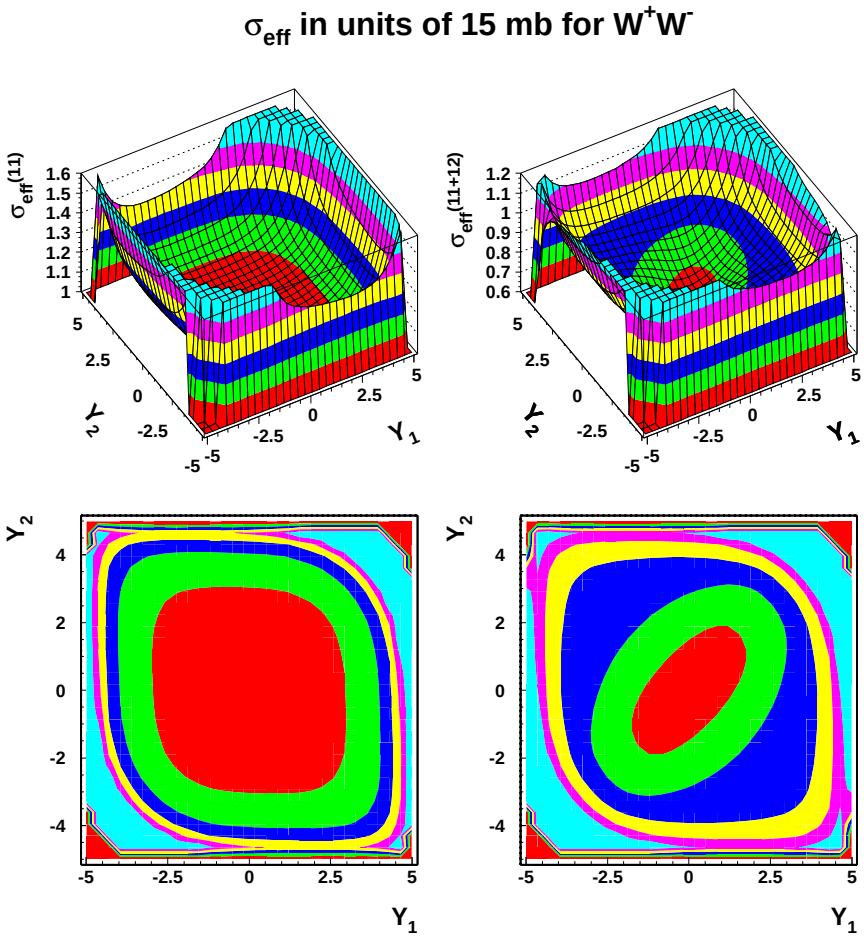

Figure 5.10: σ_{eff} in units of 15 mb for W^+W^- production as a function of boson rapidities for two models of the DPS cross sections, see in the text. The lines of constant values are shown below.

Figs. 5.10 and 5.11. For better visibility, we cut the maximal values to 1.6 or 1.2 at the edges of the phase space. We see that with the standard contribution to the DPS cross section, the factorization property is to good approximation valid in for central rapidities (small values of momentum fractions, see Fig. 5.4). However, approaching kinematic boundaries $x_1 + x_2 = z_1 + z_2 = 1$ with comparable momentum fractions, the violation of factorization becomes stronger. This picture changes after adding the single splitting contribution. Now, the violation of factorization is significant even for central rapidities. The effective cross section is smaller than 15 mb and stays in between 60%-80% of this value.

5.3.5 Experimental status and outlook

In recent years, analyses of the double parton scattering have been performed by the LHC experimental groups. The CMS [61] and ATLAS [60] Collaborations measured the DPS using $W + 2$-jet events in the proton-proton collisions at the LHC center-of-mass

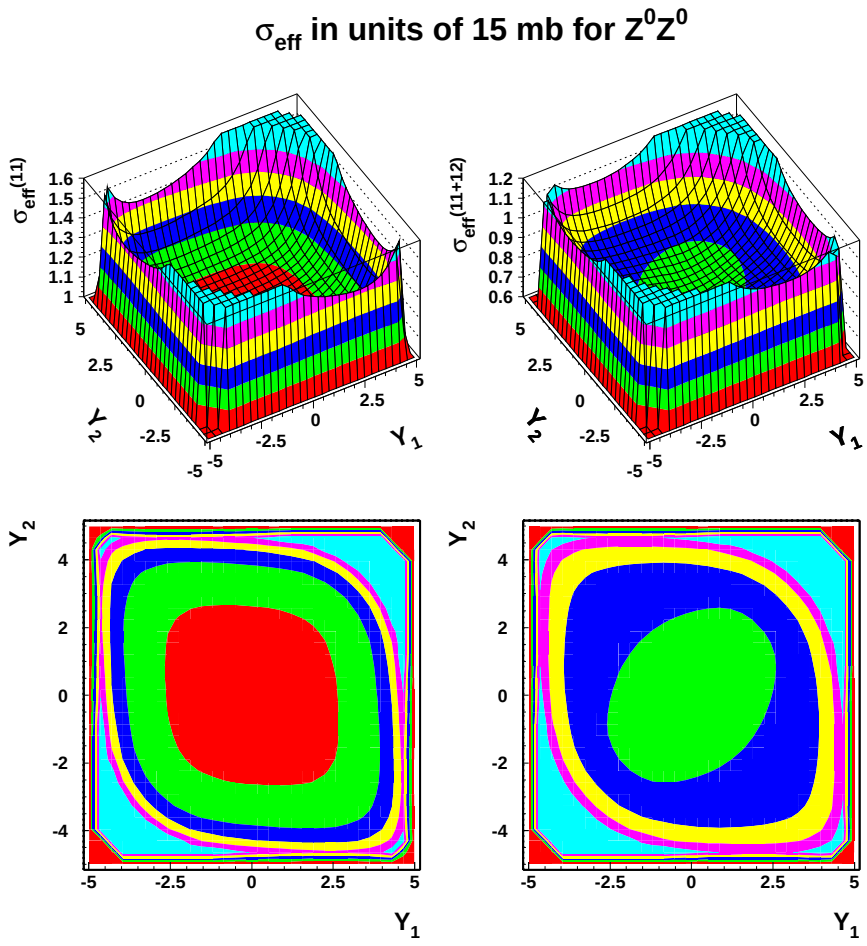

Figure 5.11: The same as in Fig. 5.10 but for the Z^0Z^0 production.

energy $\sqrt{s} = 7$ TeV. The results of these measurements allow to determine the value of the effective cross section which characterizes the effective transverse area of hard partonic interactions in collisions between protons. The measured value of the effective cross section were estimated to be $\sigma_{\text{eff}} = 20.7 \pm 0.8\ (\text{stat.}) \pm 6.6\ (\text{syst.})$ mb by CMS and $\sigma_{\text{eff}} = 15\ \pm 3\ (\text{stat.})\ ^{+5}_{-3}\ (\text{syst.})$ mb by ATLAS. The CMS and ATLAS results are in reasonable agreement with the measurements from Tevatron conducted by the D0 Collaboration with jet events in the $p\bar{p}$ collisions at the energy $\sqrt{s} = 1.96$ TeV [79]. It was found that $\sigma_{\text{eff}}^{\text{incl}} = 12.7 \pm 0.2\ (\text{stat.}) \pm 1.3\ (\text{syst.})$ mb for $\gamma + 3$-jet events and $\sigma_{\text{eff}}^{\text{HF}} = 14.6 \pm 0.6\ (\text{stat.}) \pm 3.2\ (\text{syst.})$ mb for $\gamma + b/c$-jet + 2-jet final states.

The LHCb Collaboration also measured the DPS events with the J/Ψ meson and open charm (C) hadron or double same-charge charm hadrons (CC) [80]. The extracted values of the effective cross section are in agreement with the results from Tevatron, CMS and ATLAS, see Fig. 5.12. Although the results from the CC sample give higher values of σ_{eff}, they are still in reasonable agreement with the rest of the measurements. Double open-charm production, which allows to study different properties of double parton scattering, is the subject of further research conducted by the LHCb Collaboration, see [81]

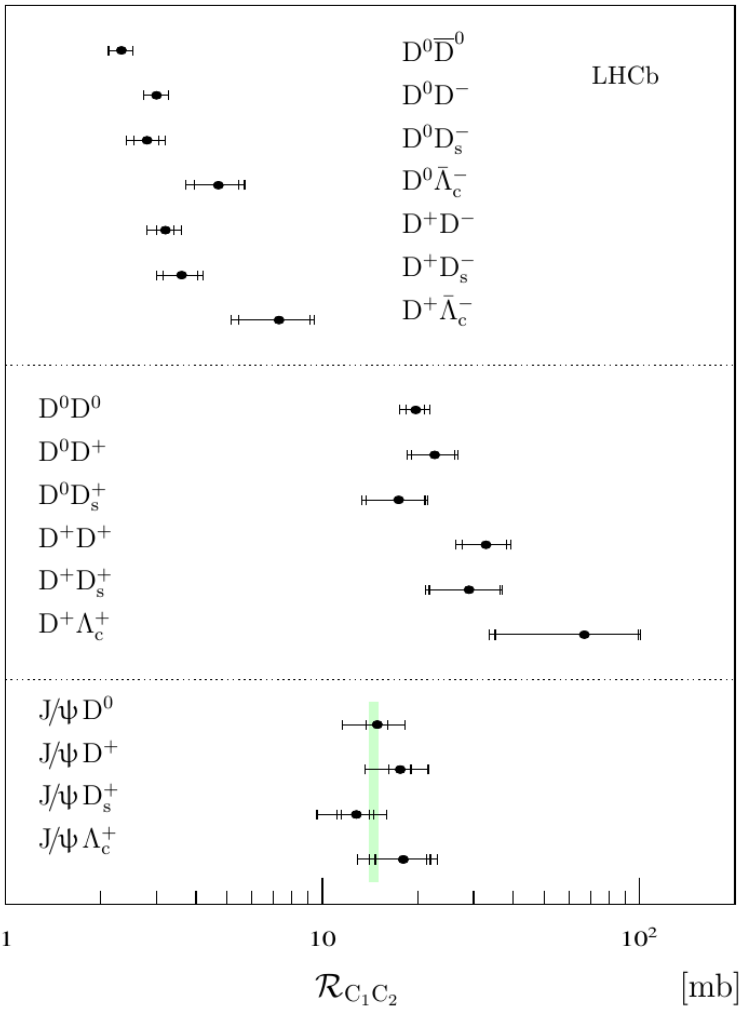

Figure 5.12: Ratios $R_{C_1C_2} \equiv \alpha' \frac{\sigma_{C_1} \times \sigma_{C_2}}{\sigma_{C_1C_2}}$ measured by LHCb (points) in comparison with the DPS cross-section measured at Tevatron (shaded area) [80]. For the J/Ψ C and CC production these ratios have a clear interpretation as the effective cross-section.

and [82] for theoretical predictions. There are also studies suggesting the relevance of double parton scattering for Higgs measurements at the LHC [83]. The current state of the DPS experimental data has been summarized in [84].

The experiments carried out by the CMS, ATLAS, D0 and LHCb Collaborations revealed the increased significance of the double parton scattering in high energy proton-proton collisions. The discussion of experimental results is still preformed with the simplified formula (5.19) for the DPS, using the notion of the effective cross section. However, with higher energy, $\sqrt{s} = 14$ TeV, and higher luminosity, the LHC measurements will be sensitive to more subtle results on the DPS, discussed in this thesis.

Summary

In this thesis, we presented results of two original analyses of high energy scattering processes with hard scales which can be measured at the LHC at CERN. They are selected in such a way that they provide new information on the quark-gluon (partonic) structure of the proton. The main theoretical tool to study these processes is quantum chromodynamics (QCD) - the basic theory of strong interactions.

The continuous progress in the construction of modern high energy accelerators, like HERA, Tevatron, RHIC and the LHC, has opened a possibility to study the structure of hadrons in the kinematic range of small values of the Bjorken variable x. In this range parton densities become so high that they saturate and the methods of perturbative QCD used to describe such effects reach the limits of applicability. One of the most characteristic processes which allows to study the small x regime at hadronic colliders is the Drell-Yan production of lepton pairs from the scattering of strongly interacting quarks and gluons. In Chapter 2, we performed the analysis of the Drell-Yan production for the LHC energy, using the color dipole approach which naturally includes parton saturation effects at small x. We showed that these effects lead to the suppression of the Drell-Yan cross section in comparison to the predictions from the collinear factorization approach in which parton saturation effects are not taken into account.

The large center-of-mass energy of the LHC also allows to gain information on parton correlations in the proton through the double parton scattering processes, described in Chapters 3 and 4. These correlations are encoded in double parton distribution functions (DPDFs) which are more general than single parton distribution functions (PDFs), studied so far in the high energy scattering experiments. The DPDFs evolve with hard scales of the DPS processes, which dependence is described by QCD evolution equations analogous to the well know DGLAP evolution equations for the PDFs. For the purpose of our studies, we constructed a numerical program which solves the evolution equations for DPDFs in the leading logarithmic approximation. The Chebyshev expansion method which we used for the construction is presented in Appendix A.

There are interesting new sum rules which obey the new evolution equations. In Chapter 4, we present an attempt to build initial conditions for the DPDFs evolution which obey the new sum rules and are built out of the existing single PDFs to reduce

arbitrariness in the specification of such initial conditions. The form which we found obeys the new momentum and valence quark number sum rules but fails to be symmetric with respect to the interchange of two partons. This leads to negative values of some DPDFs in the region of large momentum fractions (> 0.5). Our studies showed the limits of phenomenologically motivated approach to the description of the DPDFs.

Two partons in a hadron, which take part in the DPS, can originate directly from the hadron or can be produced from a single parton through its splitting. These two mechanisms are taken into account in the evolution equations for the DPDFs. It is an interesting question how important the splitting contribution is for the DPS cross sections. Up till now, a rigorous analysis of such a contribution has not been performed. In Chapter 5, we present such an analysis for the W^+W^- and Z^0Z^0 electroweak boson production in double parton scattering. We found that the splitting contribution plays an important role for the DPS cross sections, making the standard way of their estimation no longer valid.

Acknowledgments

First and foremost, I would like to express my gratitude to my supervisor Professor Krzysztof Golec-Biernat for his guidance, attention and invaluable help during the course of this thesis.

I also wish to thank the members of the Department of Theory of Structure of Matter (NZ41) for creating a friendly atmosphere for work and study.

I am especially grateful to my family and friends for their support throughout my PhD studies. I thank you all.

This thesis was supported by the Polish NCN grants: DEC-2011/01/B/ST2/03915 and DEC-2012/05/N/ST2/02678.

Appendix A

Chebyshev polynomial method

The Chebyshev polynomial method allows to construct an efficient numerical program which solves evolution equations for parton distributions by reducing the system of integro-differential equations to a set of ordinary differential equations.

A.1 Chebyshev polynomial expansion

In general, any function $f(\bar{x})$ with $\bar{x} \in [-1,1]$ can be approximated by a finite number N of Chebyshev polynomials in the following [85]

$$f(\bar{x}) \simeq \sum_{k=1}^{N} v_k c_k T_{k-1}(\bar{x}), \tag{A.1}$$

where $v_k = 1$ except $v_1 = 1/2$ and the Chebyshev polynomials T are defined by

$$T_{k-1}(\bar{x}) = \cos((k-1)\arccos\bar{x}), \qquad k = 1,2,\ldots. \tag{A.2}$$

The expansion coefficients c_k in eq. A.1 are given by

$$c_k = \frac{2}{N}\sum_{n=1}^{N} f(\bar{x}_n)\, T_{k-1}(\bar{x}_n), \tag{A.3}$$

in which variables $\bar{x}_n$ are zeros of the N^{th} polynomial, $T_N(\bar{x}_n) = 0$,

$$\bar{x}_n = \cos\left(\frac{\pi(n-1/2)}{N}\right), \qquad n = 1,2,\ldots,N. \tag{A.4}$$

From the definition of the Chebyshev polynomials [85], we find the following relation

$$T_{k-1}(\bar{x}_n) = \cos\left(\frac{\pi(k-1)(n-1/2)}{N}\right). \tag{A.5}$$

For a function $f(x)$ with $x \in [a,b]$, we need a one-to-one transformation

$$\bar{x} = \bar{\mathscr{X}}(x) \in [-1,1]\,, \tag{A.6}$$

with the inverse transformation

$$x = \mathscr{X}(\bar{x}) \in [a,b]\,. \tag{A.7}$$

Defining the function $\bar{f}$ such that $f(x) = \bar{f}(\bar{x})$, we find

$$f(x) \simeq \sum_{k=1}^{N} v_k\, c_k\, T_{k-1}(\bar{x})\,. \tag{A.8}$$

The expansion coefficients are given by

$$c_k = \frac{2}{N} \sum_{n=1}^{N} f(x_n)\, T_{k-1}(\bar{x}_n)\,, \tag{A.9}$$

with $x_n = \mathscr{X}(\bar{x}_n)$ being the images of the Chebyshev nodes (A.4) in the interval $[a,b]$.

The generalization to functions of two variables $(x,y) \in I \subset R^2$ needs the invertible transformation to the set of points $(\bar{x},\bar{y}) \in [-1,1] \times [-1,1]$,

$$\bar{x} = \bar{X}(x,y)\,, \qquad\qquad \bar{y} = \bar{Y}(x,y)\,, \tag{A.10}$$

with the inverse

$$x = X(\bar{x},\bar{y})\,, \qquad\qquad y = Y(\bar{x},\bar{y})\,. \tag{A.11}$$

Now

$$f(x,y) \simeq \sum_{k=1}^{N} \sum_{l=1}^{M} v_k v_l\, d_{kl}\, T_{k-1}(\bar{x})\, T_{l-1}(\bar{y})\,, \tag{A.12}$$

with the coefficients

$$d_{kl} = \frac{2}{N}\frac{2}{M} \sum_{n=1}^{N} \sum_{m=1}^{M} f(x_{nm}, y_{nm})\, T_{k-1}(\bar{x}_n)\, T_{l-1}(\bar{y}_m)\,, \tag{A.13}$$

where x_{nm} and y_{nm} are the images of the Chebyshev nodes x_n and y_m, given by eq. (A.4) with N and M, respectively,

$$x_{nm} = X(\bar{x}_n, \bar{y}_m)\,, \qquad y_{nm} = Y(\bar{x}_n, \bar{y}_m)\,. \tag{A.14}$$

For the inverse relation, we have

$$\bar{x}_n = \bar{X}(x_{nm}, y_{nm}), \qquad \bar{y}_m = \bar{Y}(x_{nm}, y_{nm}). \tag{A.15}$$

A.2 Solving evolution equations

Let us apply the Chebyshev polynomial expansion to the prototype evolution equation, see eq. (4.47) for the comparison,

$$\partial_t f(x,t) = \int K(x,u)\, f(x/u,t)\, du - f(x,t)\, k(x), \tag{A.16}$$

where $K(x,u)$ and $k(x)$ are known functions and $x \in [0,1]$. Thus, the coefficients c_k in the Chebyshev approximation formula (A.8) depend on time

$$c_k(t) = \frac{2}{N} \sum_{n=1}^{N} f(x_n,t)\, T_{k-1}(\bar{x}_n), \tag{A.17}$$

where x_n are the images of the Chebyshev nodes (A.4) through a one-to-one transformation,

$$x_n = \mathscr{X}(\tilde{x}_n), \qquad \tilde{x}_n = \bar{\mathscr{X}}(x_n) \in [-1,1]. \tag{A.18}$$

In order to compute them we differentiate both sides of eq. (A.17) with respect to t and use eq. (A.16),

$$\begin{aligned} \partial_t c_k &= \frac{2}{N} \sum_{n=1}^{N} \partial_t f(x_n,t)\, T_{k-1}(\bar{x}_n) \\ &= \frac{2}{N} \sum_{n=1}^{N} \left\{ \int K(x_n,u)\, f(x_n/u,t)\, du - f(x_n,t)\, k(x_n) \right\} T_{k-1}(\bar{x}_n). \end{aligned} \tag{A.19}$$

Approximating the function under the integral by the Chebyshev expansion,

$$f(x_n/u,t) \simeq \sum_{l=1}^{N} v_l\, c_l(t)\, T_{l-1}(\bar{\mathscr{X}}(x_n/u)), \tag{A.20}$$

we find the set of linear differential equations

$$\partial_t c_k = \sum_{l=1}^{N} \mathscr{A}_{kl}\, c_l(t), \qquad k = 1,2,\ldots,N \tag{A.21}$$

with the matrix $\mathscr{A}$

$$\mathscr{A}_{kl} = \frac{2}{N} v_l \sum_{n=1}^{N} \left\{ \int K(x_n,u)\, T_{l-1}(\bar{X}(x_n/u))\, du - k(x_n)\, T_{l-1}(\bar{x}_n) \right\} T_{k-1}(\tilde{x}_n)\,. \quad \text{(A.22)}$$

Equations (A.22) can be easily solved with efficient numerical methods once initial conditions $c_k(0)$ are specified.

Analogously, the method for the double parton distribution functions can be illustrated with the following prototype equation, see eq. (4.46) for the comparison,

$$\begin{aligned} \partial_t F(x,y,t) &= \int K(x,y,u)\, F(x/u,y,t)\, du - F(x,y,t)\, k(x,y) \\ &+ P(x,y)\, f(x+y,t)\,, \end{aligned} \quad \text{(A.23)}$$

where $K(x,y,u)$, $k(x,y)$ and $P(x,y)$ are known functions, $f(x+y,t)$ obeys eq. (A.16) and $(x,y) \in [0,1]\times[0,1]$, The expansion coefficients d_{kl} in the Chebyshev expansion (A.12) depend on time

$$d_{kl}(t) = \frac{2}{N}\frac{2}{M} \sum_{n=1}^{N} \sum_{m=1}^{M} F(x_{nm},y_{nm},t)\, T_{k-1}(\bar{x}_n)\, T_{l-1}(\bar{y}_m)\,, \quad \text{(A.24)}$$

where (x_{nm},y_{nm}) and (x_n,y_m) obey relations (A.14) and (A.15). Differentiating both sides with respect to t, and using eq. (A.23), we find

$$\begin{aligned} \partial_t d_{kl} &= \frac{2}{N}\frac{2}{M} \sum_{n=1}^{N} \sum_{m=1}^{M} \partial_t F(x_{nm},y_{nm})\, T_{k-1}(\bar{x}_n)\, T_{l-1}(\bar{y}_m) \\ &= \frac{2}{N}\frac{2}{M} \sum_{n=1}^{N} \sum_{m=1}^{M} \left\{ \int K(x_{nm},y_{nm},u)\, F(x_{nm}/u,y_{nm},t)\, du - F(x_{nm},y_{nm},t)\, k(x_{nm},y_{nm}) \right. \\ &+ \left. P(x_{nm},y_{nm})\, f(x_{nm}+y_{nm},t) \right\} T_{k-1}(\bar{x}_n)\, T_{l-1}(\bar{y}_m)\,. \end{aligned} \quad \text{(A.25)}$$

Approximating the functions under the integral

$$F(x_{nm}/u,y_{nm},t) = \sum_{k'=1}^{N} \sum_{l'=1}^{M} v_{k'}\, v_{l'}\, d_{k'l'}\, T_{k'-1}(\bar{X}(x_{nm}/u,y_{nm}))\, T_{l'-1}(\bar{Y}(x_{nm}/u,y_{nm})) \quad \text{(A.26)}$$

and

$$f(x_{nm}+y_{nm},t) \simeq \sum_{j=1}^{\mathscr{N}} v_j\, c_j(t)\, T_{j-1}(\bar{\mathscr{X}}(x_{nm}+y_{nm}))\,, \quad \text{(A.27)}$$

and substituting into eq. (A.25), we obtain the following set of linear differential equations

$$\partial_t d_{kl} = \sum_{k'=1}^{N} \sum_{l'=1}^{M} \mathscr{B}_{kl|k'l'}\, d_{k'l'}(t) + \sum_{j=1}^{\mathscr{N}} \mathscr{C}_{klj}\, c_j(t)\,, \tag{A.28}$$

where $k = 1,2,\ldots,N$ and $l = 1,2,\ldots,M$. The matrix $\mathscr{B}$ is given by

$$\mathscr{B}_{kl|k'l'} = \frac{2}{N}\frac{2}{M} v_{k'} v_{l'} \sum_{n=1}^{N} \sum_{m=1}^{M} \left\{ \int K(x_{nm}, y_{nm}, u)\, T_{k'-1}(\bar{X}(x_{nm}/u, y_{nm})) \right. \tag{A.29}$$

$$\left. \times\; T_{l'-1}(\bar{Y}(x_{nm}/u, y_{nm}))\, du - k(x_{nm}, y_{nm})\, T_{k'-1}(\bar{x}_n)\, T_{l'-1}(\bar{y}_m) \right\} T_{k-1}(\bar{x}_n)\, T_{l-1}(\bar{y}_m),$$

while the matrix $\mathscr{C}$ reads

$$\mathscr{C}_{klj} = \frac{2}{N}\frac{2}{M} v_j \sum_{n=1}^{N} \sum_{m=1}^{M} P(x_{nm}, y_{nm})\, T_{k-1}(\bar{x}_n)\, T_{l-1}(\bar{y}_m)\, T_{j-1}(\bar{\mathscr{X}}(x_{nm} + y_{nm}))\,. \tag{A.30}$$

Eqs. (A.28) are solved together with eqs. (A.21) after specifying initial conditions $c_k(0)$ and $d_{kl}(0)$.

The presented method allows to compute the matrices $\mathscr{A}$, $\mathscr{B}$ and $\mathscr{C}$ in advance and provide them as an input for the numerical procedure. This is the main advantage of this method which leads to a significant reduction of the computation time.

Bibliography

[1] F. Halzen and A. Martin, *Quarks and leptons: an introductory course in modern particle physics* (Wiley, 1984).

[2] R. Ellis, W. Stirling and B. Webber, *QCD and Collider Physics*Cambridge Monographs on Particle Physics, Nuclear Physics and Cosmology (Cambridge University Press, 2003).

[3] G. Altarelli and G. Parisi, Nucl.Phys. **B126**, 298 (1977).

[4] Y. L. Dokshitzer, Sov.Phys.JETP **46**, 641 (1977).

[5] V. Gribov and L. Lipatov, Sov.J.Nucl.Phys. **15**, 438 (1972).

[6] H1 and ZEUS Collaboration, F. Aaron *et al.*, JHEP **1001**, 109 (2010), [0911.0884].

[7] K. J. Golec-Biernat and M. Wusthoff, Phys.Rev. **D59**, 014017 (1998), [hep-ph/9807513].

[8] K. J. Golec-Biernat and M. Wusthoff, Phys.Rev. **D60**, 114023 (1999), [hep-ph/9903358].

[9] K. Golec-Biernat, J.Phys. **G28**, 1057 (2002), [hep-ph/0109010].

[10] E. Iancu, K. Itakura and S. Munier, Phys. Lett. **B590**, 199 (2004).

[11] K. J. Golec-Biernat and S. Sapeta, Phys. Rev. **D74**.

[12] J. Bartels, K. Golec-Biernat and H. Kowalski, Phys. Rev. **D66**, 014001 (2002).

[13] J. Bartels, K. J. Golec-Biernat and H. Kowalski, Acta Phys.Polon. **B33**, 2853 (2002), [hep-ph/0207031].

[14] I. Balitsky, Nucl.Phys. **B463**, 99 (1996), [hep-ph/9509348].

[15] Y. V. Kovchegov, Phys.Rev. **D60**, 034008 (1999), [hep-ph/9901281].

[16] Y. V. Kovchegov, Phys.Rev. **D61**, 074018 (2000), [hep-ph/9905214].

[17] G. Soyez, Phys. Lett. **B655**, 32 (2007).

[18] K. J. Golec-Biernat, Acta Phys.Polon. **B35**, 3103 (2004).

[19] A. Stasto, K. J. Golec-Biernat and J. Kwiecinski, Phys.Rev.Lett. **86**, 596 (2001), [hep-ph/0007192].

[20] S. Drell and T.-M. Yan, Annals Phys. **66**, 578 (1971).

[21] G. Altarelli, R. K. Ellis and G. Martinelli, Nucl. Phys. **B143**, 521 (1978).

[22] G. Altarelli, R. K. Ellis and G. Martinelli, Nucl. Phys. **B157**, 461 (1979).

[23] J. Kubar-Andre and F. E. Paige, Phys. Rev. D **19**, 221 (1979).

[24] J. Kubar, M. Le Bellac, J. Meunier and G. Plaut, Nucl.Phys. **B175**, 251 (1980).

[25] S. J. Brodsky, A. Hebecker and E. Quack, Phys. Rev. **D55**, 2584 (1997).

[26] B. Z. Kopeliovich, J. Raufeisen and A. V. Tarasov, Phys. Lett. **B503**, 91 (2001).

[27] B. Z. Kopeliovich, A. V. Tarasov and A. Schafer, Phys. Rev. **C59**, 1609 (1999).

[28] M. A. Betemps, M. B. Gay Ducati and M. V. T. Machado, Phys. Rev. **D66**, 014018 (2002).

[29] F. Gelis and J. Jalilian-Marian, Phys.Rev. **D66**, 094014 (2002), [hep-ph/0208141].

[30] F. Gelis and J. Jalilian-Marian, Phys. Rev. **D76**, 074015 (2007).

[31] G. Moreno *et al.*, Phys.Rev. **D43**, 2815 (1991).

[32] K. Golec-Biernat, E. Lewandowska and A. M. Stasto, Phys.Rev. **D82**, 094010 (2010), [1008.2652].

[33] E. Lewandowska, Acta Phys.Polon. **B42**, 1497 (2011).

[34] E772, P. L. McGaughey *et al.*, Phys. Rev. **D50**, 3038 (1994).

[35] P. M. Nadolsky *et al.*, Phys. Rev. D **78**, 013004 (2008).

[36] A. Martin, W. Stirling, R. Thorne and G. Watt, Eur.Phys.J. **C63**, 189 (2009), [0901.0002].

[37] Axial Field Spectrometer Collaboration, T. Akesson *et al.*, Z.Phys. **C34**, 163 (1987).

[38] B. Blok, Y. Dokshitzer, L. Frankfurt and M. Strikman, Phys.Rev. **D83**, 071501 (2011), [1009.2714].

[39] A. M. Snigirev, Phys. Rev. **D68**, 114012 (2003), [hep-ph/0304172].

[40] V. L. Korotkikh and A. M. Snigirev, Phys. Lett. **B594**, 171 (2004), [hep-ph/0404155].

[41] J. R. Gaunt and W. J. Stirling, JHEP **03**, 005 (2010), [0910.4347].

[42] F. A. Ceccopieri, Phys. Lett. **B697**, 482 (2011), [1011.6586].

[43] J. R. Gaunt and W. J. Stirling, JHEP **1106**, 048 (2011), [1103.1888].

[44] M. Ryskin and A. Snigirev, Phys.Rev. **D83**, 114047 (2011), [1103.3495].

[45] M. Diehl and A. Schafer, Phys. Lett. **B698**, 389 (2011), [1102.3081].

[46] M. Diehl, D. Ostermeier and A. Schafer, JHEP **1203**, 089 (2012), [1111.0910].

[47] J. Bartels and M. G. Ryskin, 1105.1638.

[48] M. Ryskin and A. Snigirev, Phys.Rev. **D86**, 014018 (2012), [1203.2330].

[49] A. V. Manohar and W. J. Waalewijn, Phys.Rev. **D85**, 114009 (2012), [1202.3794].

[50] A. Snigirev, N. Snigireva and G. Zinovjev, Phys.Rev. **D90**, 014015 (2014), [1403.6947].

[51] A. Del Fabbro and D. Treleani, Phys. Rev. **D61**, 077502 (2000), [hep-ph/9911358].

[52] A. Kulesza and W. J. Stirling, Phys. Lett. **B475**, 168 (2000), [hep-ph/9912232].

[53] A. Del Fabbro and D. Treleani, Phys. Rev. **D66**, 074012 (2002), [hep-ph/0207311].

[54] E. Cattaruzza, A. Del Fabbro and D. Treleani, Phys. Rev. **D72**, 034022 (2005), [hep-ph/0507052].

[55] J. R. Gaunt, C.-H. Kom, A. Kulesza and W. J. Stirling, Eur. Phys. J. **C69**, 53 (2010), [1003.3953].

[56] C. Kom, A. Kulesza and W. Stirling, Phys.Rev.Lett. **107**, 082002 (2011), [1105.4186].

[57] CDF Collaboration, F. Abe *et al.*, Phys.Rev.Lett. **79**, 584 (1997).

[58] CDF Collaboration, F. Abe *et al.*, Phys.Rev. **D56**, 3811 (1997).

[59] D0 Collaboration, V. Abazov *et al.*, Phys.Rev. **D81**, 052012 (2010), [0912.5104].

[60] ATLAS Collaboration, G. Aad *et al.*, New J.Phys. **15**, 033038 (2013), [1301.6872].

[61] CMS Collaboration, S. Chatrchyan *et al.*, JHEP **1403**, 032 (2014), [1312.5729].

[62] J. R. Gaunt, *Double parton scattering in proton-proton collisions*, PhD thesis, University of Cambridge, 2012.

[63] E. Lewandowska and K. Golec-Biernat, PoS **DIS2013**, 075 (2013), [1311.7392].

[64] K. Golec-Biernat and E. Lewandowska, Phys.Rev. **D90**, 014032 (2014), [1402.4079].

[65] UA1 Collaboration, G. Arnison *et al.*, Phys.Lett. **B122**, 103 (1983).

[66] UA2 Collaboration, M. Banner *et al.*, Phys.Lett. **B122**, 476 (1983).

[67] N. Cabibbo, Phys.Rev.Lett. **10**, 531 (1963).

[68] M. Kobayashi and T. Maskawa, Prog.Theor.Phys. **49**, 652 (1973).

[69] UA1 Collaboration, C. Albajar *et al.*, Z.Phys. **C44**, 15 (1989).

[70] UA2 Collaboration, J. Alitti *et al.*, Phys.Lett. **B276**, 365 (1992).

[71] D0 Collaboration, S. Abachi *et al.*, Phys.Rev.Lett. **75**, 1456 (1995), [hep-ex/9505013].

[72] CDF Collaboration, F. Abe *et al.*, Phys.Rev.Lett. **76**, 3070 (1996), [hep-ex/9509010].

[73] A. D. Martin, W. J. Stirling and R. Roberts, Phys.Lett. **B354**, 155 (1995), [hep-ph/9502336].

[74] A. Snigirev, Phys.Atom.Nucl. **74**, 158 (2011).

[75] K. Golec-Biernat and E. Lewandowska, Phys.Rev. **D90**, 094032 (2014), [1407.4038].

[76] B. Blok, Y. Dokshitser, L. Frankfurt and M. Strikman, Eur.Phys.J. **C72**, 1963 (2012), [1106.5533].

[77] A. V. Manohar and W. J. Waalewijn, Phys.Lett. **B713**, 196 (2012), [1202.5034].

[78] J. R. Gaunt, JHEP **1301**, 042 (2013), [1207.0480].

[79] D0 Collaboration, V. M. Abazov *et al.*, Phys.Rev. **D89**, 072006 (2014), [1402.1550].

[80] LHCb Collaboration, R. Aaij *et al.*, JHEP **1206**, 141 (2012), [1205.0975].

[81] M. G. Echevarria, T. Kasemets, P. J. Mulders and C. Pisano, 1501.07291.

[82] J. R. Gaunt, R. Maciula and A. Szczurek, Phys.Rev. **D90**, 054017 (2014), [1407.5821].

[83] M. W. Krasny and W. Placzek, Acta Phys.Polon. **B45**, 71 (2014), [1305.1769].

[84] P. Antonioli, 1409.3687.

[85] W. H. Press, S. A. Teukolsky, W. T. Vetterling and B. P. Flannery, ISBN-9780521430647.